NUMERICAL STUDY OF THE THERMAL PERFORMANCE OF SOLAR CHIMNEYS FOR VENTILATION IN BUILDINGS

Thesis submitted for the Degree of Master of Science in Engineering in Sustainable Energy Engineering

Deepti Charitar

CHRDEE002

Supervisor: Dr Amos Madhlopa

Energy Research Centre

Department of Mechanical Engineering

August 2015

PLAGIARISM DECLARATION

1. I know the meaning of plagiarism and declare that all the work in the document, save for that which is properly acknowledged, is my own.
2. I know that plagiarism is wrong. Plagiarism is to use another's work and to pretend that it is one's own.
3. I have used the prescribed Harvard UCT referencing style for citation and referencing. Each significant contribution to, and quotation in this thesis from the work, or works, of other people has been attributed, and has been cited and referenced.
4. This thesis is my own work.
5. I have not allowed, and will not allow, anyone to copy my work with the intention of passing it off as his or her own work.

Signature: SIGNED

ABSTRACT

Building ventilation is crucial for improving the indoor air quality and thermal comfort. Nowadays, mechanical ventilation systems such as air conditioning and fans are most commonly used in buildings. However, these devices consume a lot of electricity which is mainly generated from the combustion of fossil fuels, resulting in the release of greenhouse gases and thereby contributing to climate change. Consequently, it is essential to switch to natural ventilation systems which are environmentally friendly as they are based on renewable sources of energy. One such type of natural ventilation system is the solar chimney which can either be roof-mounted or wall-mounted in buildings.

The aim of this study was to develop a mathematical model for assessing the thermal performance of roof-mounted (inclined) and wall-mounted (vertical) solar chimneys. The model was validated using numerical simulations in MATLAB. Different configurations of solar chimneys were designed and modelled in MATLAB in order to compare their performances, in terms of the ventilation rate expressed as the number of air changes per hour, ACH. Raw climatic data, including the intensities of global and diffuse solar radiation on a horizontal plane, wind speed and ambient temperature were obtained for Stellenbosch, located in the Western Cape Province of South Africa. This was used for the MATLAB modelling of the solar chimneys. The effects of inclination angle, air gap, chimney height and view factor on the thermal performance of solar chimneys were explored in this study.

Results show that there is good agreement between the modelled data obtained from this investigation and experimental values reported in literature. The root mean square errors for the models with and without the view factor were found to be 13% and 20% respectively. Moreover, it was found that an inclination angle of 60° is the optimum tilt angle for Stellenbosch as the maximum ventilation rate was obtained at this angle. In addition, the ventilation rate was found to increase with an increase in the air gap. An increase in ACH was also observed when the chimney height was increased.

Furthermore, it was also observed that the view factor is an important parameter to be considered when designing solar chimneys in order to obtain more realistic values for the ventilation rate. The inclusion of the view factor also resulted in an increase in ACH. The overall conclusion is that inclined roof-mounted solar chimneys give a better thermal performance than vertical wall-mounted solar chimneys. It is also concluded that the inclusion of the view factor improves the accuracy of modelling of a solar chimney.

ACKNOWLEDGEMENTS

I would like to acknowledge the following people who have helped me during this research, without whom I would have been unable to complete my thesis:

- My family, for their financial support throughout my dissertation.
- Dr Amos Madhlopa, for his excellent guidance, patience, motivation and insightful comments throughout the project. I would also like to express my gratitude towards him for his tremendous assistance on the MATLAB program which I used in this thesis.
- The Energy Research Centre, for providing me the opportunity to carry out my research within their Renewable Energy research group.
- The Mechanical Engineering Department, for providing me access to their computer laboratory which was an environment conducive to research.

TABLE OF CONTENTS

LIST OF FIGURES

LIST OF TABLES

LIST OF ACRONYMS

ACH	Air Changes per Hour
ASHRAE	American Society of Heating, Refrigerating and Air-conditioning Engineers
CFD	Computational Fluid Dynamics
DME	Department of Minerals and Energy
DoE	Department of Energy
GHG	Greenhouse Gas
GM	Greenwich Meridian
IEA	International Energy Agency
IPCC	Intergovernmental Panel on Climate Change
NASA	National Aeronautics and Space Administration
RSC	Roof Solar Chimney
SABS	South African Bureau of Standards
SANS	South African National Standards
SC	Solar Chimney
UNEP	United Nations Environment Programme
VF	View Factor
WSC	Wall Solar Chimney

NOMENCLATURE

Symbol	Definition	Unit
A_g	Area of glass	m^2
A_i	Anisotropic index	Dimensionless
A_{in}	Cross sectional area of inlet to air flow channel	m^2
A_{out}	Cross sectional area of outlet to air flow channel	m^2
A_w	Area of absorber wall	m^2
C_d	Coefficient of discharge of air channel inlet	Dimensionless
c_{fl}	Specific heat capacity of air	$Jkg^{-1}K^{-1}$
d	Air gap (between glass cover and absorber wall)	m
f	Modulating factor	Dimensionless
F_{w-g}	View factor between absorber wall and glass cover	Dimensionless
g	Acceleration due to gravity	ms^{-2}
G_{SC}	Solar Constant	Wm^{-2}
H	Incident solar radiation on vertical wall	Wm^{-2}
h_c	Conductive heat transfer coefficient for glass	$Wm^{-2}K^{-1}$
h_g	Convective heat transfer coefficient between glass cover and air	$Wm^{-2}K^{-1}$
H_r	Height of room to be ventilated	m
h_{rs}	Radiative heat transfer coefficient from the top of glass cover to the sky	$Wm^{-2}K^{-1}$
h_{rwg}	Radiative heat transfer between absorber wall and glass cover	$Wm^{-2}K^{-1}$

h_w	Convective heat transfer coefficient between absorber wall and air	$Wm^{-2}K^{-1}$
h_{wind}	Convective heat transfer over glass cover due to wind	$Wm^{-2}K^{-1}$
I_b	Beam radiation on horizontal plane	Wm^{-2}
$I_{b,t}$	Beam radiation on inclined plane	Wm^{-2}
I_d	Diffuse radiation on horizontal plane	Wm^{-2}
$I_{d,t}$	Diffuse radiation on inclined plane	Wm^{-2}
I_g	Global solar radiation on horizontal plane	Wm^{-2}
I_{gr}	Ground-reflected radiation	Wm^{-2}
I_o	Extraterrestrial radiation	Wm^{-2}
I_t	Total solar radiation on inclined plane	Wm^{-2}
K_{ec}	Extinction coefficient	m^{-1}
k_f	Thermal conductivity of air	$Wm^{-1}K^{-1}$
k_{ins}	Thermal conductivity of wall insulation	$Wm^{-1}K^{-1}$
L_{abs}	Height of absorber wall	m
L_g	Height of glass cover	m
L_{lo}	Longitude of the specific location	°
L_r	Length of room to be ventilated	m
L_s	Stack height	m
L_{st}	Standard meridian for the local time zone	°
m	Mass flow rate of air inside the channel of the solar chimney	kgs^{-1}
n	Day of the year	Dimensionless

n_1	Refractive index of air	Dimensionless
n_2	Refractive index of glass	Dimensionless
q	Heat transfer to air stream	Wm^{-2}
R_b	Ratio of beam radiation on tilted surface to that on horizontal surface	Dimensionless
S_1	Solar radiation absorbed by glass cover	Wm^{-2}
S_2	Solar radiation absorbed by absorber wall	Wm^{-2}
T_a	Temperature of ambient air	K
T_f	Mean temperature of air in flow channel of chimney	K
$T_{f,i}$	Temperature of air at inlet of chimney	K
$T_{f,o}$	Temperature of air at outlet of chimney	K
T_g	Mean temperature of glass cover	K
T_r	Room temperature (inside building)	K
T_w	Mean temperature of absorber wall	K
U_b	Overall heat transfer coefficient between absorber and room	$Wm^{-2}K^{-1}$
U_t	Overall heat transfer coefficient from top of glass cover	$Wm^{-2}K^{-1}$
V	Wind speed	ms^{-1}
V_{rate}	Ventilation rate	$m^3\ s^{-1}$
V_{room}	Volume of room to be ventilated	m^3
W_{abs}	Width of absorber wall	m
W_g	Width of glass	m
w_{ins}	Thickness of insulation behind the absorber	m

W_r	Width of room to be ventilated	m
z	Inlet height of wall-mounted solar chimney	m
z_{glass}	Thickness of glass cover	m

Greek Symbols

α	Absorptance of glass cover	Dimensionless
α_{wall}	Absorptivity of absorber wall	Dimensionless
γ	Surface azimuth angle	°
γ_{MTA}	Constant for mean temperature approximation	Dimensionless
δ	Declination angle	°
η	Efficiency	Dimensionless
μ_f	Dynamic viscosity of air	Pa.s
ν_f	Kinematic viscosity of air	m^2s^{-1}
τ	Transmittance of glass cover	Dimensionless
ϕ	Latitude	°
ω	Hour angle	°
ω_{ss}	Sunset hour angle	°
β	Angle of inclination of solar chimney with the horizontal	°
θ_1	Angle of incidence of beam radiation on a surface	°
θ_z	Zenith angle	°
ρ	Reflectance of glass cover	Dimensionless
ρ_f	Density of air kg/m^3	kg/m^3

ρ_g	Albedo	Dimensionless
σ	Stefan-Boltzmann constant	$Wm^{-2}K^{-4}$

Chapter 1

INTRODUCTION

This chapter gives an overview of the two main types of ventilation systems in buildings, namely natural and mechanical ventilation. The need for natural ventilation, with particular focus on solar energy is also discussed as well as other solar energy applications. The problem statement, aims and objectives of this research are also stated and lastly, a thesis structure is included at the end of this chapter.

1.1 Ventilation

Ventilation can be defined as the supply and removal of air, to and from any space, in order to control the level of air contaminants, humidity or temperature within that space (American Society of Heating, Refrigerating and Air-conditioning Engineers [ASHRAE], 2001a). Air may or may not undergo conditioning during the process of ventilation (ASHRAE, 1999). Since ventilation in buildings plays a major role on the health, comfort and productivity of their occupants, ventilation standards have been issued in many countries around the world (Persily, 2015: 61). It is estimated that the minimum volume of fresh air needed for the purpose of breathing is approximately 1.2 litres per second per person but for comfort purposes, it is essential to supply more than this minimum amount in order to meet the occupants' oxygen requirements, for dilution of odours, dilution of carbon dioxide concentration and to minimise the increase in air temperature in case there are extreme sensible heat gains (Jones, 1994: 450).

A ventilation system in a building is an important design criterion as it helps to improve thermal comfort and the indoor air quality (ASHRAE, 2001a). The latter is dependent on the following factors (Ng *et al*., 2011: 3217):

a) Climatic parameters including humidity, velocity of air, temperature and levels of air contaminants.
b) Parameters related to the occupants such as moisture, carbon dioxide, odours and tobacco smoke.
c) Parameters related to the building and outdoor sources such as formaldehydes, volatile organic compounds, radon, biological agents and airborne particulates.

The ventilation process in buildings can either take place naturally or mechanically. Natural ventilation is dependent on wind or thermal buoyancy for the movement of air while an external power input is required for mechanical ventilation (Mora-Pérez, Guillén-Guillamón & López-Jiménez, 2015: 73).

1.1.1 Natural ventilation

Natural ventilation can be defined as the movement of air due to wind or thermal properties, or diffusion which can occur through any purposeful openings in a building (ASHRAE, 2001a). Temperature differences between indoor and outdoor air lead to differences in wind and air densities, which in turn result in pressure differences across the shell of the building. Movement of air is then induced due to these pressure gradients. Some natural ventilation openings in buildings include doors, windows, roof ventilators or vertical flues (ASHRAE, 2001b). There are two main types of natural ventilation, namely wind-driven ventilation and stack-driven ventilation.

Wind-driven ventilation works on the principle of the effects of the wind. As wind blows over a building, a positive pressure is created on the windward side of the building while a negative pressure is created on the leeward side of the building. In this way, a pressure difference is created and airflow is hence induced through the building (Khan, Su & Riffat, 2008: 1586). Wind-driven ventilation is dependent on two parameters, firstly, on the average driving pressure at the opening of the building and secondly, on fluctuating pressures around the opening (Khan, Su & Riffat, 2008: 1586).

Stack-driven ventilation occurs as a result of a difference in temperature between the inside and outside of a building. When the inside temperature is higher than the outside temperature, the warm indoor air rises and exits the building, while cooler outdoor air is drawn into the building (Khan, Su & Riffat, 2008: 1586).

1.1.2 Mechanical Ventilation

Mechanical ventilation involves the use of devices which are machine-driven (ASHRAE, 2001a). In this type of ventilation, also known as forced ventilation, the pressure differences across the shell of the building are induced by different types of mechanical devices (ASHRAE, 2001b). Air conditioners and fans are examples of devices used for the purpose of mechanical ventilation.

a) Air conditioners

One of the most common types of mechanical ventilation systems used in buildings nowadays is the air conditioning system which can control the temperature, humidity, supply of outdoor air, filtration of airborne particles and the movement of air within the occupied space (McDowall, 2007: 3). The major component of an air conditioning system is the refrigeration unit which consists of a series of equipment connected in a sequential order so as to produce the refrigeration effect (Wang, 2001). Refrigeration can be defined as the extraction of heat from a lower temperature heat source, transferred to a higher temperature heat sink, using a working fluid known as the refrigerant for the absorption and transmission of heat so as to keep the temperature of the heat source lower than the temperature of the surroundings (Wang, Lavan & Norton, 2000: 35). This is in accordance with the Second Law of Thermodynamics which explains that a heat engine must exchange heat with both a low-temperature sink and a high-temperature source in order to keep operating (Çengel & Boles, 2006: 287). There are various types of refrigeration systems that are used for air conditioning purposes, namely vapour compression systems, absorption systems and air or gas expansion systems.

A vapour compression system is the most commonly used refrigeration system for air conditioning. In this system, the refrigerant is activated to a higher pressure and higher temperature by the compressor. The refrigerant is then condensed to liquid form after transferring its heat to the sink. The liquefied refrigerant is then throttled to a low pressure and low temperature vapour during the process of evaporation. On the other hand, in an absorption system, the refrigeration effect is caused by thermal energy input, for instance direct-fired furnace, waste heat, hot water or steam. Concerning an air or gas expansion system, mechanical energy is used to compress the air or gas to a high pressure. The air or gas is then cooled and expanded to low pressure, thereby causing the refrigeration effect as the temperature drops (Wang, 2001).

b) Fans

Fans are commonly used for ventilation purposes in buildings. There are two major types of fans, namely centrifugal and axial. They can be distinguished from each other by the airflow path through the fans. In the case of a centrifugal fan, the velocity of the airstream is increased by a rotating impeller. The air gains kinetic energy as it moves from the impeller hub to the tips of the blade. This kinetic energy is then transformed to an increase in static pressure as the velocity of the air decreases before entering the discharge (US Department of

Energy [US DoE], 2003: 3). In general, centrifugal pumps can generate high pressure and as such, they are used commonly for 'dirty' environments with high moisture content and high particulate matter. On the other hand, in an axial fan system, the airstream moves along the fan axis. Axial fans are typically used for 'clean' environments, having low pressure and low volume (US DoE, 2003: 4).

1.1.3 The need for natural ventilation

The operation of mechanical ventilation systems requires electricity which is mainly generated from fossil fuels worldwide. Combustion of fossil fuels for the generation of electricity releases greenhouse gases (GHGs) such as carbon dioxide and nitrous oxide (European Commission, 2015). This increase in greenhouse gas emissions in turn leads to climate change (Çengel & Boles, 2006: 89). Consequently, it is essential to find ways of reducing the consumption of fossil fuels in an attempt to protect the environment. One such strategy is to make use of natural ventilation in buildings instead of the conventional mechanical ventilation systems since natural ventilation can be driven by renewable energy and consequently, it promotes sustainable exploitation of energy resources. The natural ventilation strategy discussed in this research is based on solar energy, which currently has a wide range of applications.

1.2 Solar Energy Applications

The sun is a sphere of extremely hot gaseous matter situated approximately 1.5×10^{11} m away from the earth and it has a diameter of 1.39×10^{9} m (Garg & Prakash, 2000: 2). In fact, the sun can be considered as a fusion reactor in continuous operation, "with its constituent gases as the containing vessel retained by gravitational forces" (Duffie & Beckman, 2013: 3). The sun is made up of approximately 74 % hydrogen, 25 % helium and the rest is made up of negligible quantities of heavier elements (Kalogirou, 2014: 1). Moreover, the surface temperature of the sun is estimated to be approximately 5800 K (Chen, 2011: 69).

The major process responsible for the supply of energy from the sun is a reaction whereby four atoms of hydrogen combine to form one atom of helium. The mass of the helium atom is less than the sum of the masses of the 4 atoms of hydrogen, the remaining mass having been converted to energy (Duffie & Beckman, 2013: 3). This is in accordance to the Einstein's mass-energy equivalence equation, where energy is equal to the product of mass and speed of light squared. The energy that is crucial for solar applications is that radiation from the sun

which is emitted in the ultraviolet, visible and infrared regions, corresponding to a radiation wavelength in the range of 0.15 to 3.0 micrometres (Kalogirou, 2014: 75).

Solar radiation can either be converted directly into electricity via the photoelectric effect or absorbed as heat as required for solar thermal applications. Various methods exist for collecting solar energy for the generation of electricity or heat, including flat plate collectors, evacuated tubes, concentrators, solar ponds and appropriate architecture (Da Rosa, 2005: 455).

1.2.1 Conversion of solar radiation into electricity

In 1839, the French physicist Edmund Bequerel first observed the photoelectric effect which causes certain materials to produce an electric current when exposed to light (National Aeronautics and Space Administration [NASA], 2011). Figure 1.1 illustrates the photoelectric effect. As sunlight strikes the surface of the semi-conductor, its atoms gain kinetic energy, causing a movement of the atoms within the semi-conductor, hence leading to the production of an electric current. This is the principle used in photovoltaic panels for electricity generation in houses or buildings, both as grid or off-grid electricity.

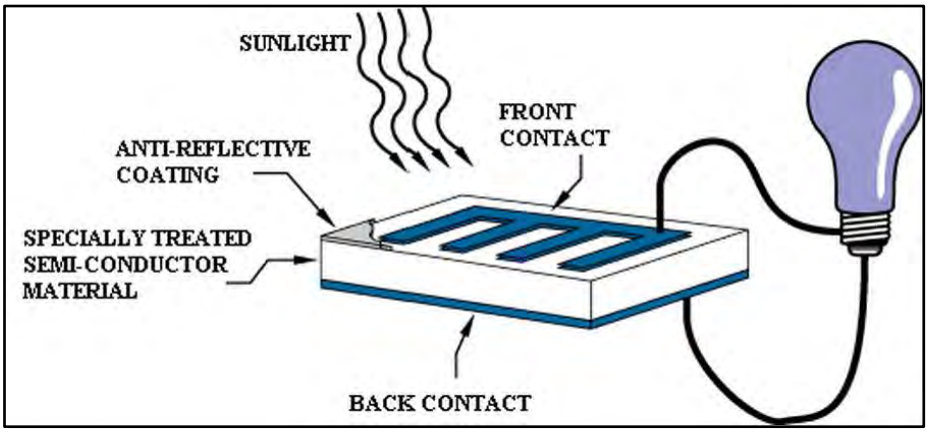

Figure 1.1: The Photoelectric effect.
Source: NASA (2011)

1.2.2 Absorption of solar radiation as heat

In the case of solar thermal applications, a solar collector is required in order to absorb solar radiation as heat which is then transferred to the working fluid (water, oil or air) of the system (Tian & Zhao, 2013: 539). This can be used for obtaining hot water as in the case of solar water heaters or for providing natural ventilation in buildings using the stack effect. A solar chimney falls under solar thermal applications.

A solar chimney is a passive cooling strategy which can be used for ventilation in buildings. As its name suggests, it uses solar radiation to allow exchange of heat through natural circulation of air. The mechanism of air flow across the system is through thermal buoyancy (Zhai, Song & Wang, 2011: 3757). Solar energy heats up the air inside the solar chimney and causes the air to expand. This expansion of air causes air density to decrease and thus, hot air rises and comes out at the top of the chimney (Lee & Strand, 2009: 615).

Solar chimneys can either be vertical or inclined and can be categorised into two groups: wall-mounted solar chimneys and roof-mounted solar chimneys. A solar chimney typically consists of an absorber wall, an air gap and a glazed wall (Zhai, Song & Wang, 2011: 3758). The latter allows sufficient heat to be accumulated from solar radiation in order to induce the natural upward movement of air, known as the chimney effect (Bansal *et al*., 2005: 1302). Figure 1.2 shows a simple schematic of a solar chimney.

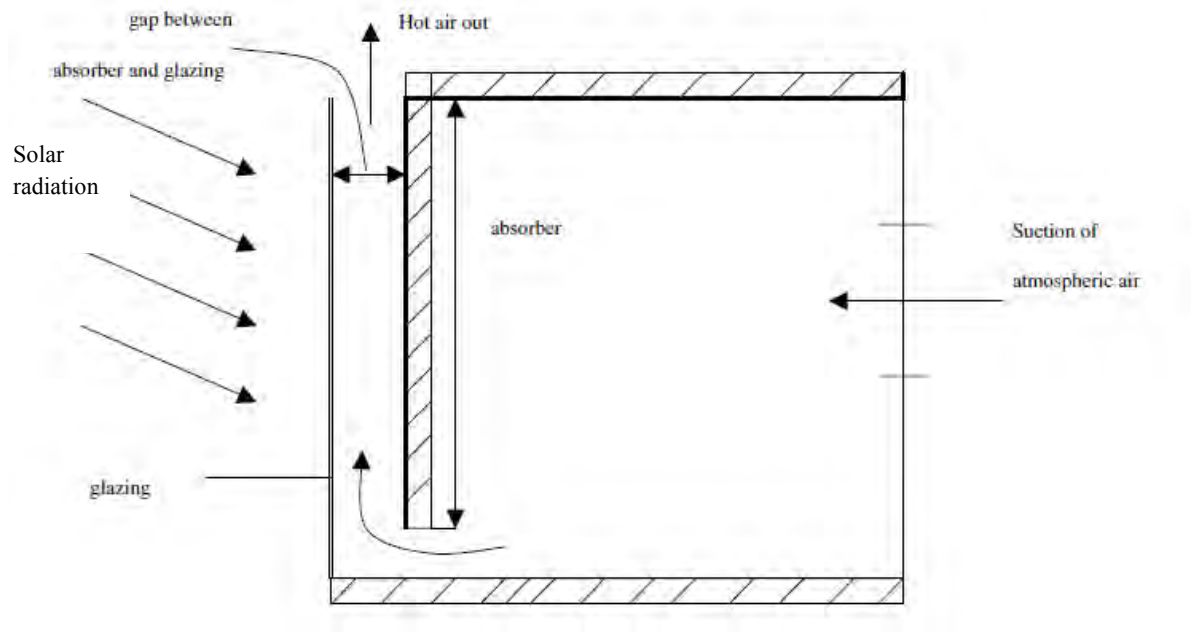

Figure 1.2: Schematic of a solar chimney.
Source: Mathur et al. (2006: 930)

As can be observed from Figure 1.2, the main components of a solar chimney are the absorber wall (or collector) and the glass wall. The collector absorbs solar radiation and heats up the air inside the solar chimney. As the air is heated, it expands and becomes less dense. The hot air rises out at the top of the chimney and air from the room is in turn drawn through the inlet of the solar chimney. In this way, the solar chimney causes natural circulation of air through the room.

1.3 Problem Statement

It is estimated that buildings represent 32% of final energy consumption globally (IEA, 2014). It is further claimed that more than one third of total energy use and related GHG emissions come from buildings, both in developing and developed countries. Most of this energy is used for heating, cooling and ventilation purposes (United Nations Environment Programme [UNEP], 2009: 5).

The building sector contributes significantly to the emissions of greenhouse gases which occur as a result of the combustion of fossil fuels for the generation of electricity. GHGs in turn lead to climate change which has negative impacts on the environment. Moreover, waste residues such as coal fly ash, are also produced during combustion of fossil fuels and the disposal of these waste materials represents a major issue for the environment. Furthermore, fossil fuels are finite energy sources and it is therefore crucial to investigate ways in which electricity consumption can be minimized in buildings. One such strategy is to install solar chimneys on the walls or roofs of buildings.

Natural ventilation is one of the most important design criteria in buildings since it has various advantages over mechanical ventilation systems, with regards to energy requirements and environmental benefits (Khanal & Lei, 2011: 1811). It is further claimed that solar chimneys are being given global attention due to their potential for reducing heat gain and inducing ventilation without causing environmental harm (Zhai, Song & Wang, 2011: 3757). Various numerical and experimental studies have been conducted on solar chimneys in order to study their performance under varying climatic conditions and varying design parameters. However, in previous investigations on solar chimneys, the view factor is a parameter which has most often been ignored. In fact, the effect of the view factor on the performance of solar chimneys has not been mentioned in any previous study. It is thus desirable to investigate and compare the thermal performance of wall-mounted and roof-mounted solar chimneys in order to identify which configuration would be more efficient for a building, as well as to investigate the effect of the view factor which has most often been ignored in previous studies.

1.4 Scope of study

This study investigates the thermal performance of wall-mounted and roof-mounted solar chimneys under identical climatic conditions. Different parameters were investigated in order to optimize the thermal performance of the solar chimneys. The study is limited to theoretical research only as no practical experiments were carried out. Nonetheless, numerical results obtained from this investigation were compared with experimental values from literature in order to validate the mathematical model developed in this study. The MATLAB software was used as a platform to simulate various system configurations.

1.5 Aim and Objectives

The aim of this study is to assess the thermal performance of roof and wall solar chimneys, in terms of the ventilation rate.

The specific objectives of this research are to:

a) Design roof-mounted and wall-mounted solar chimneys.
b) Develop and validate a mathematical model for the solar chimneys.
c) Simulate the thermal performance of the solar chimneys.
d) Determine which configuration of the solar chimney is more efficient.

1.6 Thesis organisation

This thesis comprises of 5 chapters. In chapter 1, the two types of ventilation are discussed, as well as the need for natural ventilation. The problem statement, aims and objectives are also stated. Chapter 2 is the literature review which gives a background on the physics of solar radiation, examines the mechanisms of heat transfer and gives a comprehensive description on solar chimneys. The methodology adopted for the mathematical model and simulation of the solar chimneys in MATLAB is discussed in Chapter 3. The results from the MATLAB simulation are presented in Chapter 4, as well as a discussion on the results obtained. Chapter 5 gives the conclusions and recommendations which could be drawn based on the results and discussion. After chapter 5, a list of the references which were used in the context of this study is given, followed by the appendix section which shows correlations for physical properties of air which were developed in Excel, as well as the simulation program which was written in MATLAB for investigating the performance of the solar chimneys.

Chapter 2

LITERATURE REVIEW

This chapter discusses the drivers for natural ventilation, examines the physics of solar radiation and gives an explanation on the geographical and astronomical terms associated with solar radiation which have been used in the context of this investigation. Moreover, the modelling of solar radiation on inclined surfaces is also discussed, as well as the laws of thermodynamics and the three modes of heat transfer, namely conduction, convection and radiation. A detailed description of solar chimneys is also provided. Furthermore, the factors affecting the performance of solar chimneys are also discussed, based on previous numerical studies carried out on solar chimneys.

2.1 Drivers for natural ventilation in buildings

Natural ventilation in buildings is considered as an effective means of saving energy which would have been otherwise used by mechanical ventilation systems (Gontikaki *et al*., 2010). There are numerous advantages of using natural ventilation in buildings, as compared to conventional mechanical ventilation systems.

2.1.1 Dependence on fossil fuels for electricity generation

The primary source of energy for the generation of electricity is mainly derived from fossil fuels. Figure 2.1 shows the global share of electricity generation by energy source (International Energy Agency [IEA], 2013a). As can be observed from Figure 2.1, fossil fuels (coal, oil and natural gas) account for 68% of electricity generated globally.

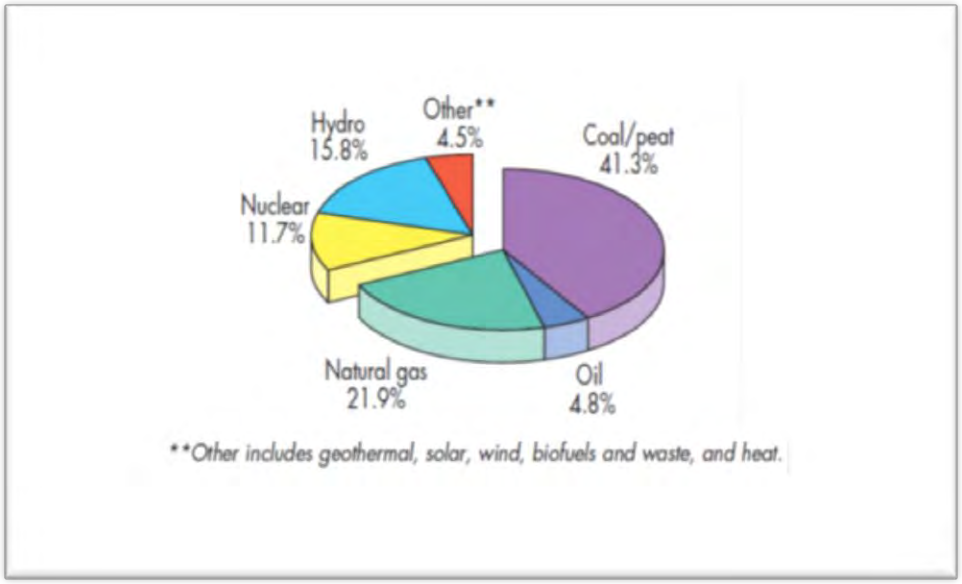

Figure 2.1: Global share of electricity generation by energy source in 2011.
Source: IEA (2013a)

Furthermore, the building industry is considered as one of the major energy-consuming economic sectors (Gordon, 2001: 1). Figure 2.2 shows the global share of final energy consumption by buildings and other sectors for the year 2010. The buildings sector accounted for 35 % of the final energy consumption in 2010 and this represents the largest share of final energy consumption amongst all the different sectors, as can be illustrated from Figure 2.2.

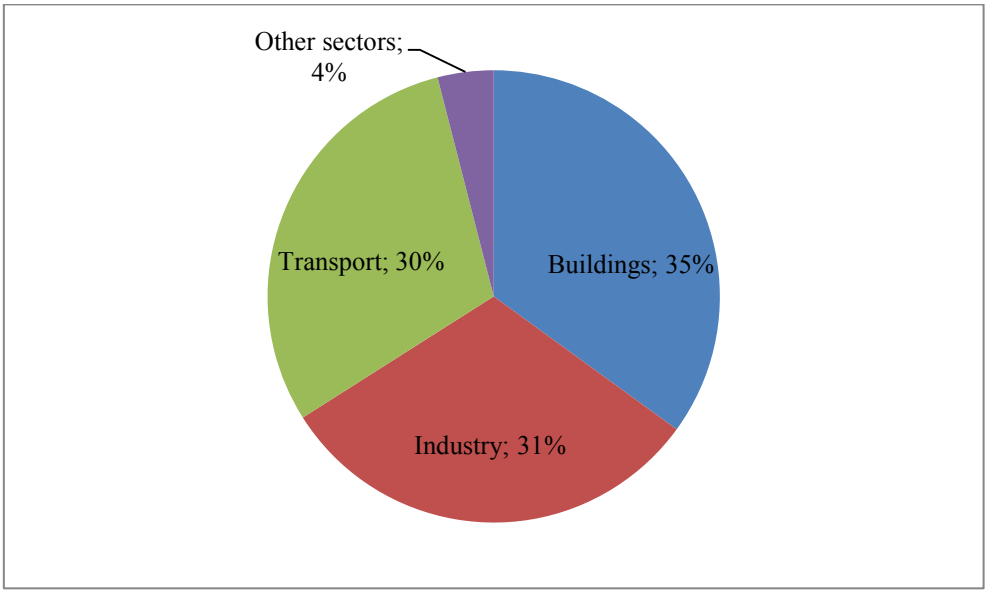

Figure 2.2: Global share of final energy consumption by buildings and other sectors in 2010.
Other sectors include agriculture, forestry, fishing and other non-specified.
Source: Adapted from IEA (2013b)

In the context of this study, the main focus will be on South Africa and therefore, it is essential to analyse the energy sector in the country. Figure 2.3 shows the share of electricity generation in South Africa by energy source. The country is heavily dependent on coal for electricity generation. In fact, 91.7% of the total electricity generated in 2006 was derived from coal (Department of Energy [DoE], 2009: 45) as can be depicted by Figure 2.3.

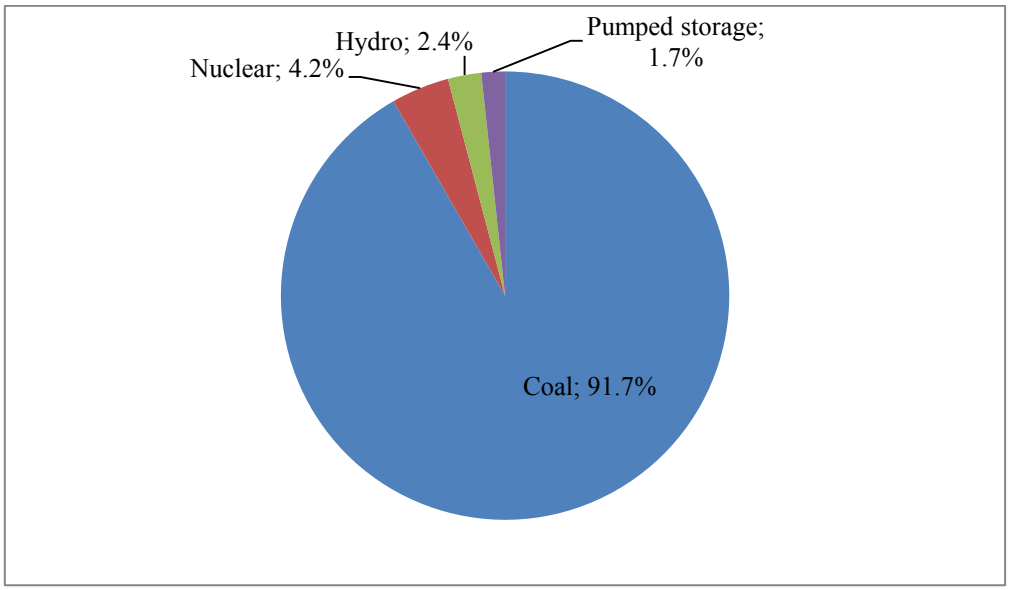

Figure 2.3: Electricity generation in South Africa by type of fuel in 2006.
Source: Adapted from DoE (2009: 45)

Figure 2.4 shows the final energy consumption in the buildings sector in South Africa from the years 1971 to 2010. It is estimated that residential buildings consumed 617 PJ of final energy in 2010 while non-residential buildings consumed 181 PJ of final energy during that same year; hence a total of 798 PJ of final energy being consumed by the buildings sector in 2010 in South Africa (IEA, 2015b).

Figure 2.4: Final energy consumption in the buildings sector in South Africa.
Source: IEA (2015b)

It is further estimated that the buildings sector's share of the total final energy consumption in 2010 was 31 %; residential and non-residential sectors representing 24 % and 7 % of the total share respectively, as can be observed from Figure 2.5.

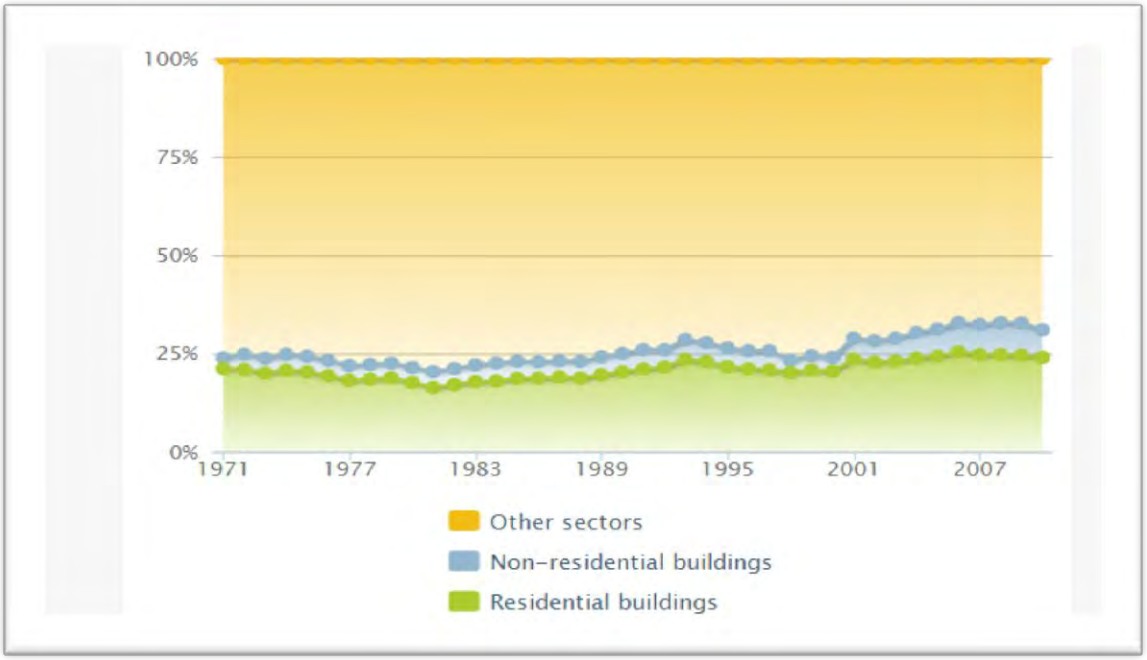

Figure 2.5: Buildings sector's share of the total final energy consumption in South Africa.
Source: IEA (2015b)

The overall observation is that the building sector consumes large amounts of energy, both on the national and international scale. Since there is heavy reliance on fossil fuels for electricity generation worldwide, it is important to implement renewable energy sources in the buildings sector. One such strategy is to make use of natural ventilation in buildings, in order to reduce the electricity consumption associated with mechanical ventilation.

2.2.2 Climate change

Another driver for natural ventilation is climate change. The latter is a phenomenon which can be defined as an alteration in the state of the climate that can be observed by fluctuations in the mean and/or variability of its properties, and that continues for a prolonged period (usually decades), as a result of human activities or natural causes (Intergovernmental Panel on Climate Change [IPCC], 2012: 5). Climate change is closely linked to an increase in the concentration of greenhouse gases (GHGs) in the atmosphere; in fact it has been observed that the sea level is increasing due to the storage of heat in the oceans which has been occurring over the past few decades as a result of an increase in GHG concentration in the atmosphere (IPCC, 2013: 1142). The average global sea level increased by 3.2 ± 0.4 mm per annum over the years 1993 to 2011 while the average global surface temperature has been increasing by 0.14 to 0.17°C per decade since 1971 (Kalogirou, 2014: 16-19).

Melting of glaciers occurs as a result of the increase in the temperature of the earth. It has been further stated that ocean thermal expansion due to storage of excess heat and loss of mass from glaciers due to melting are the main contributors to the increase in sea level; and also the rate of increase in sea level was higher in the 20th century as compared to the 19th century and it has been predicted that the rate of increase in sea level in the 21st century would be even higher than that of the 20th century (IPCC, 2013: 1142). As a result of an increase in the sea level, coastal and low lying areas are being flooded and eroded (European Commission, 2015).

Concerning South Africa, various studies have been carried out in order to investigate the potential impacts of climate change in the country. Firstly, according to the Long Term Adaptation Scenarios (LTAS), with regards to the biodiversity sector, it was found that the grassland biome is under the most threat of considerable structural change due to infringement by woody vegetation as a result of increases in temperature and carbon dioxide. The Nama Karoo biome, the Indian Ocean coastal belt, the Fynbos biome, and the Forest

biome are the four other biomes which have also been evaluated to be under substantial threat due to climate change (Ziervogel *et al*., 2014: 608).

Secondly, concerning the agricultural sector, hugely negative estimated impacts have been revealed for crops such as maize and wheat. Moreover, the net range suitability for certain pests and pathogens in South Africa and on the African continent as a whole, is expected to increase due to climate change. Thirdly, regarding the water sector, various complexities are expected to occur including higher occurrences of droughts and floods (Ziervogel *et al*., 2014: 609). It is therefore essential to take measures which will help combat the impacts of climate change, for instance, switching to renewable sources of energy.

2.2.3 Disposal of waste residues from combustion of fossil fuels

Since South Africa is largely dependent on coal for electricity generation, it is worth analysing the issues surrounding coal combustion, besides the emissions of GHGs. A complex mixture of chemicals such as oxides of sulphur, oxides of nitrogen, carbon monoxide, acid gases, organic compounds and solid waste products such as coal fly ash are released into the atmosphere during coal combustion (Meawad, Bojinova & Pelovski, 2010: 2549). Disposal of coal fly ash represents a major concern to the environment since it can cause contamination of ground water due to leaching of heavy metals and emissions of particulate matter from the ash (González, Navia & Moreno, 2009: 976).

In fact, South Africa produced 30 Mt of coal fly ash in 1992 and was amongst the top five producers of coal fly ash globally (Manz, 1997: 695). Consequently, it is essential to reduce the amount of electricity produced from coal in order to minimize the production of this waste product in an attempt to reduce environmental harm.

2.2.4 Energy Security

Ensuring energy security is another driver for natural ventilation in buildings. Energy security can be defined as "the uninterrupted availability of energy sources at an affordable price" (IEA, 2015b). According to the *Energy Security Master Plan of South Africa*, energy security is to "ensure that diverse energy resources, in sustainable quantities and at affordable prices, are available to the South African economy in support of economic growth and poverty alleviation, taking into account environment management requirements and interactions among economic sectors " (Department of Minerals and Energy [DME], 2007: 13).

South Africa is currently facing an energy security crisis and emergencies in electricity supply were declared both in 2008 and at the beginning of 2014 (Trollip *et al*., 2014: 8). Since fossil fuels are finite sources of energy (non-renewable), they will not always be readily available and as such, it is important to invest in alternative energy sources in order to ensure energy security. Furthermore, this electricity crisis is also having negative impacts on the South African economy (Trollip *et al*., 2014: 16).

2.2.5 High costs of mechanical ventilation systems

Air conditioning is widely used in buildings as a means of mechanical ventilation. According to the United Nations Environment Programme (2002), as cited by Santamouris and Kolokotsa (2013: 75), air conditioning and refrigeration account for nearly 15 % of the global electricity consumption. Since electricity is required for the operation of mechanical ventilation systems, the costs of operating such systems are often high. On the other hand, natural ventilation systems require less complex structures and since they only entail free resources like the sun and wind to operate, the costs associated with such systems are lower compared to mechanical systems. It has also been stated that environmentally friendly and low cost systems need to be employed in buildings since the energy consumption of the buildings sector is projected to increase due to increasing world population and improving standard of living (Gordon, 2001: 21).

Consequently, it can be noted that natural ventilation in buildings can help to combat the effects of climate change, minimize production of waste materials and also ensure energy security. Moreover, since natural ventilation systems are more affordable than mechanical ventilation systems (World Health Organization, 2009), they can help to improve thermal comfort and indoor air quality, especially in developing countries where electricity access is a major issue.

2.2 Physics of solar radiation

Solar energy reaches the surface of the Earth as radiation, with components mainly from the visible, infrared and ultraviolet regions of the electromagnetic spectrum (Chen, 2011: 41). It consists of two components, namely beam radiation, also known as direct radiation, and diffuse radiation which is also known as scattered radiation. The sum of direct and diffuse radiation is commonly referred to as global radiation. Beam radiation at normal incidence is usually measured using a pyrheliometer while global radiation is typically measured using a pyranometer (Myers, 2013: 19).

A pyranometer is used to measure the global radiation on a surface as it has a hemispherical view of the surroundings while a pyrheliometer has a restricted view of the surroundings and consequently, it is used to measure direct radiation by being pointed towards the sun (Goswami, Kreith & Kreider, 2000: 63).

2.2.1 Direct radiation

Direct or beam radiation is defined as radiation which is obtained from the sun without undergoing any scattering by the atmosphere (Duffie & Beckman, 2013: 10). It reaches the earth's surface with no change in direction (Goswami, Kreith & Kreider, 2000: 43). Direct radiation comes directly from the disk of the sun (Bourne, 2009: 6), as can be depicted from Figure 2.6.

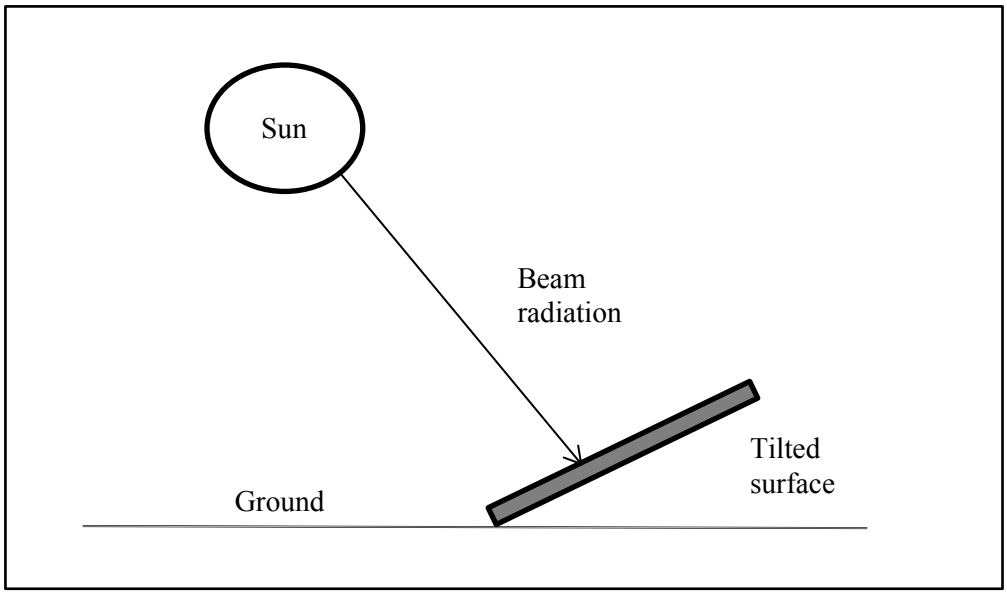

Figure 2.6: Beam radiation on a tilted surface.

2.2.2 Diffuse radiation

Diffuse or scattered radiation is defined as the solar radiation striking the surface of the earth after being scattered by the atmosphere (Myers, 2013: 9). According to Jones (1994: 142), diffuse radiation originates from four fundamental phenomena. Firstly, direct radiation is scattered in all directions in the atmosphere when it strikes oxygen and nitrogen molecules. This effect is more prominent for short wavelengths and consequently, the sky appears blue Secondly, direct radiation is also scattered by water vapour molecules present in the atmosphere. Thirdly, selective absorption by ideal gases and water vapour also takes place, which result in diffuse radiation. Fourthly, diffuse radiation occurs as a result of scattering caused by dust particles in the atmosphere. Figure 2.7 gives an illustration of diffuse radiation.

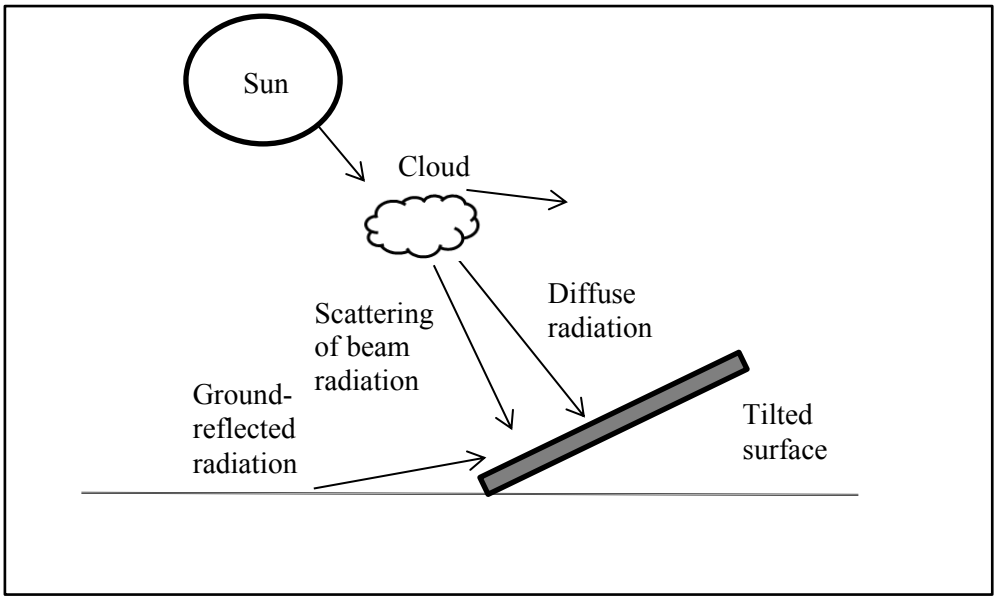

Figure 2.7: Diffuse radiation on a tilted surface.

2.2.3 Geographical and Astronomical parameters

The total power output of the sun is estimated to be 3.8 x 10^{20} MW, which is radiated in all direction and only a small percentage of that total radiation strikes the surface of the Earth (Kalogirou, 2014: 51). According to Chen (2011: 1), the annual total energy from the sun which reaches the surface of the earth is approximately 5.46 x 10^{24} J but only around 0.01 % of that total energy is needed to meet the annual global energy need. Nonetheless, the amount of solar radiation which can be captured on the surface of the earth is not constant and is hugely dependent on the earth-sun geometry at any given time (Gordon, 2001: 498). In the context of this research, many geographical and astronomical terms associated with the earth-sun relationship are used and these are described in the following paragraphs.

2.2.3.1 Latitude and longitude

Any location on the surface of the earth can be specified by two coordinates, namely the latitude and the longitude (Chen, 2011: 78). The latitude, ϕ, of a location refers to the angular location of a place on the surface of the earth with respect to the equatorial plane (Jones, 1994: 144). A positive value for the latitude means that the location is in the Northern Hemisphere while a negative value means that the location is in the Southern Hemisphere.

On the other hand, the longitude of a location is always given with respect to the zero line of longitude which runs through Greenwich in England (Myers, 2013: 3). The line of zero longitude is commonly referred to as the Greenwich Meridian and longitudes are typically measured east or west of the Greenwich Meridian (Garg & Prakash, 2000: 9). The convention which is used is as follows: a positive value for longitude means that the location is to the east of the Greenwich Meridian while a negative value means that the location is to the west of the Greenwich Meridian.

2.2.3.2 Declination angle

The declination angle, typically represented by δ, refers to the angular position of the sun from the equatorial plane (Jones, 1994: 143). It is the angle between the equatorial plane and the orbital plane of the earth (Myers, 2013: 4). The convention that will be used in this research is as follows: positive angle refers to the north of the equator while negative angle refers to the south of the equator. The declination angle, δ can be calculated as follows (Goswami, Kreith & Kreider, 2000: 24):

$$\delta = 23.45 * \sin\left[360 * \frac{284 + n}{365}\right] \tag{2.1}$$

Where n = day of the year; $1 \leq n \geq 365$.

Nonetheless, a more accurate equation can be used for calculating the declination angle, as given by equation (2.2) (Duffie & Beckman, 2013: 14):

$$\delta = \tag{2.2}$$
$$\left(\frac{180}{\pi}\right)(0.006918 - 0.399912\cos B + 0.070257\sin B - 0.006758\cos 2B +$$
$$0.000907\sin 2B - 0.002697\cos 3B + 0.00148\sin 3B)$$

$$B = (n-1) * \frac{360}{365} \tag{2.3}$$

2.2.3.3 Solar Time

Another important definition in the context of this research is the solar time. At a given location, the solar time can be estimated by using the difference between the standard meridian for the local time zone and the longitude of the location, and taking into account the annual deviation in the rate of the rotation of the earth around the sun (Behar, Khellaf & Mohammedi, 2015: 239). The solar time can be expressed (in minutes) as given by equation (2.4) (Goswami, Kreith & Kreider, 2000: 26):

$$Solar\ time = Standard\ time + 4(L_{st} - L_{lo}) + E_{time} \tag{2.4}$$

Where L_{st} and L_{lo} refer to the standard meridian for the local time zone and the longitude of the specific location respectively. The local standard meridian can be computed by multiplying the time difference between the Greenwich Meridian Time and the local standard time by 15 (Duffie & Beckman, 2013: 11). E_{time} refers to the Equation of time and is given as follows (Myers, 2013: 5):

$$\begin{aligned} E_{time} = 229.18\ (&0.0000075 \\ &+ 0.001868 \cos B\ - 0.032077 \sin B\ - 0.014615 \cos 2B \\ &- 0.040849 \sin 2B) \end{aligned} \tag{2.5}$$

2.2.3.4 Hour Angle and Sunset hour angle

The hour angle, denoted by ω, is the angular displacement of the sun from the local longitudinal line due to the earth's rotation on its own axis at an average rate of 15° per hour and is given by the following equation (Behar, Khellaf & Mohammedi, 2015: 239):

$$\omega = 15 * (solar\ time - 12) \tag{2.6}$$

The sunset hour angle (ω_{ss}) is another parameter which is used in the context of this research. It is a function of the latitude of the location and the declination angle. The sunset hour angle can be expressed as follows (Duffie & Beckman, 2013: 17):

$$\omega_{ss} = -\tan\phi \tan\delta \tag{2.7}$$

2.2.3.5 Solar Zenith Angle and Surface Azimuth Angle

The solar zenith angle, θ_z, is the angle between the normal to a horizontal plane and the direction of the sun in the sky, given by the following equation (Myers, 2013: 5):

$$\cos\theta_z = \sin\phi\sin\delta + \cos\phi\cos\delta\cos\omega \tag{2.8}$$

On the other hand, the surface azimuth angle usually denoted by γ, is defined as "the deviation of the projection on a horizontal plane of the normal to the surface from the local meridian'' (Duffie & Beckman, 2013: 13).

2.2.3.6 Angle of incidence

The angle of incidence of beam radiation on a surface, symbolised as θ_1, is a function of the declination angle (δ), latitude of the location (ϕ), surface azimuth angle (γ), hour angle (ω) and the angle between the surface and the horizontal (β). The cosine of the angle of incidence can be expressed as follows (Chen, 2011: 87):

$$\cos\theta_1 = \tag{2.9}$$
$$\sin\delta\sin\phi\cos\beta - \sin\delta\cos\phi\sin\beta\cos\gamma + \cos\delta\cos\phi\cos\beta\cos\omega +$$
$$\cos\delta\sin\phi\sin\beta\cos\gamma\cos\omega + \cos\delta\sin\beta\sin\gamma\sin\omega$$

2.2.3.7 Albedo

The albedo of a surface is defined as the reflectivity of a surface to solar radiation (Sailor, Resh & Segura, 2005: 589). It is a ratio of the reflected solar radiation to the total radiation striking the surface (Behar, Khellaf & Mohammedi, 2015: 240). This parameter, denoted by ρ_g, is used in estimating the ground reflected radiation which is in turn used to calculate the total solar radiation on an inclined plane.

2.2.4 Modelling of solar radiation on inclined planes

In order to compute the total solar radiation that can be captured on an inclined surface, various equations need to be solved. There are numerous terms which are used in those equations and these are discussed in the following paragraphs.

2.2.4.1 Solar constant

The solar constant, denoted by G_{SC}, is defined as the average amount of radiation from the sun captured on a surface which is perpendicular to the rays of the sun outside the atmosphere at average earth-sun distance (Goswami, Kreith & Kreider, 2000: 41). According to Chen

(2011: 67), the solar constant has a value of 1366 ± 3 W/m^2 while according to Duffie and Beckman (2013: 5), the solar constant is assigned a value of 1367 W/m^2 which was adopted by the World Radiation Centre. Consequently, in this research, a value of 1367 W/m^2 was used for all the calculations.

2.2.4.2 Extraterrestrial solar radiation

Extraterrestrial solar radiation, I_o, is defined as the hypothetical amount of solar energy that would be available on a horizontal plane on the surface of the Earth in the absence of an atmosphere (Madhlopa, 2009: 21). Extraterrestrial radiation at any time during the day on a horizontal plane can be calculated as follows (Sailor, Resh & Segura, 2006: 593):

$$I_o = G_{SC} * \left[1 + 0.033 * \cos\frac{360n}{365}\right] * \cos\theta_z \tag{2.10}$$

2.2.4.3 Beam, diffuse and ground-reflected solar radiation on a tilted surface

The total solar radiation on a tilted surface, I_t, can be expressed as the sum of three components, namely, beam ($I_{b,t}$), diffuse ($I_{d,t}$) and ground-reflected (I_{gr}) radiation (Goswami, Kreith & Kreider, 2000: 47). The solar radiation on a tilted surface is obtained by converting the solar radiation on a horizontal surface to the tilted surface of interest since global and diffuse radiation levels are typically measured on horizontal surfaces (Demain, Journée & Bertrand, 2013: 710).

An important parameter used in the calculation of solar radiation on a tilted plane is the geometric factor (R_b). The latter is defined as the ratio of beam radiation on a tilted plane to the beam radiation on a horizontal plane (I_b) at any given time (Duffie & Beckman, 2013: 23).

$$R_b = \frac{I_{b,t}}{I_b} = \frac{\cos\theta}{\cos\theta_z} \tag{2.11}$$

The intensity of beam radiation on a tilted plane can be calculated by multiplying the beam radiation component on a horizontal surface with the geometric factor, as given by following equation (Wlodarczyk & Nowak, 2009: 128):

$$I_{b,t} = I_b * R_b \tag{2.12}$$

Various models have been proposed to estimate the diffuse solar radiation on an inclined plane. Some of these models are isotropic while others are anisotropic. Isotropic models are based on the assumption that the intensity of diffuse radiation from the sky is uniform over the sky dome. On the other hand, anisotropic models take into consideration the non-uniformity of the diffuse sky radiation near the disk of the sun (circumsolar diffuse) and also account for the isotropic diffuse radiation from the rest of the sky dome (Khalil & Shaffie, 2013: 857). Figure 2.8 illustrates the various components of solar radiation on a tilted surface.

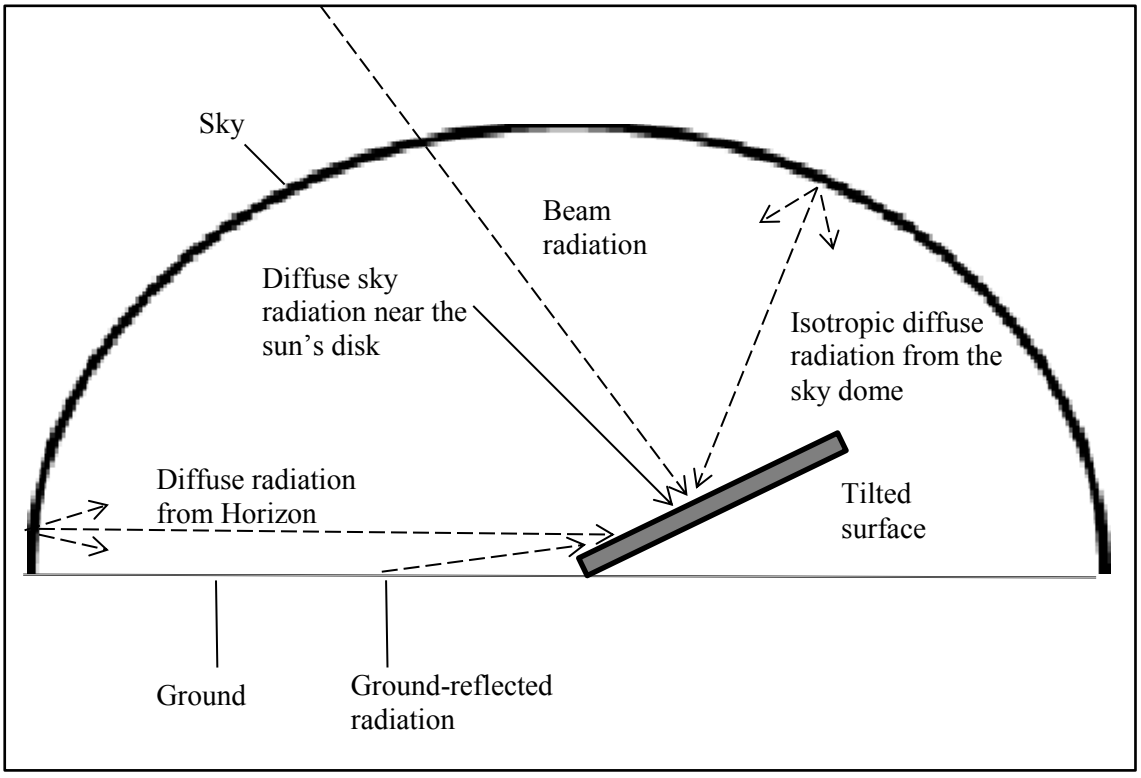

Figure 2.8: Components of solar radiation on a tilted surface.

It has been observed that the diffuse solar radiation on an inclined surface comprises of 3 parts, namely an isotropic diffuse component which is obtained uniformly from the sky dome; a circumsolar diffuse component which is obtained due to the forward scattering of solar radiation, concentrated near the disk of the sun; and a horizon brightening component which is most evident in clear skies and concentrated near the horizon (Demain, Journée & Bertrand, 2013: 711). These different components are depicted in Figure 2.8. A brief description of some solar radiation models is given in Table 2.1.

Table 2.1: Solar Radiation Models.
Source: Compiled from Evseev & Kudish (2009:379)

Model	Description and equation
Liu-Jordan (1961)	Assumes isotropic diffuse radiation: $\Psi = \cos^2\left(\frac{\beta}{2}\right)$ (2.13)
Temps-Coulson (1977)	Assumes clear sky conditions: $\Psi = \cos^2\left(\frac{\beta}{2}\right)\ [1 + \sin^3\left(\frac{\beta}{2}\right)]\ [1 + \cos^2\theta \sin^3\theta_z]$ (2.14)
Hay (1979)	Assumes linearity of the isotropic and circumsolar diffuse radiation components: $\Psi = A_i R_b + (1 - A_i)\cos^2\left(\frac{\beta}{2}\right)$ (2.15)

The various symbols that are used in Table 2.1 have already been defined at an earlier stage in this thesis and new parameters are described as follows:

Ψ is the ratio of diffuse radiation on a tilted surface to the horizontal diffuse radiation (Evseev & Kudish, 2009: 379).

A_i, the anisotropic index, refers to the transmittance of the atmosphere for beam radiation and can be expressed as follows (Duffie and Beckman, 2013: 92):

$$A_i = \frac{I_b}{I_o} \tag{2.16}$$

In the Temps-Coulson model (1977), horizon brightening was accounted for, by the inclusion of a correction factor of $1 + sin^3\left(\frac{\beta}{2}\right)$ (Evseev & Kudish, 2009: 379). This correction factor was revised by Klucher (1979) to incorporate a modulating factor, f, in order to account for cloudiness. Furthermore, a similar term to that of Klucher was added by Reindl et al. (1990) to the Hay model. This modulating factor is given by Duffie and Beckman (2013: 92):

$$f = \sqrt{\frac{I_b}{I_g}} \tag{2.17}$$

Where, I_g = Global solar radiation on a horizontal surface.

The Reindl equation can be expressed as follows (Wlodarczyk & Nowak, 2009: 132):

$$I_{d,t} = I_d \left\{ (1 - A_i) \left(\frac{1 + cos\beta}{2} \right) \left[1 + f sin^3 \left(\frac{\beta}{2} \right) \right] + A_i R_b \right\} \tag{2.18}$$

In this study, the above equation was used for calculating the diffuse solar radiation on a tilted surface as it is an improvement over the isotropic model and it accounts for horizon brightening and cloudiness (Duffie & Beckman, 2013: 92). The third component of solar radiation on an inclined plane, the ground-reflected radiation, is given by the following equation (Demain, Journée & Bertrand, 2013: 714):

$$I_{gr} = \frac{1}{2} * \rho_g * I_g * (1 - \cos\beta) \tag{2.19}$$

The total solar radiation on an inclined plane can thus be expressed as follows (Goswami, Kreith & Kreider, 2000: 47) :

$$I_t = I_{b,t} + I_{d,t} + I_{gr} \tag{2.20}$$

Equation (2.20**)** can be expressed explicitly by the following equation (Duffie & Beckman, 2013: 92):

$$I_t = (I_b + I_d A_i)\, R_b + I_d (1 - A_i) \left(\frac{1 + cos\beta}{2} \right) [1 + f \sin^3 \left(\frac{\beta}{2} \right)] + I_g\, \rho_g \left(\frac{1 - cos\beta}{2} \right) \tag{2.21}$$

In order to understand the working principle of a solar chimney, it is also essential to know the theory of thermodynamics and heat transfer.

2.3 Thermodynamics

Thermodynamics is the study of various energy interactions, particularly work and heat, with matter, which result in noticeable and quantifiable changes in the properties of a substance at a macroscopic level (Nag, 2008: xxiii). Thermodynamics can be sub-categorized into macroscopic (or classical) thermodynamics which deals with the net changes that affect a system and microscopic (or statistical) thermodynamics which deals with changes happening to or within the molecules inside the system (Winterbone & Turan, 2015: 1). There are four laws of thermodynamics, namely, the Zeroth Law, the First Law, the Second Law and the Third Law. The laws of thermodynamics encapsulate the characteristics of energy and its conversion from one form to another (Atkins, 2010).

2.3.1 The Zeroth Law of Thermodynamics

The Zeroth Law of thermodynamics states that *"if two systems are at the same time in thermal equilibrium with a third system, they are in thermal equilibrium with each other"* (Al-Shemmeri, 2010: 33). In other words, if body A is in thermal equilibrium with body B and body B is in thermal equilibrium with body C, then body A and C will be in thermal equilibrium with each other (Nag, 2008: 26).

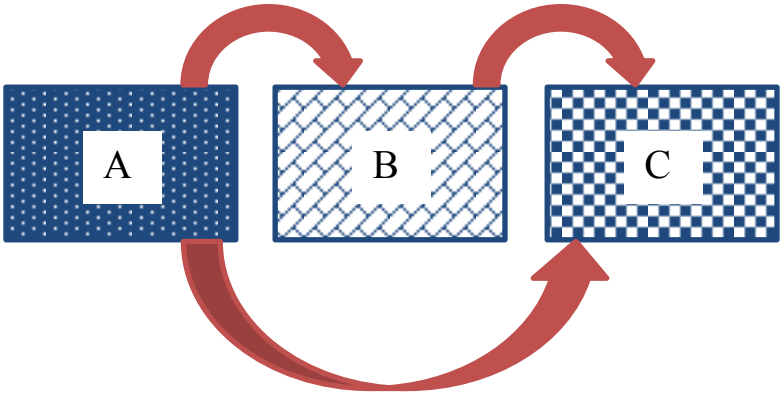

Figure 2.9: Zeroth Law of Thermodynamics

Source: Al-Shemmeri (2010: 33)

2.3.2 The First Law of Thermodynamics

The First Law of thermodynamics is based on the principle of conservation of energy. It states that energy can neither be created nor destroyed during a process; it can only be changed from one form to another. This principle can be expressed as follows: the difference between the total energy entering and leaving a system during a process is equal to the net change in the total energy of the system during that process (Çengel & Boles, 2006: 70):

$$E_{in} - E_{out} = \Delta E_{system} \quad (2.22)$$

Where, E_{in} is the total energy entering the system, E_{out} is the total energy leaving the system and ΔE_{system} represents the change in the total energy of the system.

2.3.3 The Second Law of Thermodynamics

The second law of thermodynamics is of particular relevance in matters of efficiency and can be expressed by the Kelvin-Planck statement as follows (Bergman *et al*., 2011: 31): "*It is impossible for any system to operate in a thermodynamic cycle and deliver a net amount of work to its surroundings while receiving energy by heat transfer from a single thermal reservoir.*" This means that a heat engine must exchange heat with both a low-temperature sink and a high-temperature source in order to keep operating and a heat engine cannot achieve a thermal efficiency of 100 % (Çengel & Boles, 2006: 287). The efficiency of a heat engine can be expressed by the following equation (Bergman *et al*., 2011: 32):

$$\eta = 1 - \frac{Q_{out}}{Q_{in}} \quad (2.23)$$

Where, η is the efficiency of the heat engine, Q_{in} is the heat transferred to the heat engine from the high-temperature source and Q_{out} is the heat transferred from heat engine to the low-temperature sink.

2.3.4 The Third Law of Thermodynamics

The Third Law of thermodynamics states that *"the entropy of a pure crystalline substance at absolute zero temperature is zero"* (Çengel & Boles, 2006: 347). Entropy is a property which gives an indication of the microscopic disorder of a system (Al-Shemmeri, 2010: 8). It is a measure of the change which occurs as a result of a process and it gives an indication of the direction of a process (Winterbone & Turan, 2015: 14).

In the context of this research, the First Law of thermodynamics was applied; energy balances were applied on the three main components of the solar chimney, namely, the absorber wall, the glass cover and on the air stream within the channel of the solar chimney. Since thermodynamics provides no information with regards to the nature of the interactions which occur between the system and its surroundings, it is also crucial to study the various modes of heat transfer (Bergman *et al*., 2011: 2).

2.4 Heat transfer

Heat transfer can be defined as the exchange of energy between material bodies due to a difference in temperature (Holman, 2010: 1). Heat transfer cannot occur between two systems which are at the same temperature (Çengel & Boles, 2006: 60). There are three modes of heat transfer, namely conduction, convection and radiation.

2.4.1 Conduction

Heat conduction is the transfer of energy which occurs in a stationary medium, which can either be a solid or a fluid, when there is a temperature gradient in the medium (Bergman *et al*., 2011: 2). There are two ways in which energy is transferred via conduction, namely through molecular interaction and by free electrons. In the first instance, molecules of higher energy level, being in greater motion, transfer energy to adjacent molecules of lower energy level. This process can occur in all systems in which solid, liquid and gas molecules are present and in which a temperature gradient exists. In the second instance, the heat transfer occurs due to the presence of free electrons and occurs predominantly in pure-metallic solids. The capacity of solids to conduct heat is directly proportional to the concentration of free electrons (Welty *et al*., 2008: 201). Figure 2.10 shows the various parameters which are used to calculate the rate of heat transfer.

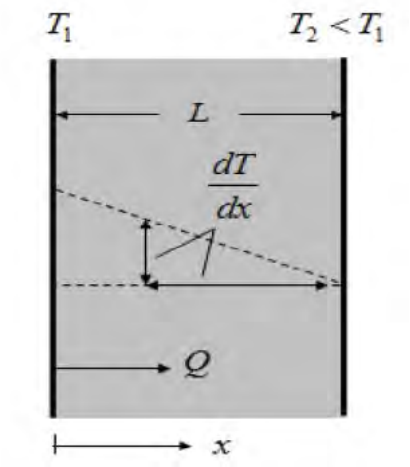

Figure 2.10: Heat transfer through conduction.
Source: Long & Sayma (2009: 9)

The rate equation for conduction is given by Fourier's law of heat conduction. The rate of heat transfer in the x direction (Q_x) is dependent on the thermal conductivity of the material (k), the temperature gradient $\left(\frac{dT}{dx}\right)$ and the area perpendicular to the direction of heat flow (A) and can be expressed as follows (Holman, 2010: 2):

$$\frac{Q_x}{A} = -k \frac{dT}{dx} \tag{2.24}$$

2.4.2 Convection

Convection is defined as the exchange of energy between a surface and an adjacent fluid (Welty *et al*., 2008: 207). There are two mechanisms through which convection occurs, firstly due to the random motion of the molecules as aggregates and secondly, due to the bulk motion of the fluid as the molecules move collectively (Bergman *et al*., 2011: 6).

There are two types of convection, namely natural and forced convection. Natural convection occurs due to buoyancy forces, which occur as a result of density differences arising due to variations in temperature within the fluid. On the other hand, forced convection entails the movement of the fluid due to the application of an external force, for instance a fan or pump (Welty *et al*., 2008: 207). The rate of heat transfer for convection is given by Newton's law of cooling. The convective heat transfer rate (Q) is a function of the convective heat transfer coefficient (h), the area perpendicular to the direction of heat flow (A) and the temperature difference between the wall temperature (T_w) and the fluid temperature (T_f) and this can be expressed by the following equation (Holman, 2010: 10):

$$Q = h\,A\,(T_w - T_f) \tag{2.25}$$

2.4.3 Radiation

The third mode of heat transfer, radiation, is the transfer of heat energy through electromagnetic waves between surfaces which are at different temperatures (Long & Sayma, 2009: 7). Radiation does not require a medium for heat transfer. In fact, maximum heat transfer occurs when there is a vacuum between two surfaces which are exchanging heat (Welty *et al*., 2008: 209). The rate of energy emission (Q) from a blackbody is dependent on the absolute temperature (T) and the area of the emitting surface (A) and is given by the following equation (Holman, 2010: 12):

$$Q = \sigma\,A\,T^4 \tag{2.26}$$

A blackbody can be defined as a perfect absorber and emitter of radiation (Duffie & Beckman, 2013: 139). Irrespective of the wavelengths or directions of the radiation that strikes the surface of the blackbody, the latter will absorb all of the incident radiation. Moreover, a blackbody emits more energy than any other surface for a given wavelength and

temperature. In addition, a blackbody is considered to be a diffuse emitter, that is, the radiation emitted from a blackbody is independent of direction (Bergman *et al*., 2011: 782).

2.4.4 Radiation shape factor

When determining the rate of radiative heat transfer between two surfaces, it is crucial to consider their geometric configurations, besides their radiation properties and temperatures. The impact of geometry on radiative heat transfer can be expressed in terms of the radiation shape factor (Goswami, Kreith & Kreider, 2000: 20). The latter is also commonly referred to as view factor, angle factor or configuration factor (Holman, 2010: 389).

The view factor ($F_{1\text{-}2}$) between any two given surfaces, *1* and *2*, can be defined as the fraction of radiation which leaves surface *1* that reaches surface 2 (Bergman *et al*., 2011: 862). The view factor can be expressed as follows (Maor & Appelbaum, 2012: 1702):

$$F_{1-2} = \frac{Radiation\ leaving\ \ surface\ 1,\ \ intercepted\ by\ surface\ 2}{Total\ radiation\ leaving\ surface\ 1} \qquad (2.27)$$

Different radiation shape factor correlations exist for different geometries. In the context of this research, the correlation which is required is that of 2 parallel and equal rectangles, since a solar chimney comprises of a rectangular glass cover which is parallel to an absorber wall of the same dimension, irrespective of whether the solar chimney is along the wall or on the roof of the building. Figure 2.11 shows the geometric configuration of a solar chimney.

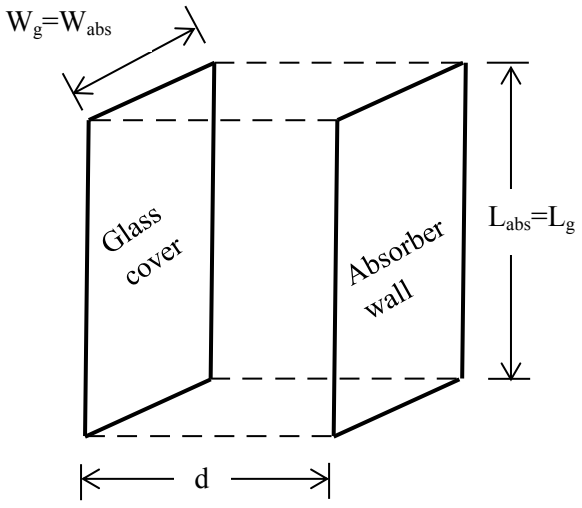

Figure 2.11: Geometric configuration of a solar chimney.

The view factor correlation for 2 parallel and equal rectangles is given by the following equation (Holman, 2010: 396):

$$F_{w-g} = \left(\frac{2}{\pi XY}\right)\{\ln\left[\frac{(1+X^2)(1+Y^2)}{1+X^2+Y^2}\right]^{\frac{1}{2}} + X(1+Y^2)^{\frac{1}{2}}\tan^{-1}[\frac{X}{(1+Y^2)^{\frac{1}{2}}}] + Y(1+X^2)^{\frac{1}{2}}\tan^{-1}[\frac{Y}{(1+X^2)^{\frac{1}{2}}}] - X\tan^{-1}X - Y\tan^{-1}Y\} \quad (2.28)$$

$$X = \frac{L_{abs}}{d} \quad (2.29)$$

$$Y = \frac{W_{abs}}{d} \quad (2.30)$$

2.5 Solar Chimneys

A solar chimney, as its name suggests, requires solar radiation for its basic function. As mentioned in Chapter 1, a solar chimney is considered as a passive cooling system which can be used for ventilation purposes. It typically consists of a glazed wall, also commonly termed as glass cover, and an absorber wall, also known as a collector, parallel to each other. The glass cover allows solar radiation to pass through and to get absorbed by the collector. Moreover, it also reduces convection heat losses to ambient air from the absorber wall (Lee *et al*., 2015: 656). On the other hand, the key function of an absorber wall is to absorb the largest amount possible of solar radiation striking its surface, re-emit as little as possible and to enable heat to be transferred efficiently to the working fluid (Goswami, Kreith & Kreider, 2000: 92). In solar chimneys, the working fluid is air which is found in the chimney channel between the glass cover and the absorber wall.

There are two types of solar chimneys, namely roof solar chimneys and wall solar chimneys (Zhai, Song & Wang, 2011: 3758). As their names suggest, roof solar chimneys are installed on the roofs of buildings and wall solar chimneys are installed along the walls of buildings.

2.5.1 Wall Solar Chimneys

A wall solar chimney is analogous to a Trombe wall (Ong & Chow, 2003: 1). The latter absorbs solar energy and re-circulates warm air to allow for passive heating of buildings. Nonetheless, the Trombe wall has a massive thermal wall compared to a solar chimney. In the case of a solar chimney, storage of heat behind the absorber wall is undesirable since the

purpose is to provide natural ventilation (Bansal *et al*., 2005: 1302). Furthermore, recirculation of warm air does not occur in a solar chimney since the warm air gets expelled out of the chimney. Figure 2.12 shows a solar chimney mounted along the walls of a building.

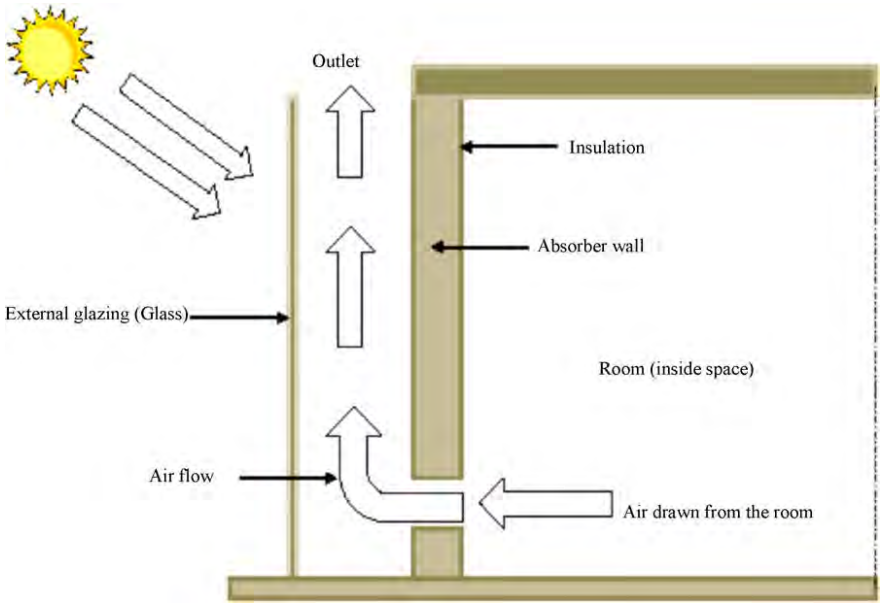

Figure 2.12: Schematic of a Wall Solar Chimney.
Source: Khanal & Lei (2011: 1813)

2.5.2 Roof Solar Chimneys

Roof solar chimneys can be easily integrated in buildings having gable roofs in order to provide thermal comfort in summer (Zhai, Song & Wang, 2011: 3759). Furthermore, Khedari, Hirunlabh and Bunnag (1997) investigated the effect of using a roof solar collector under hot climatic conditions in European style houses. The studies revealed that the amount of solar flux absorbed by the house was reduced and the natural ventilation provided by the solar chimney led to the enhancement of the thermal comfort inside the house. Figure 2.13 shows a solar chimney mounted on the roof of a building.

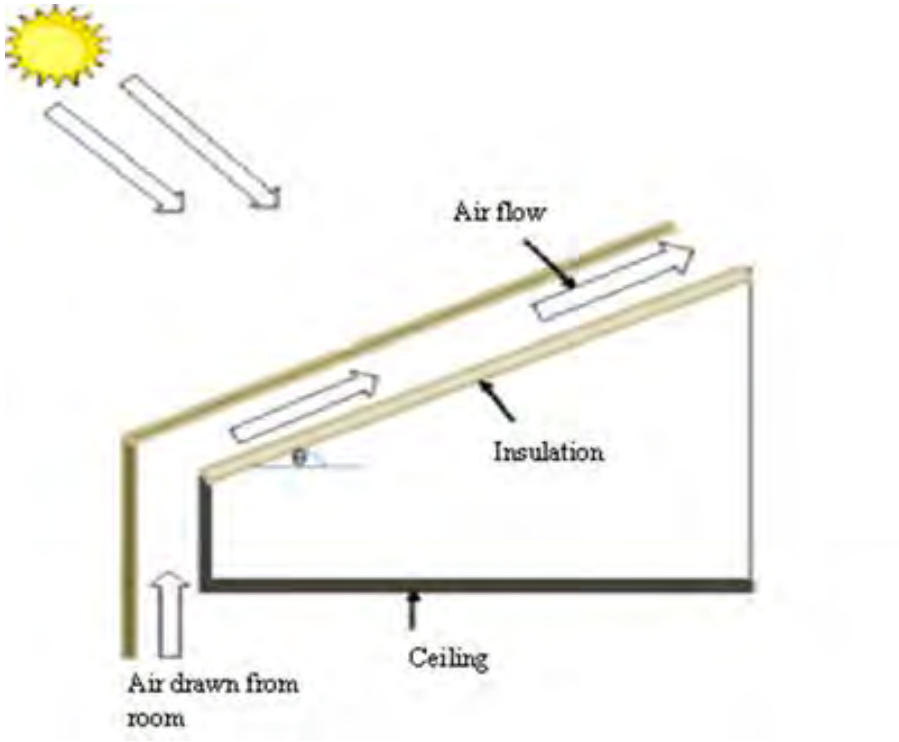

Figure 2.13: Schematic of a Roof Solar Chimney.
Source: Khanal & Lei (2011: 1817)

The absorber in a solar chimney maximises the heat energy gained from the sun, thus causing a significant temperature difference between the inside and the outside of the building (Khanal & Lei, 2011:1812). As can be observed from Figure 2.12 and Figure 2.13, solar radiation strikes the surface of the glass cover and gets transmitted to the absorber wall. The temperature of air inside the chimney channel increases as it gains heat mainly from the absorber wall via convection; thus causing a temperature gradient between the air inside the chimney channel and the air at the inlet of the solar chimney. This temperature gradient results in a density difference which in turn leads to a pressure difference between the channel and the inlet of the solar chimney, thereby causing hot air to get expelled out of the chimney and colder air to be drawn from the adjacent room. This process repeats itself and in this way, natural ventilation occurs in the room due to the solar chimney.

2.5.3 Mathematical modelling

It has been stated by Goswami, Kreith & Kreider (2000: 14) that solar energy is the most abundant permanent source of energy on earth. The concept of a solar chimney has been receiving a lot of attention globally since its operation is based on solar radiation and thus contributes to a reduction in GHG emissions. Numerous experimental and numerical studies have been carried out in order to model the performance of both wall-mounted and roof-mounted solar chimneys.

A steady-state mathematical model was developed by Bansal, Mathur and Bhandari (1993) to investigate numerically the effects of ambient temperature and solar radiation on air flow rate in a solar chimney. The mathematical model was solved using an iterative procedure. Gan and Riffat (1998) carried out a numerical study on the performance of a solar chimney based on Computational Fluid Dynamics (CFD) modelling techniques. They compared the results obtained from their numerical simulation with experimental data in order to verify their model. Hirunlabh et al. (1999) proposed a mathematical model in order to study the performance of a metallic solar wall (identical to the solar chimney concept) under the climatic conditions of Bangkok in Thailand. They used the Newton-Raphson method to solve the model and they also carried out experiments on the metallic solar wall in order to compare the numerical results with the experimental results.

AboulNaga and Abdrabboh (2000) performed a theoretical investigation on a combined wall-roof solar chimney so as to predict the ventilation rate and to determine the optimum height of the wall of the solar chimney. They made use of a spreadsheet computer program together with the ACTION Psychrometrics Software in order to study the performance of the solar chimney. Afonso and Oliveira (2000) also developed a thermal model which combines heat transfer equations with natural ventilation flow equations for the simulation of solar chimneys. They used a finite difference method in order to solve for their mathematical model. Moreover, they carried out experiments on solar chimneys in the region of Porto, in Portugal, so as to compare the results obtained from their model with values obtained experimentally.

Ong (2003) proposed a mathematical model for a solar chimney based on steady-state heat transfer. The equations developed in their model were solved using the matrix inversion method in order to predict the performance of a solar chimney. This model was further used by Ong and Chow (2003) to study the effects of air gap and solar radiation intensity on the

performance of solar chimneys. They also carried out experiments on a 2 m high by 0.45 m wide physical model of a solar chimney so as to validate the mathematical model.

A mathematical model based on one-dimensional steady-state heat transfer was developed by Bansal et al. (2005) for the prediction of airflow velocity inside a solar chimney. They used the C++ programming software so as to solve the equations developed in their model. In order to verify their model, they carried out experiments on a physical model of a solar chimney. Additionally, a model similar to the one developed by Ong (2003) was used by Mathur et al. (2006) to investigate the effects of air gap and height of absorber wall on the ventilation rate. They also carried out experiments on a physical model of a solar chimney and they compared their experimental results with values obtained from the steady-state mathematical model. The same model was further used by Mathur, Mathur and Anupma (2006). They used a computer program (the specific name of the software was not mentioned) in order to study the performance of solar chimneys at different inclination angles. They also performed experiments on a physical model of a solar chimney in order to compare the numerical results with those obtained experimentally.

Miyazaki, Akisawa and Kashiwagi (2006) carried out an investigation on the use of solar chimneys for minimizing the thermal load in office buildings under Japanese climatic conditions. They used CFD modelling techniques in conjunction with the C programming software to calculate the heating and cooling loads. A physical model was also proposed by Marti-Herrero and Heras-Celemin (2007) to assess the thermal performance of a solar chimney under Mediterranean climatic conditions. This model was based on unsteady-state heat transfer, taking into account the thermal inertia of the solar chimney. The set of equations for this model was solved using an iterative procedure. Harris and Helwig (2007) studied numerically the effects of inclination angle and type of glazing on the ventilation rate by making use of CFD modelling techniques using the PHOENICS software.

A mathematical model was developed by Bassiouny and Koura (2008) based on heat transfer processes across the solar chimney system. The system of equations was solved iteratively in the FORTRAN computer program. Sakonidou et al. (2008) developed a mathematical model to establish the optimum tilt angle of a solar chimney for maximum ventilation rate. They used solar radiation data for the region of Serres, situated in Greece in their study and they made use of the FLUENT software to solve equations from their mathematical model. Lee and Strand (2009) used the EnergyPlus software to investigate numerically the effects of

chimney height, air gap, absorptance of absorber wall and transmittance of glass cover on the performance of solar chimneys under various climatic conditions.

Yan et al. (2011) used a steady-state mathematical model of a solar chimney to investigate numerically the effects of height and width of the absorber wall, intensity of solar radiation, air inlet velocity and ratio of outlet area to inlet area. They used the MATLAB programming software in order to solve the equations from the mathematical model.

Gontikaki et al. (2010) used the ESP-r building energy modelling program in order to optimize the design of a solar chimney integrated in a multi-storey building in the Netherlands. They also used experimental data to validate their model in ESP-r. Larbi and Hella (2013) investigated numerically the performance of solar chimneys using the FLUENT computer software. The location chosen for their numerical study was Adrar, located in the south west of Algeria. They used a steady-state mathematical model based on energy balance equations associated with the glass cover, absorber wall and air inside the channel of the solar chimney. DeBlois, Bilec and Schaefer (2013) also made use of the ESP-r software in order to simulate the thermal dynamics within a roof solar chimney under the climatic conditions of Pittsburgh, in the United States of America. Jianliu and Weihua (2013) developed a mathematical model of a solar chimney based on one-dimensional steady-state heat transfer across the system. They investigated numerically the effect of inclination angle and ratio between absorber height and air gap on the performance of solar chimneys under the climatic conditions of Nanjing in China. They implemented their mathematical model into the EnergyPlus program and they also performed experiments on a physical model of a solar chimney in order to compare the results obtained from their numerical simulation with experimental results.

Additionally, Khanal and Lei (2014) used a numerical simulation to investigate the air flow pattern due to natural convection inside a solar chimney. The latter was modelled as a disproportionately heated air channel, with homogeneous heating on the absorber wall and the glass cover. Al-Kayiem, Sreejaya and Gilani (2014) also used the MATLAB program to investigate numerically the effect of chimney height and area of absorber wall on the performance of a roof-mounted solar chimney. They used a mathematical model based on steady-state heat transfer, similar to the model used by Ong (2003) and Mathur et al. (2006).

Imran, Jalil and Ahmed (2015) investigated both numerically and experimentally the performance of solar chimneys under the climatic conditions of Iraq. They developed a two-

dimensional steady-state mathematical model which was solved in the FORTRAN computer program. Suárez-López et al. (2015) developed a three-dimensional mathematical model for a solar chimney in order to investigate the dynamic and thermal performance of the fluid in a solar chimney. They used CFD modelling techniques within the FLUENT software to solve their mathematic model.

2.5.4 Parameters affecting the performance of solar chimneys

Various studies have been carried out in order to investigate the parameters which affect the performance of a solar chimney. Some of the factors which have been examined experimentally and through mathematical modelling include solar radiation level, air gap between glass cover and absorber wall, height of solar chimney, inclination angle and type of glazing.

2.5.4.1 Intensity of solar radiation

The intensity of solar radiation is the driving force in the design of a solar chimney and as such, it is the most determining factor in the performance of the solar chimney (Gontikaki *et al*., 2010). When solar radiation level increases, the temperature of air inside the solar chimney increases, leading to a higher stack pressure which causes the flow rate of air to increase (Chen *et al*., 2003: 902).

Bansal, Mathur and Bhandari (1993) investigated the effect of solar radiation on ventilation rate. A numerical analysis involving an iterative procedure was performed and it was found that the ventilation rate increases with increase in solar radiation. Chen et al. (2003) studied the effect of heat flux on ventilation rate through experimental investigations and they compared their experimental results with predicted results from numerical modelling of solar chimneys based on heat balance analysis. The heat flux was varied between 200 W/m^2 to 600 W/m^2 and an increase in air flow rate was observed as the heat flux was increased. Nevertheless, the values for the air flow rate were lower than those predicted from the numerical simulation but the same trend was observed; the numerical analysis also showed an increase in ventilation rate with an increase in the intensity of solar radiation.

The effect of the intensity of solar radiation on ventilation rate was also analysed by Ong (2003). He used a mathematical model in order to generate his results which revealed that the mass flow rate of air increases with an increase in the solar radiation level. Mathur et al. (2006) carried out a numerical study on solar chimneys, involving the use of the C++ computer programming software, which showed that the ventilation rate increases linearly

with increase in the intensity of solar radiation. Yan et al. (2011) used the MATLAB programming software to conduct a numerical analysis on the performance of solar chimneys. They found that an increase in solar radiation intensity causes an increase in the ventilation rate. Jianliu and Weihua (2013) studied the performance of solar chimneys using the EnergyPlus program. The results from their numerical study revealed that the maximum ventilation rate occurs when the intensity of solar radiation is at its peak.

Suárez-López et al. (2015) investigated the effect of solar radiation on the performance of solar chimneys using CFD techniques. They found that the mass flow rate of air increases with an increase in the intensity of solar radiation. The same trend was also observed from numerical studies carried out using the FORTRAN computer program by Imran, Jalil and Ahmed (2015) and Bassiouny and Koura (2008). In both studies, it was found that an increase in the intensity of solar radiation causes the ventilation rate to increase. Al-Kayiem, Sreejaya & Gilani (2014) also observed the same trend when they used the MATLAB program to investigate the performance of solar chimneys.

2.5.4.2 Air gap between absorber wall and glass cover

A numerical study using CFD techniques carried out by Gan and Riffat (1998) revealed that air flow rate increased as the air gap was increased from 0.1 to 0.2 m but a further increase in the air gap actually resulted in a decrease in the flow rate of air. Air flow was observed to be upwards along the solar chimney for small air gaps but for a high air gap (0.5 m), the air flow was only in the upward direction near the heated absorber wall due to buoyancy effects and it was in the downward direction along the middle of the solar chimney. This was attributed to the fact that reverse flow occurs for air gaps which are wider than the two boundary layers, namely the glass cover and the absorber wall.

Hirunlabh et al. (1999) also investigated the effect of air gap on ventilation rate, both experimentally and numerically. They found that an increase in air gap causes the ventilation rate to increase. The difference between their experimental and their simulated results were approximately 10 %.

The effect of air gap on ventilation rate was also investigated both numerically and experimentally by Chen et al. (2003). The air gap was varied from 0.1 to 0.6 m at a solar radiation level of 400 W/m^2. It was found that the air flow rate increased with increasing air gap but no optimum air gap could be determined from the experimental study. Moreover, reverse flow near the outlet of the chimney was observed for an air gap of 0.3 m. As the air

gap was increased from 0.3 to 0.6 m, reverse flow was observed further down the solar chimney. However, the increase in reverse flow did not result in a decrease in air flow rate since the chimney inlet size was increased simultaneously and thus, pressure loss was reduced at the inlet. Nevertheless, if the chimney inlet size remained constant while the air gap was increased, an optimum air gap could have been observed. The numerical analysis also showed that the ventilation rate increases continuously with increase in the air gap, with no optimum air gap being observed.

A numerical study by Mathur et al. (2006) also indicated that air flow rate increases as air gap increases. The C++ program was used for the simulation of the solar chimneys. The air gap was varied between 0.1 to 0.3 m at solar radiation levels of 300, 500 and 700 W/m^2. For each solar radiation level, it was found that an increase in air gap caused the air flow rate to increase. This was attributed to the fact that a wider air gap results in a decrease in the percentage of flow restricted due to boundary layer and this caused an increase in the air velocity. It was also observed that an increase in the air gap causes the ventilation rate to increase in a numerical investigation carried out by Imran, Jalil and Ahmed (2015). They used the FORTRAN program to run their simulations. Jing, Chen and Li (2015) carried out an experimental study to investigate the performance of solar chimneys. They compared their experimental results with numerical prediction methods from literature. Both their experimental and numerical results showed that the ventilation rate increases continuously with an increase in the air gap. Nonetheless, they found that the numerical method actually over predicts the ventilation rate, especially for solar chimneys with large air gaps.

2.5.4.3 Chimney height

The effect of chimney height on ventilation rate was investigated by Hirunlabh et al. (1999) based on an experimental and numerical analysis on a metallic solar wall (identical to the solar chimney. Their results showed that the ventilation rate increases as the height of the metallic solar wall increases. An experimental and numerical study carried out by Afonso and Oliveira (2000) showed that an increase in chimney height resulted in an increase in the ventilation rate. The chimney height was varied between 0.5 to 3 m. Ong (2003) also conducted a numerical analysis on the performance of solar chimneys and his results revealed that the mass flow rate of air increases with an increase in the height of the chimney.

Lee and Strand (2009) studied numerically the effect of chimney height on the performance of solar chimneys using the EnergyPlus program. They claimed that the ventilation rate

increases with an increase in chimney height due to the fact that a longer path is obtained for convective heat transfer between the absorber and the air stream. It was also observed in a numerical study conducted by Maerefat and Haghighi (2010) that an increase in chimney height causes the ventilation rate to increase due to the fact that the surface area of the absorber wall increases with an increase in the height of the chimney. They made use of a mathematic model based on the one developed by Ong (2003). Al-Kayiem, Sreejaya & Gilani (2014) used the MATLAB computer program to investigate the effect of chimney on the performance of a roof-mounted solar chimney. Their results showed that the ventilation rate increases as the height of the chimney increases.

2.5.4.4 Angle of inclination

The effect of inclination angle on the performance of solar chimneys was investigated both experimentally and numerically by Chen et al. (2003). Their results showed that an inclination angle of 45° results in maximum air flow rate for a solar chimney of height 1.5 m with a 0.2 m air gap. Harris and Helwig (2007) studied the effect of inclination angle on air flow rate for Edinburg in Scotland at latitude of 52°, using CFD modelling techniques. Their results showed that maximum flow rate of air could be achieved with an inclination angle of 67.5° with the horizontal. Moreover, it has been claimed that the effect of inclination angle on ventilation rate is extremely dependent on the latitude of the location (Gontikaki *et al*., 2010).

Mathur, Mathur and Anupma (2006) wrote a computer program to study the performance of solar chimneys in Jaipur in India at latitude of 27° and they found that an inclination angle of 45° gave the highest air flow rates while inclination angles of 30° and 60° gave fairly similar results. Table 2.2 shows the optimum angle of inclination of solar chimneys for different latitudes.

Table 2.2: Variation of optimum angle of inclination with latitude.
Source: Mathur, Mathur & Anupma (2006: 1160)

Latitude (°)	Optimum inclination of solar chimney (°)
0	55
5	50
10	50
15	50
20	45
25	45
30	45
35	50
40	50
45	55
50	55
55	60
60	60
65	60

Moreover, the effect of inclination angle on the performance of solar chimneys was also investigated by Imran, Jalil and Ahmed (2015) under the climatic conditions of Iraq (of latitude 33.3°). They proposed both an experimental and numerical model for a solar chimney. From their numerical model, it was found that an inclination angle of 60° gave the highest rate of ventilation. Additionally, another numerical study conducted by Jianliu and Weihua (2013) indicated that the optimum inclination angle for maximum ventilation rate is 45° in Nanjing, with a latitude of 32°. They performed the numerical simulation in the EnergyPlus program in order to predict the performance of the solar chimneys.

2.5.4.5 Type of glazing

The effect of glazing on the performance of solar chimneys was investigated numerically by Gan and Riffat (1998) based on CFD modelling techniques. Their results showed that double glazing results in higher ventilation rates. The study also revealed that for low intensities of solar radiation, the effect of glazing was much more significant than for high intensities of solar radiation. In fact, it was found that for solar radiation levels of 167 W/m^2 and 124 W/m^2, the ventilation rates decreased by 11 % and 35 % respectively, when double glazing was replaced by single glazing. Furthermore, the effect of glazing on the performance of solar chimneys was also investigated by Harris and Helwig (2007) using CFD modelling techniques. The results revealed that double glazing gives a slightly better performance than

single glazing. Nonetheless, they found that it was not cost effective to use double glazing since the improvement was not significant enough.

Chapter 3

METHODOLOGY

Numerous experimental and numerical studies have been carried on solar chimneys due to their attractiveness as a means of providing natural ventilation in buildings. Various numerical investigations conducted on solar chimneys were discussed in Chapter 2. According to Khanal and Lei (2011: 1819), some contradictory observations on the performance of solar chimneys have been reported in literature. Consequently, it is essential to carry out more research on solar chimneys in order to understand their performance better. This chapter deals with the methodology adopted for this study. A mathematical model for the solar chimney was developed, based on models which have been generated from previous studies on solar chimneys. A program was then written in the MATLAB computer software in order to solve the system of equations from the mathematical model, thereby investigating numerically the thermal performance of various configurations of solar chimneys.

3.1 Design of solar chimneys

A solar chimney needs to be designed such that the absorption of solar radiation is maximised in an attempt to maximise the ventilation rate (Bansal, Mathur & Bhandari, 1993: 374). A solar chimney typically consists of four walls, with one wall made of glass (commonly referred to as the glass cover), one wall painted black (known as the absorber wall) and the remaining two walls, together with the glass cover and the absorber wall, form a channel through which air rises due to natural convection (Ong & Chow, 2003: 3). The glass cover is parallel to the absorber wall and the distance between these two boundaries is referred to as the air gap.

There are many parameters to be considered when designing a solar chimney, including height of the chimney, air gap, type of absorber and glazing, insulation and thermal mass in the solar chimney (Harris & Helwig, 2007: 136). According to Bansal, Mathur & Bhandari (1993: 374), the temperature difference between the inlet and the outlet of the solar chimney is a critical design parameter. Solar chimneys can either be roof-mounted or wall-mounted. The model for the wall-mounted solar chimney used in this research is depicted in Figure 3.1. The temperatures of the various components of the solar chimney are also given in Figure 3.1.

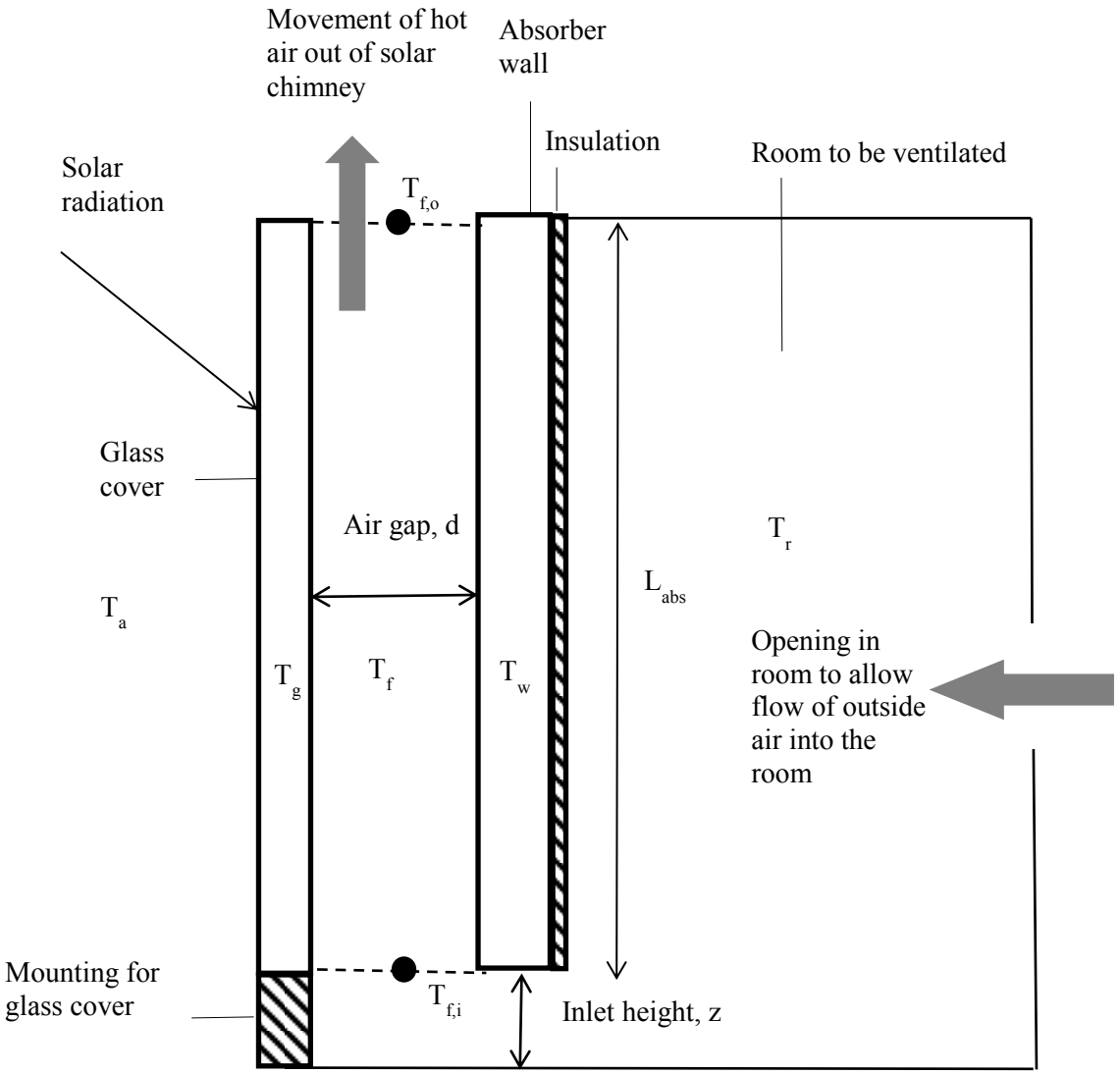

Figure 3.1: Solar chimney mounted on a wall.

The wall-mounted solar chimney, as illustrated by Figure 3.1, is vertical, hence its inclination with the horizontal is 90°. The glass cover is mounted on a concrete structure, such that it is of the same height as the absorber wall. Both the glass cover and the absorber wall are of the same dimensions; having length and width of 2 m by 1 m respectively. The air gap is 0.25 m while the thickness of insulation behind the absorber wall is 0.1 m. The inlet height to the solar chimney is 0.1 m and the room which needs to be ventilated has dimension of 3 m by 3m by 3 m.

As solar radiation strikes the surface of the glass cover, it gets transmitted to the absorber wall. The latter, being a black body, captures the solar radiation and converts it into heat, which is then transferred via convection to the air stream within the channel of the solar chimney. As this air gets heated up, its temperature increases and it expands, thus causing a

density difference between the air inside the channel of the solar chimney and air at the inlet of the solar chimney. This density difference results in a pressure difference, thus causing hot air to be expelled out of the solar chimney and causing cold air to be drawn through the inlet of the solar chimney. This is a continuous process, as long as solar radiation is available, and hence, ventilation of the room occurs naturally.

On the other hand, the roof-solar chimney was inclined at 34° to the horizontal but it had the same dimension as the vertical wall-mounted solar chimney. The roof-mounted solar chimney works on the same principle as the wall-mounted solar chimney and is illustrated in Figure 3.2.

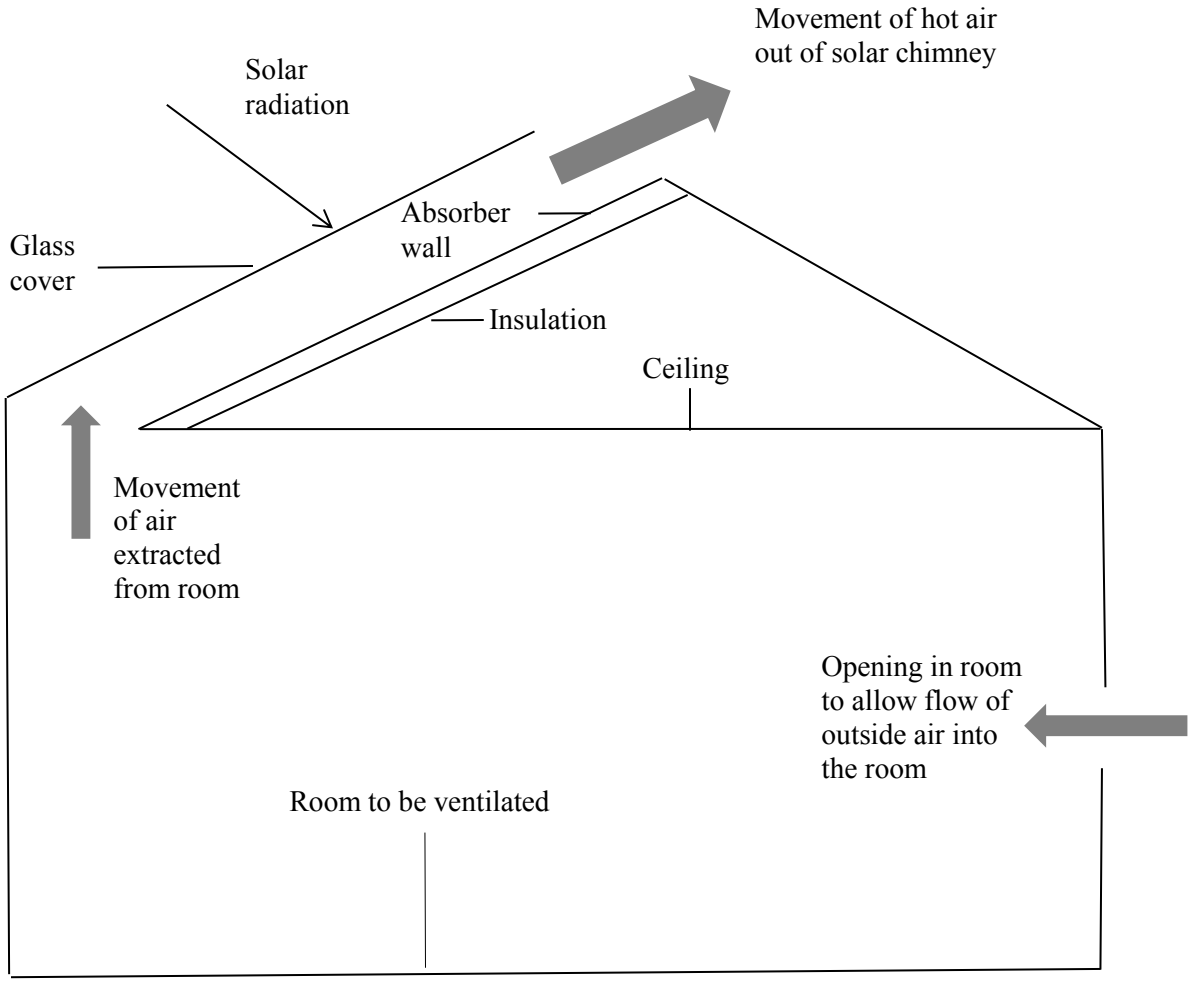

Figure 3.2: Solar chimney mounted on a roof.

3.1.1 Design parameters of solar chimneys

a) Location

In the context of this research, the specific location considered was Stellenbosch, a town located in the Western Cape province of South Africa, situated in the southern hemisphere. The latitude and longitude of Stellenbosch are 33° 56' south and 18° 46' east respectively. The location of Stellenbosch is shown in Figure 3.3.

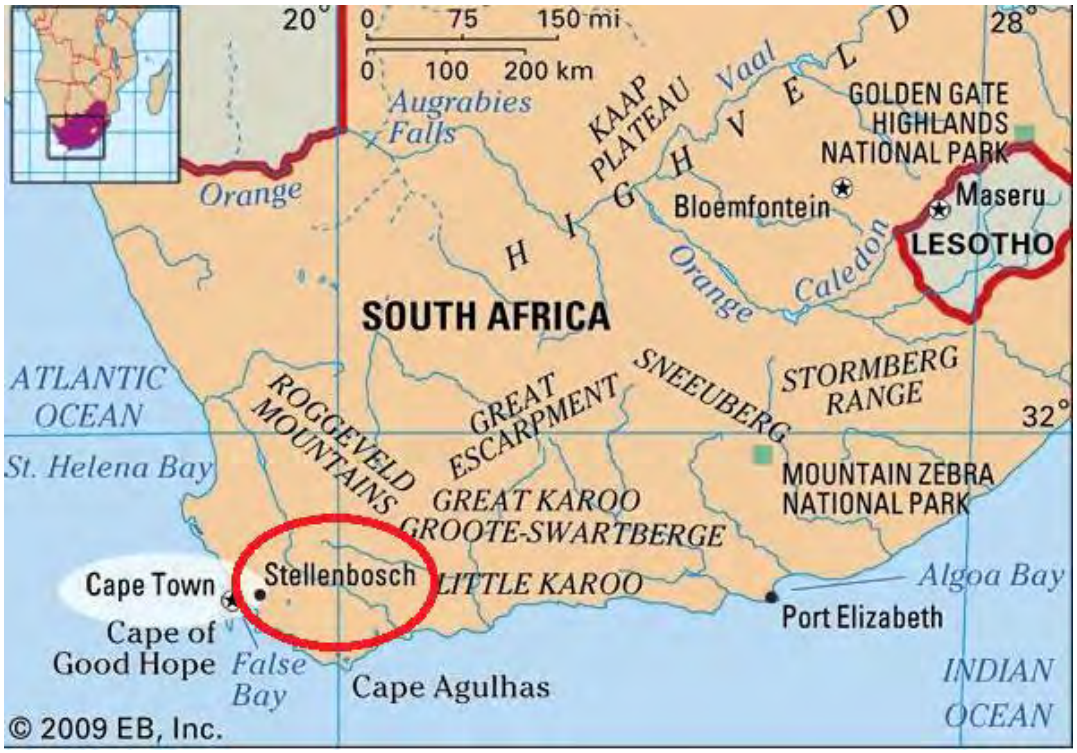

Figure 3.3: Location of Stellenbosch.
Source: Encyclopaedia Britannica (2015)

b) Orientation of solar collectors

According to Duffie and Beckman (2013: 114), solar collectors should be orientated towards the equator for maximum absorption of solar radiation, that is, solar collectors in the northern hemisphere should be south facing while those in the southern hemisphere should be north facing. Consequently, in this study, the solar chimneys were considered to be north facing in order to capture maximum solar radiation during the day.

c) Inclination angles

The inclination angles investigated in this study for the roof-mounted solar chimney are 30°, 34°, 45°, 60° and 75° while for the wall-mounted solar chimney, the inclination angle was 90°. Numerous studies have revealed the relationship which exists between the optimum tilt angle of a solar collector and the latitude of the location (ϕ), as shown in Table 3.1.

Table 3.1: Optimum tilt angle for solar collectors.
Source: Adapted from Yadav & Chandel (2013: 507)

Source	Optimum tilt angle of solar collector
Duffie & Beckman (2013)	$\phi \pm (10° \text{ to } 15°)$
Heywood (1971)	$\phi - 10°$
Lunde (1980); Garg (1982)	$\phi \pm 15°$
Chinnery (1971); Kern & Harris (1975)	$\phi + 10°$
Löf and Tybout (1973)	$\phi + (10° \text{ to } 30°)$
Hottel (1954); Yellot (1973)	$\phi + 20°$
Elminir et al. (2006)	$(\phi + 15°) \pm 15°$

'+' refers to the winter season and '-' refers to the summer season

Different correlations were obtained from different sources and it can be observed that the optimum tilt angle is different for the winter and summer seasons. However, in this investigation, the solar chimneys have a fixed tilt angle throughout the whole year and it is essential to choose an inclination angle which gives the maximum solar radiation absorption throughout the whole year. This tilt angle needs to be used as the reference angle for the purpose of comparison with other inclination angles. It has been stated by Duffie and Beckman (2013: 114) that a solar collector should be inclined at an angle equal to the latitude of the location for maximum annual absorption of solar radiation. Consequently, an angle of 34° was chosen as the reference angle for the roof-mounted solar chimney as this represents the latitude of Stellenbosch.

d) Dimensions of different components of the solar chimney

The air gap between the absorber wall and the glass wall of the solar chimney was varied from 0.15 to 0.75 m in order to investigate the effect of air gap on the thermal performance of the solar chimneys. An air gap of 0.25 m was chosen as the reference air gap.

The dimensions of the absorber wall and the glass cover were the same for both the roof and the wall solar chimneys for the purpose of comparison. The reference lengths and widths of the solar chimneys were 2 m and 1 m respectively, as mentioned earlier. The chimney height (which is equal to the length of the absorber wall and the glass cover) was varied from 0.5 m to 3 m. The thickness of the glass cover was 4 mm while the thickness of the wall insulation was 0.1 m. Moreover, the area of the inlet of the solar chimney was assumed to cover the entire base of the solar chimney and thus, the inlet area was given as follows:

$$A_i = d * W_{abs} \quad (3.1)$$

The outlet area was assumed to be equal to the inlet area and consequently, A_r, the ratio of the outlet area to the inlet area was equal to 1. The design parameters of the wall-mounted and roof-mounted solar chimneys that were used for the reference scenarios are given in Table 3.2 and the various design parameters investigated in this study are given in Table 3.3.

Table 3.2: Design parameters of solar chimneys for reference scenarios.

Design parameter	**Wall Solar Chimney**	**Roof Solar Chimney**
Orientation	North facing	North facing
Inclination angle	Vertical (90°)	34°
Dimension of absorber wall	2 m by 1 m	2 m by 1 m
Dimension of glass cover	2 m by 1 m	2 m by 1 m
Thickness of glass cover	4 mm	4 mm
Thickness of wall insulation	0.1 m	0.1 m
Air gap	0.25 m	0.25 m
Ratio of outlet area to inlet area	1	1
Dimension of room to be ventilated	3 m by 3 m by 3 m	3 m by 3 m by 3 m

Table 3.3: Parameters investigated in this study.

Design parameter	**Wall Solar Chimney**		**Roof Solar Chimney**	
	Design Value	Range Studied	Design Value	Range Studied
Inclination angle	90°	90°	34°	30° to 75°
Air gap	0.25 m	0.15 m to 0.75 m	0.25 m	0.15 m to 0.75 m
Chimney height	1 m	0.5 m to 3 m	1 m	0.5 m to 3 m

3.2 Mathematical model

In order to investigate numerically the performance of solar chimneys, various computer programs have been used, namely the C program (Miyazaki, Akisawa & Kashiwagi, 2006), C++ (Mathur *et al*., 2006), FORTRAN (Bassiouny & Koura, 2008; Imran, Jalil & Ahmed, 2015), ESP-r (Gontikaki *et al*., 2010; DeBlois, Bilec & Schaefer, 2013), EnergyPlus (Lee & Strand, 2009; Jianliu & Weihua, 2013) and MATLAB (Yan *et al*., 2011; Al-Kayiem, Sreejaya & Gilani, 2014). In addition, CFD modelling techniques were used by Harris and Helwig (2007) in the PHOENICS computer software and by Suárez-López et al. (2015) within the FLUENT software. Sakonidou et al. (2008) and Larbi and Hella (2013) also used the FLUENT software for the numerical investigation on solar chimneys.

In this research, the MATLAB program was used in order to assess the thermal performance of various configurations of solar chimneys. MATLAB was chosen for this study since it is

one of the most commonly used programming languages for performing scientific and engineering calculations (Hoffbeck, Sarwar & Rix, 2001: 77; Sen & Shaykhian, 2009: 1005; Jaluria, 2011: 5; Moore, 2012: 1).

The mathematical model which was used in this study is based on similar models used by Ong (2003); Ong and Chow (2003); Mathur et al. (2006); Larbi and Hella (2013); Al-Kayiem, Sreejaya and Gilani (2014). In order to develop a mathematical model for a solar chimney, the energy balances on three components were analysed, namely the glass cover, the absorber wall and the air inside the channel of the solar chimney. The mass balance on the air stream was also computed. Before setting up the energy and mass balances, it is important to highlight the assumptions which were made in this investigation.

3.2.1 Assumptions

The following assumptions were made for this study:

a) Steady-state conditions were assumed over the whole system.
b) Heat transfer in only one-dimension was assumed for all the heat transfer processes across the system.
c) The temperature of air at the inlet of the solar chimney was assumed to be equal to the adjacent room temperature and also equal to the ambient temperature, that is, $T_{f,i}=T_r=T_a$.

3.2.2 Energy balance equations

The same mathematical model applies for both the wall-mounted and the roof-mounted solar chimneys. Figure 3.4 shows the overall thermal network for the solar chimneys. Solar radiation strikes the surface of the glass cover and gets transmitted to the absorber wall. Heat is lost through convection from the top of the glass cover to the surroundings and by conduction from the insulted absorber wall to the adjacent room. Heat is also transferred via radiation from the absorber wall to the glass cover and via convection both from the glass cover to the air stream and from the absorber wall to the air stream. Taking into account the assumptions which have been discussed earlier and the heat transfer mechanisms which occur across the solar chimneys, the energy balance equations were developed.

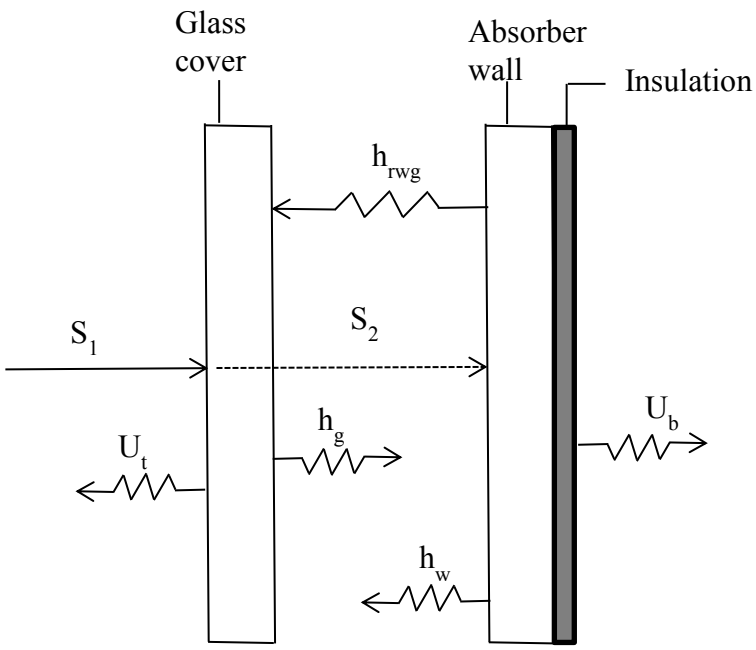

Figure 3.4: Overall thermal network for solar chimneys.

3.2.2.1 Energy Balance on glass cover

The flow of heat to the glass cover is the sum of two components, namely heat from solar radiation and radiative heat from the absorber wall while the flow of heat from the glass cover is the sum of the heat loss to the surroundings and the convective heat loss to the air inside the channel of the solar chimney. Figure 3.5 shows the flow of heat to and from the glass cover.

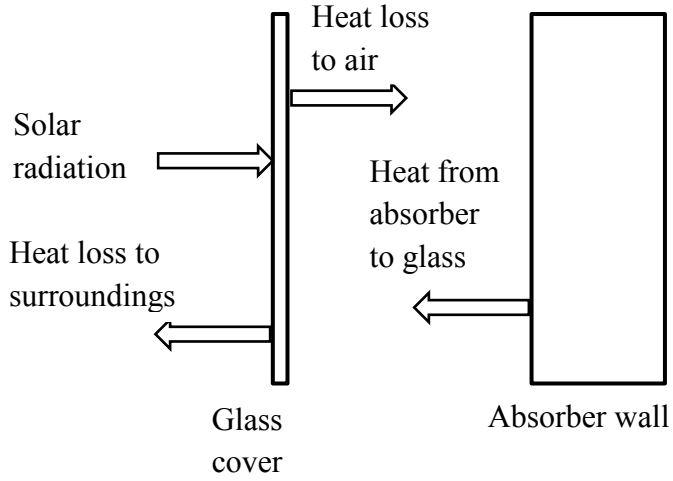

Figure 3.5: Energy balance on glass cover.

The energy balance for the glass cover can thus be given by:

$$S_1 A_g + h_{rwg} A_w (T_w - T_g) = h_g A_g (T_g - T_f) + U_t A_g (T_g - T_a) \qquad (3.2)$$

3.2.2.2 Energy Balance on absorber wall

The heat flow to the absorber wall comes from solar radiation which gets transmitted from the glass cover. On the other hand, the heat flow from the absorber wall comprises of 3 elements; convective heat to the air stream, radiative heat to the glass cover and conductive heat to the adjacent room, as can be depicted in Figure 3.6.

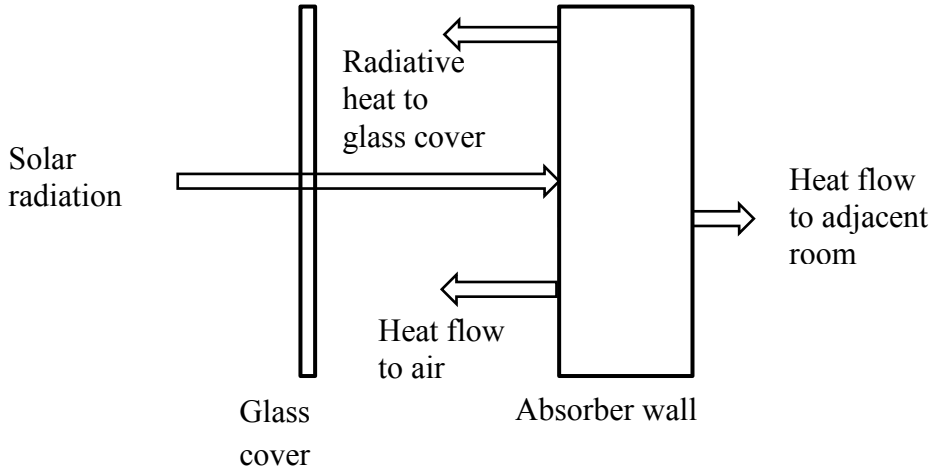

Figure 3.6: Energy balance on absorber wall

The energy balance on the absorber wall can be given as:

$$S_2 A_w = h_w A_w (T_w - T_f) + h_{rwg} A_w (T_w - T_g) + U_b A_w (T_w - T_r) \qquad (3.3)$$

3.2.2.3 Energy balance on air stream

The heat gained (q) by the air stream is the sum of the convective heat from the glass cover and the convective heat from the absorber wall. Figure 3.7 illustrates the heat gained by the air inside the solar chimney.

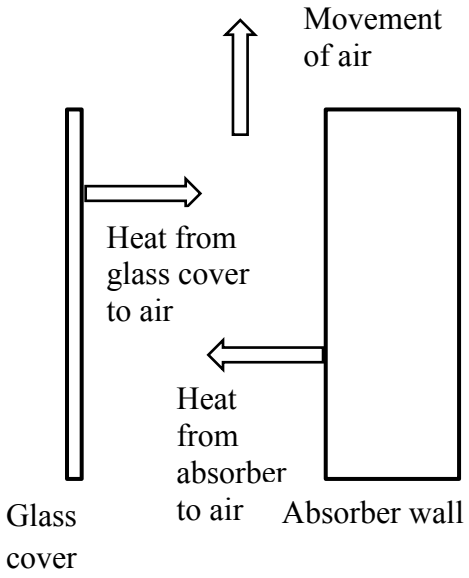

Figure 3.7: Energy balance on air stream

The energy balance equation for the air between the glass cover and absorber wall is given by:

$$q = h_w A_w (T_w - T_f) + h_g A_g (T_g - T_f) \tag{3.4}$$

The heat transferred to the air stream can also be written as:

$$q = mc_{f1}(T_{f,o} - T_{f,i}) \tag{3.5}$$

The temperature at the inlet of the solar chimney is assumed to be the same as the room temperature. The following correlation can then be used to estimate the mean air temperature of the air stream.

$$T_f = \gamma_{MTA} T_{f,o} + (1 - \gamma_{MTA}) T_{f,i} \tag{3.6}$$

The value for the constant γ_{MTA} was found to be 0.75 from experimental observations (Hirunlabh *et al*., 1999: 113) while Ong and Chow (2003: 3) determined the value of γ_{MTA}

experimentally and it was found to be 0.74. In the context of this research, the value for the constant will be taken as 0.74 as this has been commonly used in previous studies on solar chimneys.

Using equation (3.6) and making $T_{f,o}$ the subject of formula and assuming $T_{f,i} = T_r$, the following equation is obtained:

$$T_{f,o} = \frac{\left[T_f - (1 - \gamma_{MTA})T_r\right]}{\gamma_{MTA}} \tag{3.7}$$

By substituting equation (3.7) into equation (3.5), the following equation is obtained:

$$q = \frac{mc_{f1}\left[T_f - T_r\right]}{\gamma_{MTA}} \tag{3.8}$$

Substitution of equation (3.8) into equation (3.4) generates the following equation:

$$\frac{\left[-mc_{f1}T_r\right]}{\gamma_{MTA}} = h_w A_w T_w + h_g A_g T_g - T_f \left[\frac{\left(mc_{f1}\right)}{\gamma_{MTA}} + h_w A_w + h_g A_g\right] \tag{3.9}$$

Equations (3.2), (3.3) and (3.9) can be re-arranged as follows to obtain the following set of three equations:

$$\begin{aligned}(h_{rwg}A_w + h_g A_g + U_t A_g)\, T_g \; - \left(h_g A_g\right)T_f - \left(h_{rwg}A_w\right)T_w \\ = S_1 A_g + U_t A_g T_a\end{aligned} \tag{3.10}$$

$$-h_{rwg}A_w T_g - h_w A_w T_f + \left(h_w A_w + h_{rwg}A_w + U_b A_w\right)T_w = S_2 A_w + U_b A_w T_r \tag{3.11}$$

$$h_g A_g T_g - \left[h_g A_g + h_w A_w + \frac{mC_{f1}}{\gamma_{MTA}}\right]T_f \; + h_w A_w T_w \; = -\left(\frac{mC_{f1}}{\gamma_{MTA}}\right)T_r \tag{3.12}$$

3.2.2.4 Mass balance

The mass flow rate of the air stream in a solar chimney can be determined as follows (Mathur, Mathur & Anupma, 2006):

$$m = C_d \rho_{f1} A_{out} \sqrt{\frac{2gL \sin\beta \left(T_f - T_r\right)}{(1 + A_r^2) T_r}} \tag{3.13}$$

$$A_r = \frac{A_{out}}{A_{in}} \tag{3.14}$$

Equations (3.10), (3.11), (3.12) and (3.13) were then used to solve for temperatures of the glass cover, absorber wall and air stream and also to determine the mass flow rate of air. The step by step procedure of how this was done is described below.

3.2.3 Solution Procedure

In order to solve the mathematical model which has been developed in this investigation, a program was written in MATLAB. The detailed procedure of how this was done is described below.

3.2.3.1 Astronomical parameters

The geographical coordinates of Stellenbosch were entered in MATLAB. However, the latitude was assigned a negative value, accounting for the fact that Stellenbosch is located in the southern hemisphere since a location north of the equator is conventionally assigned a positive value while a location south of the equator is assigned a negative value (Garg & Prakash, 2000: 9).

The standard meridian for the local time zone was calculated as follows (Duffie & Beckman, 2013: 11):

$$L_{standard} = Time\ difference\ between\ South\ African\ time\ and\ GM\ time\ * 15 \tag{3.15}$$
$$= 2 * 15 = 30°$$

Equations (2.1) to (2.8) were then used to calculate the declination angle, solar time, hour angle, sunset hour angle and solar zenith angle. According to Mohammadi and Khorasanizadeh (2015: 508), the azimuth angle is 180° for north-facing surfaces and as reported by Duffie and Beckman (2013: 24), the optimum surface azimuth angle for solar

collectors in the southern hemisphere is 180°. Consequently, the surface azimuth angle was assumed to be 180° in the context of this research since Stellenbosch is located in the southern hemisphere and the solar chimneys are in the north-facing direction. The angle of incidence of beam radiation on a surface was then calculated using equation (2.9). According to Popoola and Burnier (2014: 54), the albedo of a surface is 0.2 if the annual temperature is greater than 0 °C and 0.7 if the yearly temperature is lower than -5 °C. In this study, the temperature data was analysed for the year 2007 and it was found that the annual temperature was greater than 0 °C and thus, the albedo was assigned a value of 0.2.

3.2.3.2 Solar radiation and attenuation

After calculating the various astronomical parameters, the total solar radiation level on an inclined surface was calculated using equations (2.10) to (2.12) and equations (2.16) to (2.21). The transmittance, reflectance and absorptance of the glass cover were computed using equations (3.17) to (3.29).

When radiation strikes a surface, some of it is reflected, some absorbed and in the case of a transparent material, some of the radiation is also transmitted. The fraction of radiation that is reflected is known as the reflectance (ρ), the fraction which is absorbed is defined as the absorptance (α) and the fraction that is transmitted is called the transmittance (τ), the sum of these 3 components adding up to 1, as given by the following equation (Goswami, Kreith & Kreider, 2000: 82) :

$$\alpha + \tau + \rho = 1 \tag{3.16}$$

The transmittance, absorptance and reflectance associated with the perpendicular component of unpolarised radiation for a single cover, as used in this study, can be determined from the following equations (Duffie & Beckman, 2013: 202-206):

$$\tau_{perpendicular} = \frac{\tau_a \left(1 - r_{perpendicular}\right)^2}{1 - \left(r_{perpendicular}\tau_a\right)^2} \tag{3.17}$$

$$\alpha_{perpendicular} = \frac{(1 - \tau_a)\left(1 - r_{perpendicular}\right)}{\left(1 - r_{perpendicular}\tau_a\right)} \tag{3.18}$$

$$\rho_{perpendicular} = 1 - (\tau_{perpendicular} + \alpha_{perpendicular}) \tag{3.19}$$

Similar equations can be used to compute the transmittance, absorptance and reflectance associated with the parallel component of radiation.

$$\tau_{parallel} = \frac{\tau_a\left(1 - r_{parallel}\right)^2}{1 - \left(r_{parallel}\tau_a\right)^2} \tag{3.20}$$

$$\alpha_{parallel} = \frac{(1 - \tau_a)\left(1 - r_{parallel}\right)}{\left(1 - r_{parallel}\tau_a\right)} \tag{3.21}$$

$$\rho_{parallel} = 1 - (\tau_{parallel} + \alpha_{parallel}) \tag{3.22}$$

$$\tau_a = \exp\ (-K_{ec}z_{glass}/\cos\theta_2) \tag{3.23}$$

$$\theta_2 = \sin^{-1}[n_1 \sin\theta_1/n_2] \tag{3.24}$$

$$r_{perpendicular} = \frac{\sin^2(\theta_2 - \theta_1)}{\sin^2(\theta_2 + \theta_1)} \tag{3.25}$$

$$r_{parallel} = \frac{\tan^2(\theta_2 - \theta_1)}{\tan^2(\theta_2 + \theta_1)} \tag{3.26}$$

The transmittance of the single cover can then calculated by taking the average of the transmittances for the perpendicular and parallel components of radiation. The same method can be used to calculate the absorptance and reflectance of the cover.

$$\tau = \frac{1}{2}\left(\tau_{perpendicular} + \tau_{parallel}\right) \tag{3.27}$$

$$\alpha = \frac{1}{2}\left(\alpha_{perpendicular} + \alpha_{parallel}\right) \tag{3.28}$$

$$\rho = \frac{1}{2}\left(\rho_{perpendicular} + \rho_{parallel}\right) \tag{3.29}$$

In equation (3.24), the refractive indices of air and glass, n_1 and n_2, were assigned values of 1 and 1.526 respectively (Duffie & Beckman, 2013: 206). Moreover, the value of the extinction coefficient, K, in equation (3.23) was allocated an average value of 18 m^{-1} since according to Duffie and Beckman (2013: 206), K varies from 4 m^{-1} to 32 m^{-1} for different types of glass. The extinction coefficient refers to the characteristic of a medium that combines the effects of absorption, emission and scattering by the molecules of the medium (Goswami, Kreith & Kreider, 2000: 22).

The amount of solar radiation absorbed by the glass cover and the absorber wall, denoted by S_1 and S_2 respectively, were calculated as follows (Mathur, Mathur & Anupma, 2006: 1162):

$$S_1 = \alpha * I_t \tag{3.30}$$

$$S_2 = \alpha_{wall} * \tau * I_t \tag{3.31}$$

The values for the transmittance (τ) and the absorptance (α) of the glass cover were calculated using equations (3.27) and (3.28) respectively. The value for the absorptivity of the absorber wall (α_{wall}) was assumed to be 0.95, as used in previous studies on solar chimneys (Ong, 2003; Ong & Chow, 2003; Mathur *et al*., 2006).

3.2.3.3 Temperature of solar chimney components

The next step was to compute the temperatures of the fluid (air stream), glass cover and absorber wall, denoted by T_f, T_g and T_w respectively. In order to do so, it was crucial to determine various physical properties of air and convective heat transfer coefficients. Furthermore, it was essential to develop correlations for density, specific heat capacity, dynamic viscosity and thermal conductivity as these do not have fixed values; they are dependent on temperature and consequently, these values had to be computed hourly for the whole year.

Values for density, specific heat capacity, dynamic viscosity and thermal conductivity were obtained from Welty et al. (2008: 679) for temperatures ranging from 250 K to 1000 K. Those correlations were developed in an Excel spreadsheet. For each of the physical

property, a graph was plotted and a trend line was used to fit the data on a curve. Various trend lines of polynomial functions of orders 2, 3, 4 and 5 were made to fit the data on a curve until the coefficient of determination, also known as the R-squared value, was 1.00 such that the best fit could be obtained. The correlations which were developed for density, specific heat capacity, dynamic viscosity and thermal conductivity, as well as the equation which was used to calculate the kinetic viscosity of air are given in Appendix A.

The mean monthly hourly temperatures for each component of the solar chimney were calculated as follows:

$$T_{j,ave} = \frac{1}{n}\sum_{i=1}^{n} T_j \tag{3.32}$$

$$n = number\ of\ days\ in\ each\ month * number\ of\ hours\ in\ 1\ day \tag{3.33}$$

Where, T_j represents the instantaneous temperatures of the absorber wall, glass cover, fluid and ambient air (T_w, T_g, T_f and T_a) ; n represents the number of data points in each month and $T_{j,ave}$ represents the mean monthly hourly temperatures of the absorber wall, glass cover, fluid and ambient air ($T_{w,ave}$, $T_{g,ave}$, $T_{f,ave}$ and $T_{a,ave}$) .

It is important to note that two values were calculated for each of the physical properties at each data point, to account for the fact that the air stream is surrounded by different boundaries, namely the glass cover and the absorber wall. Other physical properties were calculated using existing equations from literature.

3.2.3.4 Convective heat transfer correlations

In addition to physical properties of air, convective heat transfer correlations were also needed to calculate the temperatures of glass cover, absorber wall and air stream. All the equations which were used in the MATLAB simulation are given below.

a) Prandtl number

The Prandtl number is a dimensionless constant, which is a function of dynamic viscosity, specific heat capacity and thermal conductivity. It can be expressed as the following (Mathur *et al*., 2006: 934).

For glass cover and air stream,

$$Pr = \frac{\mu_f C_f}{k_f} \tag{3.34}$$

For absorber wall and air stream,

$$Pr_1 = \frac{\mu_{f1} C_{f1}}{k_{f1}} \tag{3.35}$$

b) Grashof number

The Grashof number is a measure of the ratio of buoyancy forces to viscous forces (Bergman *et al*., 2011: 409).

For glass cover and air stream,

$$Gr = \frac{g\ \beta\ \Delta T\ L_{stack}^3}{\nu_f^2} \tag{3.36}$$

$$\beta = \frac{1}{T_m} \tag{3.37}$$

$$\Delta T = T_g - T_f \tag{3.38}$$

For inclined solar chimneys: $L_{stack} = L_{abs} \sin\beta$ (3.39)

For wall-mounted solar chimneys: $L_{stack} = L_{abs} + \frac{z}{2}$ (3.40)

For absorber wall and air stream,

$$Gr_1 = \frac{g\ \beta_1\ \Delta T_1\ L_{stack}^3}{\nu_{f1}^2} \tag{3.41}$$

$$\beta_1 = \frac{1}{T_{m1}} \tag{3.42}$$

$$\Delta T_1 = T_w - T_f \tag{3.43}$$

c) Rayleigh number

The Rayleigh number is the product of the Grashof number and the Prandtl number (Welty *et al*., 2008: 299).

For glass cover and air stream,

$$Ra = Gr\ Pr \tag{3.44}$$

For absorber wall and air stream,

$$Ra_1 = Gr_1\ Pr_1 \tag{3.45}$$

d) Nusselt's number

The Nusselt's number is a function of the Rayleigh number and the Prandtl number, as expressed by the following equations (Holman, 2010: 335):

For glass cover and air stream,
Scenario 1: for Ra < 10^9,

$$Nu_f = 0.68 + \frac{0.670\ Ra^{\frac{1}{4}}}{\left[1 + \left(\frac{0.492}{Pr}\right)^{\frac{9}{16}}\right]^{\frac{4}{9}}} \tag{3.46}$$

Scenario 2: for $10^{-1} < Ra < 10^{12}$,

$$Nu_f = \left\{ 0.825 + \frac{0.387\, Ra^{\frac{1}{6}}}{\left[1 + \left(\frac{0.492}{Pr}\right)^{\frac{9}{16}}\right]^{\frac{8}{27}}} \right\}^2 \tag{3.47}$$

For absorber wall and air stream,

Scenario 1: for $Ra < 10^9$,

$$Nu_{f1} = 0.68 + \frac{0.670\, Ra_1^{\frac{1}{4}}}{\left[1 + \left(\frac{0.492}{Pr_1}\right)^{\frac{9}{16}}\right]^{\frac{4}{9}}} \tag{3.48}$$

Scenario 2: for $10^{-1} < Ra < 10^{12}$,

$$Nu_{f1} = \left\{ 0.825 + \frac{0.387\, Ra_1^{\frac{1}{6}}}{\left[1 + \left(\frac{0.492}{Pr_1}\right)^{\frac{9}{16}}\right]^{\frac{8}{27}}} \right\}^2 \tag{3.49}$$

It has been further stated by Welty et al. (2008: 300) that equations (3.46) to (3.49) can be used for plane surfaces inclined at an angle of up to 60° with the vertical; which means that the minimum angle of inclination with the horizontal needs to be at least 30°. In this investigation, the minimum tilt angle with the horizontal for the roof-mounted solar chimney was 30° and thus, equations (3.46) to (3.49) could be used.

3.2.3.5 Heat transfer coefficients

The next step was to calculate the various heat transfer coefficients in equations (3.2), (3.3) and (3.4), which represent the energy balance equations of the solar chimney system.

a) Radiative heat transfer coefficient between wall and glass

The radiative heat transfer coefficient between the absorber wall and the glass cover was computed as follows (Ong, 2003: 1055):

$$h_{rwg} = \frac{\left[\sigma\left(T_g^2 + T_w^2\right)\left(T_g + T_w\right)\right]}{\left(\frac{1}{\varepsilon_g} + \frac{1}{\varepsilon_w} - 1\right)} \tag{3.50}$$

The symbols ε_g and ε_w refer to the emissivity of the glass cover and absorber wall, assumed to be 0.90 and 0.95 respectively, as given in the study conducted by Mathur et al. (2006: 928). The Stefan-Boltzmann constant (σ) is 5.67 x 10^{-8} $Wm^{-2}K^{-4}$ (Bergman *et al*., 2011: 9).

Since the effect of view factor on the performance of solar chimneys was also investigated in this research, it was important to calculate the radiative heat transfer coefficient between the absorber wall and the glass cover, taking into account the view factor between these two components. This heat transfer coefficient was calculated as follows (Duffie & Beckman, 2013: 148):

$$h_{rwg} = \frac{\left[\sigma\left(T_g^2 + T_w^2\right)\left(T_g + T_w\right)\right]}{\left(\frac{1-\varepsilon_w}{\varepsilon_w} + \left(\frac{1-\varepsilon_g}{\varepsilon_g A_g}\right)A_{abs} + \frac{1}{F_{w-g}}\right)} \tag{3.51}$$

b) Convective heat transfer coefficient between glass and air and between wall and air

The convective heat transfer coefficient between the glass cover and the air stream, h_g, and the convective heat transfer coefficient between the absorber wall and the air stream, h_w, can be calculated from the following equations (Marti-Herrero & Heras-Celemin, 2007: 618):

$$h_g = \frac{Nu\ k_f}{L_g} \tag{3.52}$$

$$h_w = \frac{Nu_1\ k_{f1}}{L_{abs}} \tag{3.53}$$

c) Heat transfer coefficient between absorber wall and adjacent room

The overall heat transfer coefficient between the insulation layer of the absorber wall and the room that needs to be ventilated is given by the following equation (Larbi & Hella, 2013: 631):

$$U_b = \frac{k_{ins}}{w_{ins}} \tag{3.54}$$

The insulation material considered for this study was polyurethane, having a thermal conductivity of 0.027 $Wm^{-1}K^{-1}$ at room temperature (National Physical Laboratory, 2015).

d) Overall heat transfer coefficient from top of glass cover

Heat is lost to the atmosphere from the top of the glass cover mainly due to radiation from the glass cover to the sky and due to convection by wind (Madhlopa, 2009: 43). The overall heat transfer loss coefficient can thus be given as follows:

$$U_t = h_{rs} + h_{wind} \tag{3.55}$$

The radiative heat transfer coefficient between the glass cover and the sky can be expressed as follows (Duffie & Beckman, 2013: 243):

$$h_{rs} = \sigma\, \varepsilon_g \left(T_g^2 + T_s^2\right)\left(T_g + T_s\right) \tag{3.56}$$

The heat transfer coefficient by convection due to wind can be calculated using the correlation developed in 1977 by Wattmuf, Charters and Proctor (cited by El-Sebaii, 2005: 27):

For $V \leq 5$ m/s,

$$h_{wind} = 2.8 + 3\,V \tag{3.57}$$

For $V > 5$ m/s,

$$h_{wind} = 6.15\,V^{0.8} \tag{3.58}$$

3.2.3.6 Climatic data

There are two main climatic factors which affect the performance of a solar chimney, namely the intensity of solar radiation and the wind speed. The intensity of solar radiation is the driving force behind the operation of a solar chimney (Gontikaki *et al*., 2010). As mentioned earlier in this thesis, a higher level of solar radiation causes the temperature of air inside the solar chimney to increase, thereby leading to a higher stack pressure and higher ventilation rates (Chen *et al*., 2003: 902). Previous studies on solar chimneys have shown that the ventilation rate increases as the intensity of solar radiation increases (Bansal, Mathur & Bhandari, 1993; Chen *et al*., 2003; Ong, 2003, Mathur *et al.*, 2006; Bassiouny & Koura, 2008; Jianliu &Weihua, 2013; Al-Kayiem, Sreejaya & Gilani, 2014; Suárez-López *et al.*, 2015; Imran, Jalil & Ahmed, 2015). The ambient temperature is also a climatic parameter which is needed to assess the performance of solar chimneys; the ambient temperature and the intensity of solar radiation are directly related.

Wind is considered as the second most dominant climatic factor which affects the performance of solar chimneys as it can either improve or hinder air flow at the outlet of the solar chimney (Gontikaki *et al*., 2010). In an experimental investigation on solar chimneys conducted by Arce *et al*. (2009), it was found that the highest flow rate of air was achieved when the wind velocity was at its peak while the lowest air flow rate occurred when the wind velocity was at its minimum.

The climatic data that were required for this research include solar radiation level, wind speed and temperature. The raw data obtained for this study were on an hourly basis for the year 2007 in Stellenbosch, thereby comprising of 8760 data points (365 days multiplied by 24 hours). The following raw data were obtained:

a) The intensities of global radiation and diffuse radiation, in Wh/m^2, on a horizontal surface.
b) Wind speed, in m/s.
c) Temperature, in °C.

This set of climatic data was obtained from the South African Solar Radiation Database and according to Ciolkosz (2009), as cited by Madhlopa et al. (2015: 328), the quality of this set of meteorological data is acceptable. Figure 3.8 and Figure 3.9 show the climatic data which were used in this investigation. The hourly values for each climatic parameter have been

averaged for each month such that one mean value is obtained monthly, for the purpose of showing the raw sets of data that were obtained.

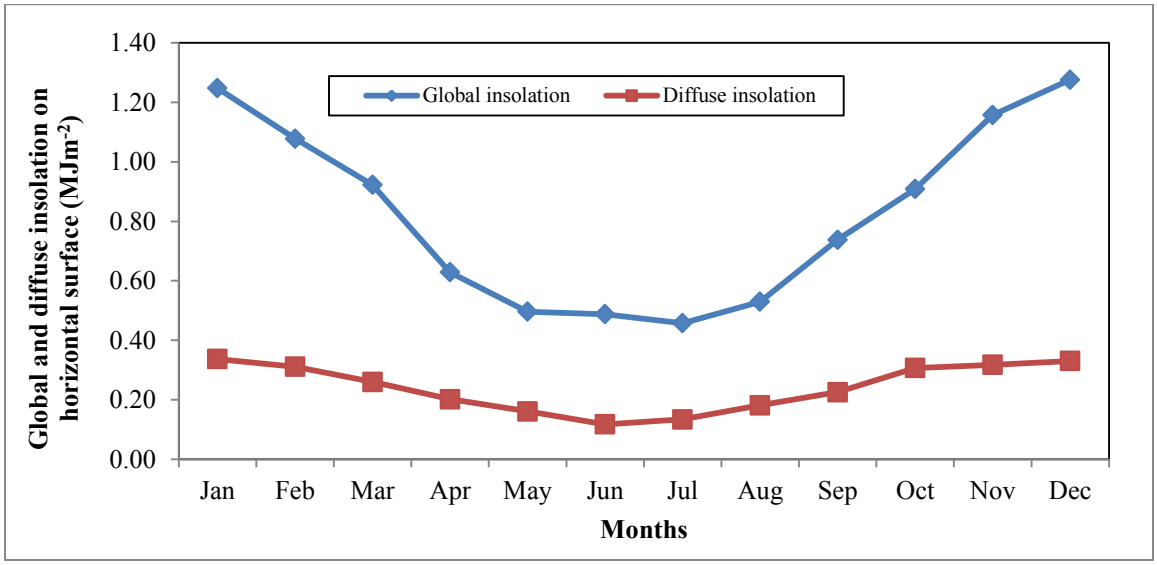

Figure 3.8: Mean monthly global (I_g) and diffuse insolation (I_d) on a horizontal surface at Stellenbosch in 2007.

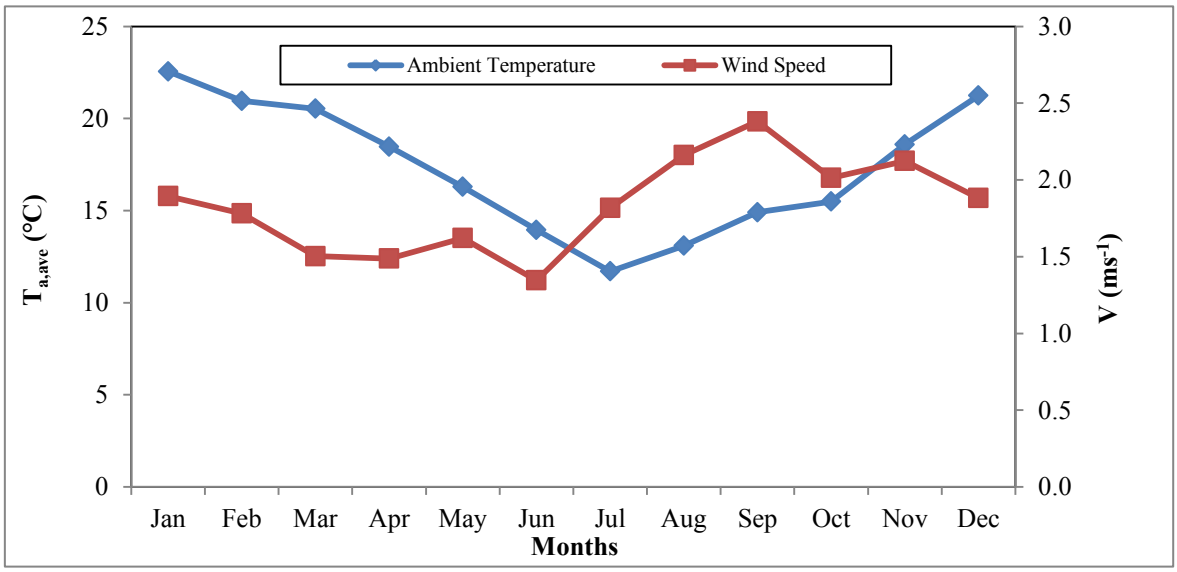

Figure 3.9: Mean monthly hourly ambient air temperature and wind speed at Stellenbosch in 2007.

3.2.3.7 Simulation in MATLAB

After developing the various correlations for the physical properties of air and calculating all the heat transfer coefficients, three equations were solved for the three unknown temperatures (T_f, T_g and T_w). Equation (3.12) was re-arranged to write T_f in terms of T_g and T_w. Likewise, equations (3.10) and (3.11) were re-arranged to make T_g and T_w the subject of formula respectively, as shown by the following equations:

$$T_f = \frac{h_g A_g T_g + h_w A_w T_w + \frac{mC_{f1}T_r}{\gamma_{MTA}}}{h_g A_g + h_w A_w + \frac{mC_{f1}}{\gamma_{MTA}}} \tag{3.59}$$

$$T_g = \frac{S_1 A_g + U_t A_g T_a + h_g A_g T_f + h_{rwg} A_w T_w}{h_g A_g + h_{rwg} A_w + U_t A_g} \tag{3.60}$$

$$T_w = \frac{S_2 A_w + U_b A_w T_r + h_{rwg} A_w T_g + h_w A_w T_f}{h_w A_w + h_{rwg} A_w + U_b A_w} \tag{3.61}$$

Equations (3.59), (3.60) and (3.61), together with equation (3.13), comprising of a set of linear simultaneous equations, were then solved in MATLAB. According to Jaluria (2011: 173), there are two methods which can be adopted for solving a set of linear simultaneous equations, namely direct and iterative methods. Examples of direct methods include Gaussian elimination method, Cramer's Rule and LU decomposition method while iterative methods include the Jacobi method, the Gauss-Seidel method and the Successive over-relaxation method (Butt, 2009: 148).

In this study, the iterative method was chosen to solve for the unknowns because fluid properties and the coefficients of convective and radiative heat transfer are temperature-dependent. An iterative procedure can be defined as a method which is carried out repeatedly, using the output from the first step as the input to the second step, and so on, until the solutions converge (Cheney & Kincaid, 2009:647). The Gauss-Seidel iterative procedure was used for this investigation as it is the most commonly used method amongst the iterative methods and it also gives good accuracy since the new estimates are used for the arithmetic operations as soon as they are available (Butt, 2009: 208-216).

Figure 3.10 shows the step by step procedure which was used to solve for the numerous equations associated with the performance of the solar chimneys in MATLAB. First of all, it was important to input all the constants and design parameters for the solar chimneys in MATLAB. The initial temperatures for the fluid, glass and absorber wall were then estimated. All the required equations associated were subsequently entered in MATLAB and were solved using an iterative process until the solutions converged.

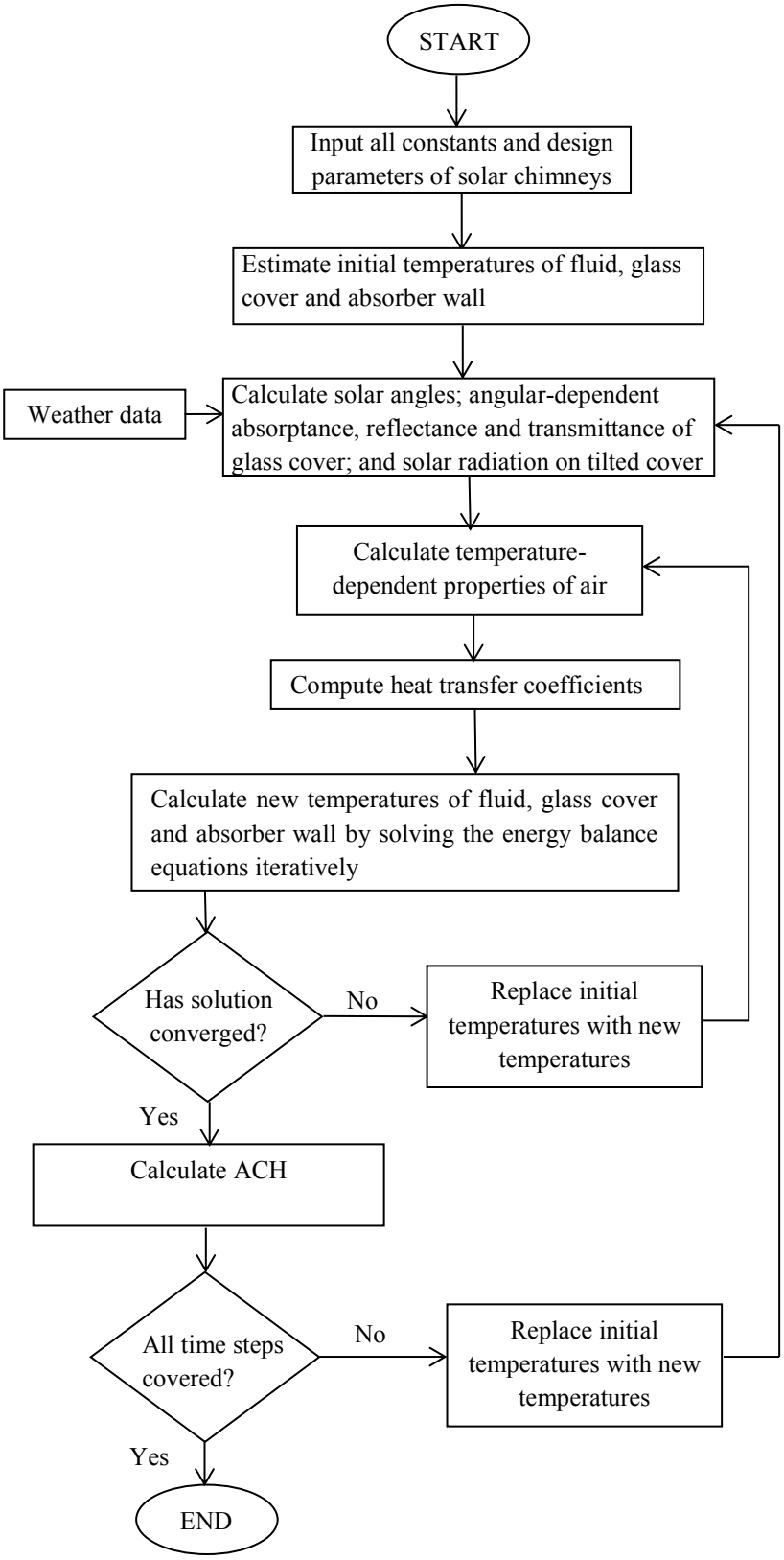

Figure 3.10: Algorithm for solving system of equations in MATLAB.

3.3 Assessment of the performance of the solar chimneys

The performance of a solar chimney is usually determined by the ventilation rate (V_{rate}), which is typically expressed in m^3/s and is given by the following equation (Mathur *et al*., 2006: 932):

$$V_{rate} = \frac{m}{\rho_{f1}} \tag{3.62}$$

In several studies, the number of air changes per hour (ACH) is the parameter which is used to assess the performance of solar chimneys. ACH is typically another way of expressing the ventilation rate. ACH is an important parameter to analyse as it is a ventilation standard which needs to be met in many countries. For instance in India, a minimum of 3 ACH is needed for residential buildings, according to ventilation standards (Mathur *et al*., 2006: 933). In South Africa, buildings such as educational buildings (classrooms and libraries), meeting and waiting spaces in offices and lobbies of hotels need to have a minimum ACH of 2 while the minimum ACH requirement for conference rooms, kitchens, assembly rooms or rooms associated with medical care are much higher, ranging from 6 to 20 according to SANS 10400-O: 2011 (South African Bureau of Standards [SABS], 2011). The ACH can be computed using equation (3.63**)** as given by Mathur et al. (2006: 933):

$$ACH = \frac{V_{rate} * 3600}{V_{room}} \tag{3.63}$$

The volume of the room that needed to be ventilated was calculated as follows:

$$V_{room} = L_r * W_r * H_r \tag{3.64}$$

In this study the performance of the solar chimneys was assessed based on the ACH, which is an indicator of the ventilation rate. The effects of inclination angle, air gap, chimney height and view factor on the ACH were examined. The total ACH was calculated for each month and this was then divided by the number of hours in each month so that the ACH values could be reported as average number of air changes per hour for each month.

3.4 Statistical Analysis

In an attempt to validate the mathematical model developed in this study, simulation values were compared with published values from literature, precisely from a study conducted by Mathur, Mathur and Anupma (2006). The same design parameters that they used for their study were put into the MATLAB program in order to compute the performance of their solar chimney numerically using the mathematical model developed in this investigation. Mathur, Mathur and Anumpa (2006) performed a numerical and experimental study on an inclined solar chimney, without taking into account the view factor. Since the present study considers both the performance of solar chimneys with and without view factor, the numerical values obtained from each of the two scenarios (with and without view factor) were compared to the values published in literature.

The performance of the inclined solar chimney (in terms of the air flow velocity at the exit) was investigated for intensities of solar radiation ranging from 500 W/m^2 to 750 W/m^2 for an absorber height of 1 m and absorber width of 1 m, with the air gap being 0.35 m at a tilt angle of 45° at different ambient temperatures. Moreover, the thermal conductivity of the insulation material was taken to be 0.037 Wm^{-1}K^{-1} and the wind speed was also assumed to be zero in order to use the same exact parameters that were used by Mathur, Mathur and Anumpa (2006).The air flow velocity at exit was calculated as follows (Mathur, Mathur & Anupma, 2006: 1159):

$$v_o = \frac{m}{\rho_{f1} A_{out}} \tag{3.65}$$

The root mean square of percentage deviation (e) was calculated as follows (Tripathi & Tiwari, 2004: 74):

$$e = \sqrt{\frac{1}{n}\sum_{i=1}^{n} e_i^2} \tag{3.66}$$

$$e_i = \left(\frac{X_i - Y_i}{X_i}\right) * 100 \tag{3.67}$$

Where, X_i refers to the value obtained from this numerical simulation (predicted value), Y_i refers to the experimental value obtained from Mathur, Mathur and Anupma (2006), and n is the number of observations

Chapter 4

RESULTS AND DISCUSSION

In this study, various configurations of solar chimneys were modelled in MATLAB and their performances were assessed in terms of the ventilation rate, expressed as the number of air changes per hour. Several numerical studies conducted on solar chimneys were discussed in Chapter 2, as well as the different parameters which affect the performance of solar chimneys, namely solar radiation intensity, air gap, chimney height, angle of inclination and type of glazing. However, the effect of the view factor has most often been ignored in previous studies on solar chimneys. In this research, the effect of inclination angle, air gap, chimney height and view factor on the thermal performance of wall-mounted and roof-mounted solar chimneys were investigated. The model validation and the results from the MATLAB simulation as well as a discussion on the results are presented in this chapter.

4.1 Incident solar radiation on inclined and vertical surfaces

The incident solar radiation (diffuse, direct and ground-reflected) on an inclined surface with a tilt angle of 34° and on a vertical surface was calculated in MATLAB. There was a need to calculate the incident solar radiation on these surfaces as the raw data only gave the global and diffuse solar radiation on a horizontal surface. The calculated values were then exported to Excel to plot the required graphs. The hourly values for the incident solar radiation were averaged for each month such that one mean value could be obtained for each month across the whole year.

It can be observed from Figure 4.1 that the highest value for the incident solar radiation on both surfaces was achieved in the month of December while the lowest value was obtained in the month of July. Moreover, the incident solar radiation was higher for the months of October to March as compared to the months of April to September. This is because the Southern Hemisphere is tilted towards the sun during the months of October to March while it is tilted away from the sun during the months of April to September; this seasonal weather variation occurring due to the rotation of the earth around the sun, about an axis tilted at an angle of 23.5° to the orbital plane (Myers, 2013: 1).

Moreover, it can be observed that the incident solar radiation is much higher for the inclined surface, as compared to the vertical surface throughout the whole year. The highest amounts of solar energy for the inclined and vertical surfaces were 1.03 MJ/m^2/hour and 0.32 MJ/m^2/hour respectively for the month of December as can be observed from Figure 4.1. The amount of solar energy incident on the inclined surface was thus more than three times higher than that on the vertical surface. This is due to the fact that the amount of solar radiation captured on a surface decreases with increase in inclination angle (Bassiouny & Korah, 2009: 194). Furthermore, the optimum tilt angle of a solar collector is that angle which allows solar radiation to strike the surface perpendicularly (Handoyo, Ichsani & Prabowo, 2013: 166). Consequently, the amount of solar radiation incident on the inclined surface is higher since it allows the rays of the sun to strike its surface at an angle closer to 90° than the vertical surface.

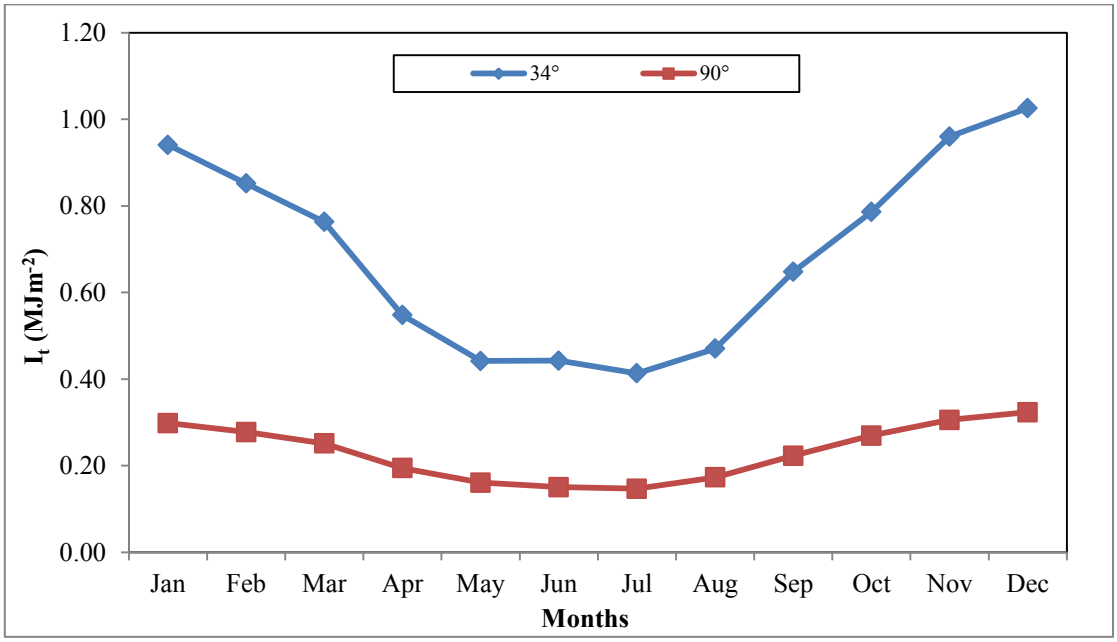

Figure 4.1: Mean monthly hourly incident insolation on inclined and vertical surfaces (I_t) at Stellenbosch, situated in the Western Cape Province of South Africa.

It has been further stated that maximum solar radiation can be captured on a solar collector if it is inclined at an angle which is nearly equal to the latitude of the location (Benghanem, 2011: 1427). Therefore, since 34° represents the latitude of Stellenbosch, the amount of solar radiation incident on the inclined surface (with tilt angle of 34°) is higher than that on the vertical surface.

4.2 Model Validation

Table 4.1 shows the comparison between the experimental data from Mathur, Mathur and Anupma (2006) and the modelled values from the present study. The errors for Model 1(with view factor) and Model 2 (without view factor) were found to be 13 % and 20 % respectively. Consequently, it can be noted that the results obtained from this present investigation are in good agreement with those obtained from literature. Furthermore, it is observed that the inclusion of the view factor improves the accuracy of modelling of a solar chimney by nearly 7 %.

Table 4.1: Comparison between experimental results from Mathur, Mathur and Anupma (2006) and numerical results obtained from the model in this study for an inclined solar chimney (45°).
Model 1 includes the view factor while Model 2 does not.

S	**T_a**	**Air flow velocity at exit (m/s)**		
(W/m^2)	**(K)**	Experimental	Model 1	Model 2
500	299.2	0.174	0.1600	0.1517
550	302.6	0.184	0.1661	0.1572
600	306	0.1948	0.1719	0.1623
650	310.3	0.1979	0.1776	0.1672
700	312.2	0.2132	0.1832	0.1722
750	313	0.2201	0.1888	0.1771

4.3 Temperatures of system components

4.3.1 Temperature of absorber wall, glass cover, fluid and ambient air

The hourly temperatures of the absorber wall, glass cover, fluid (air within the chimney channel; between the absorber wall and the glass cover) and ambient air for each month were averaged such that one mean value for temperature was obtained monthly for each component of the inclined and vertical solar chimneys.

The coldest month in Stellenbosch during that particular year was July while the hottest month was January, hence accounting for the trough and crest respectively at these two months, as represented by the ambient temperature curve on Figure 4.2 and Figure 4.3. Moreover, it can be observed from Figure 4.2 and Figure 4.3 that the absorber wall temperature ranks first, followed by the glass cover temperature, fluid temperature and ambient temperature, in descending order of magnitude, for both the inclined solar chimney and the vertical solar chimney. This was anticipated since the absorber wall was modelled as

a black body which can trap much more heat than the glass cover, hence accounting for the higher temperature.

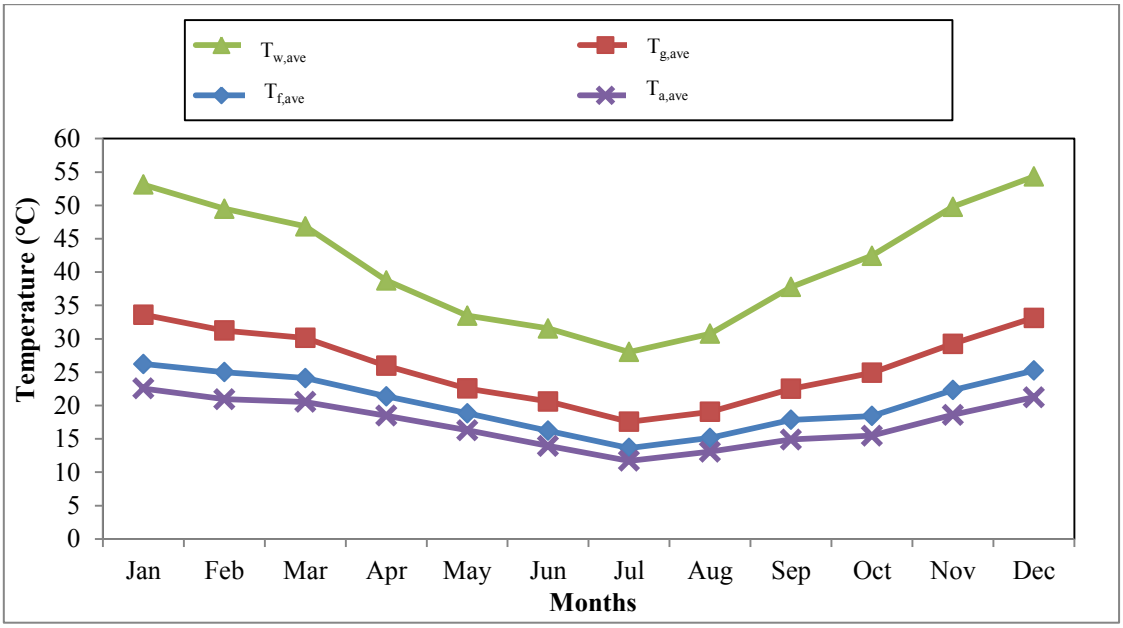

Figure 4.2: Mean monthly hourly temperatures of the absorber wall ($T_{w,ave}$), glass cover ($T_{g,ave}$), fluid ($T_{f,ave}$) and ambient air ($T_{a,ave}$) for the solar chimney inclined at 34° to the horizontal with d=0.25 m and $L_{abs}=L_g=2$ m.

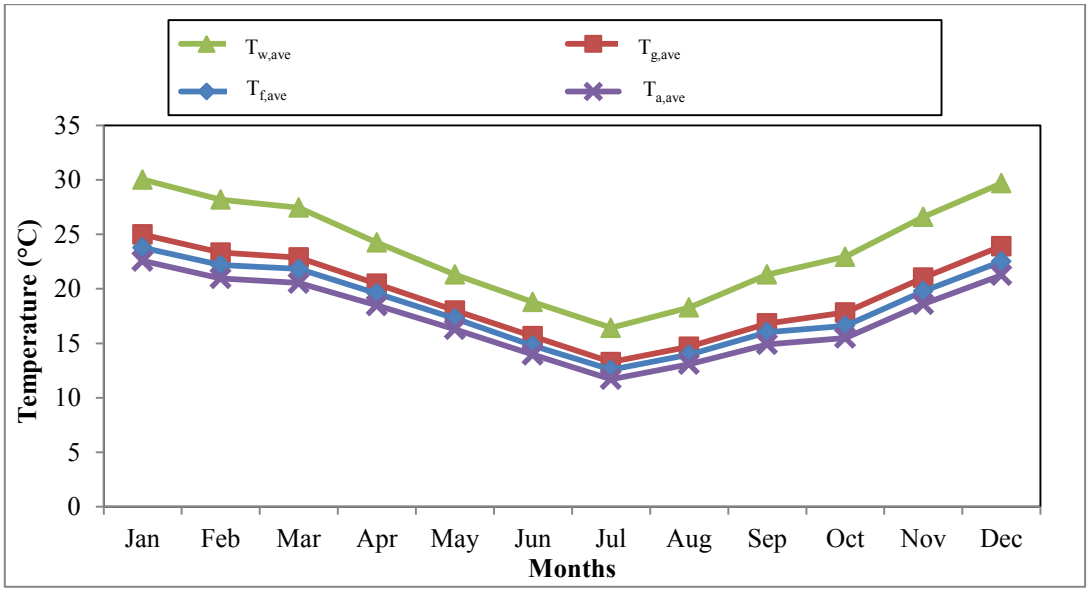

Figure 4.3: Mean monthly hourly temperatures of the absorber wall ($T_{w,ave}$), glass cover ($T_{g,ave}$), fluid ($T_{f,ave}$) and ambient air ($T_{a,ave}$) for the vertical solar chimney with d=0.25 m and $L_{abs}=L_g=2$ m.

The results obtained in this study are in agreement with those obtained from previous studies. In a numerical study conducted by Ong (2003), it was found that the temperature of the absorber wall always exceeds the temperature of both the glass cover and the fluid. A numerical study carried out by Larbi and Hella (2013) also revealed that the absorber wall

temperature is higher than that of the glass cover and the fluid due to thermal radiation absorption by the absorber wall.

Furthermore, the temperatures of the fluid, glass cover and absorber wall for both solar chimney configurations are higher during summer as compared to winter. The intensity of solar radiation is higher during summer and therefore, more energy can be absorbed by the glass cover and the absorber wall, and more heat can be transferred via convection to the air stream. Consequently, this causes the fluid, glass and absorber wall temperatures to be higher when the solar radiation level is higher. The temperature results obtained in this study are in accordance with the results obtained from previous studies which showed an increase in fluid, glass and wall temperatures as the intensity of solar radiation increases (Ong, 2003; Bassiouny & Koura, 2008; Jianliu & Weihua, 2013).

4.3.2 Comparison between temperatures of inclined solar chimney and vertical solar chimney

Figure 4.4, Figure 4.5 and Figure 4.6 respectively show the comparison between the fluid temperatures, glass cover temperatures and absorber wall temperatures of the inclined solar chimney and the vertical solar chimney. It can be observed from Figure 4.4, Figure 4.5 and Figure 4.6 that all temperatures of the three components (fluid, glass cover and absorber wall) for the inclined solar chimney are higher than those of the corresponding components of the vertical solar chimney. This is due to the fact that the amount of solar radiation captured on a surface decreases with increase in inclination angle (Bassiouny & Korah, 2009: 194), as mentioned earlier. Moreover, it was also discussed that a solar chimney with a tilt angle equivalent to the latitude of the location can absorb maximum solar radiation. Consequently, the solar chimney inclined at 34° can absorb more solar radiation than the vertical solar chimney, thus causing the temperatures of its glass, absorber wall and fluid to be higher than the corresponding temperatures of the components of the vertical solar chimney.

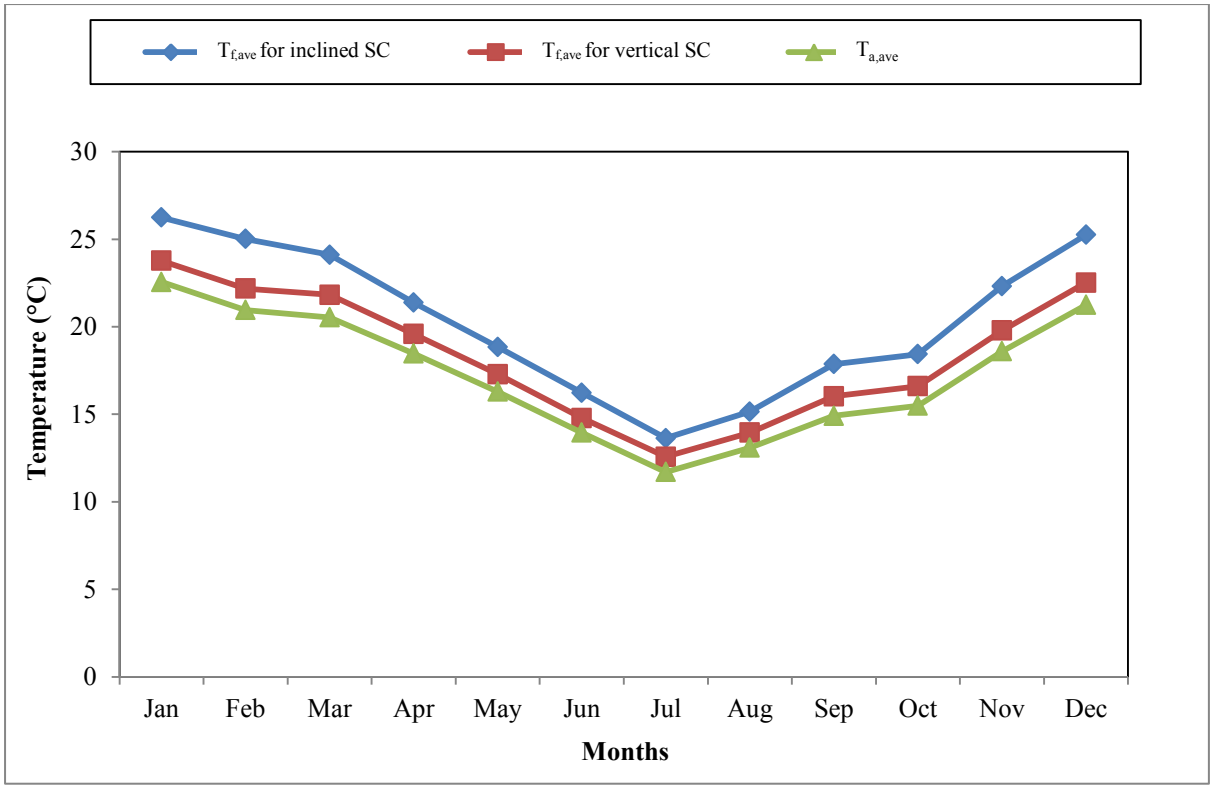

Figure 4.4: Mean monthly hourly fluid temperatures ($T_{f,ave}$) for inclined solar chimney with tilt angle of 34° and vertical solar chimney; with d=0.25 m and L_{abs}=L_g=2 m.

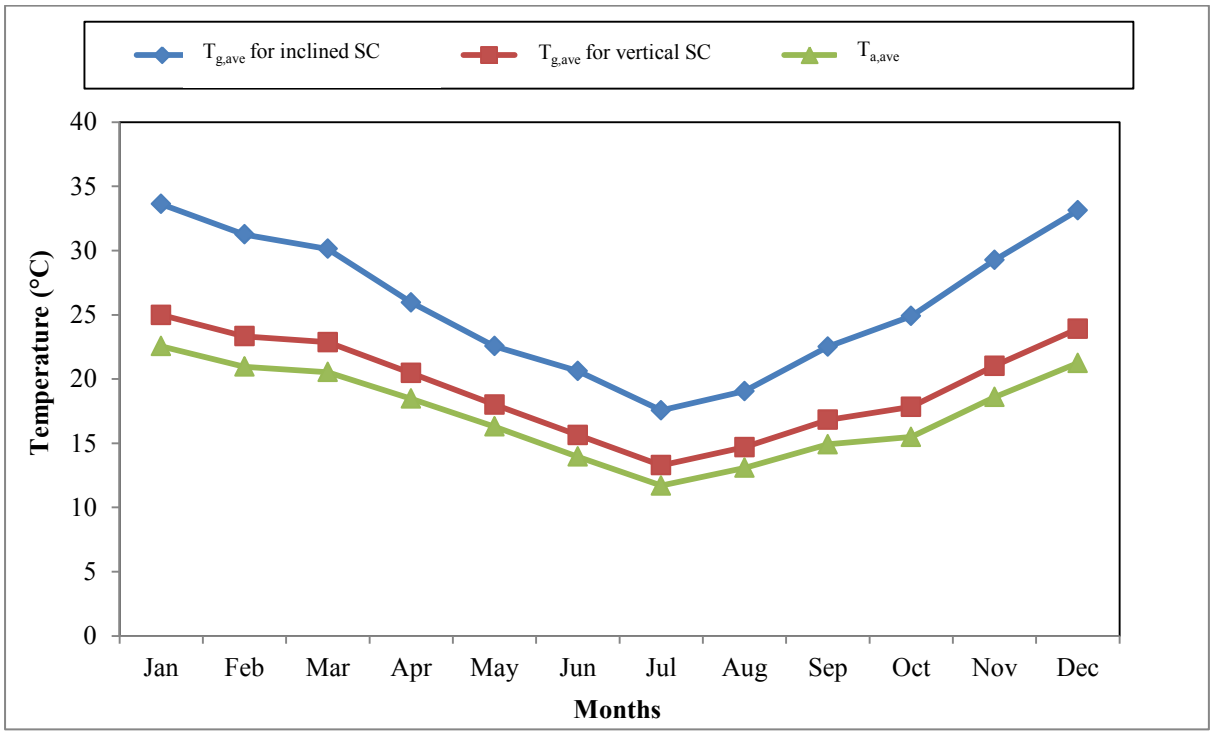

Figure 4.5: Mean monthly hourly glass cover temperatures ($T_{g,ave}$) for inclined solar chimney with tilt angle of 34° and vertical solar chimney; with d=0.25 m and L_{abs}=L_g=2 m.

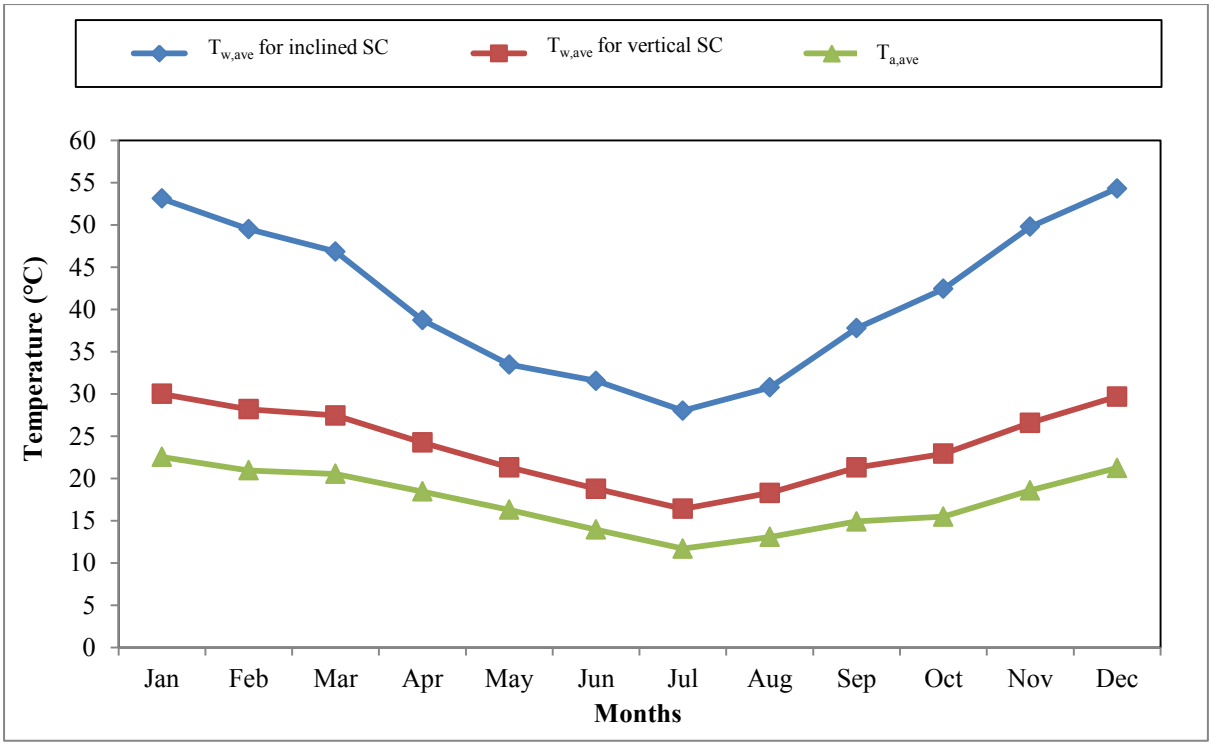

Figure 4.6: Mean monthly hourly absorber wall temperatures ($T_{w,ave}$) for inclined solar chimney with tilt angle of 34° and vertical solar chimney; with d=0.25 m and L_{abs}=L_g=2 m.

4.3 Effect of inclination angle on ACH

According to the South African Weather Service (2015), the seasons in South Africa are as follows: autumn in March to May, winter in June to August, spring in September to November and summer in December to February. In the context of this investigation, the results are shown for winter (June to August) and summer (December to February). As can be observed Figure 4.7, the ACH increases with an increase in inclination angle from 30° to 60°, but a further increase in inclination angle causes the ACH to decrease. An inclination angle of 60° was found to be the optimum angle of inclination for Stellenbosch, both for winter and summer seasons, while the vertical solar chimney gave the worst performance, having the lowest ACH throughout winter and summer.

For the solar chimney inclined at an angle of 60° to the horizontal, the highest ACH recorded in winter was 4.3, occurring in the month of August. On the other hand, for the vertical solar chimney, the highest ACH obtained for the winter season was 3.6, also occurring in the month of August. Concerning the summer season, for the solar chimney having an inclination angle of 60°, it was found that the highest ACH achieved was during the month of December, at an average value of 5.9. For the vertical solar chimney, it was found that the highest ACH was 4.6, occurring during the month of December as illustrated by Figure 4.7. Thus, it can be

gathered that the inclined solar chimney having a tilt angle of 60° can provide around 20 % higher ventilation higher rate than the vertical solar chimney, both in winter and summer.

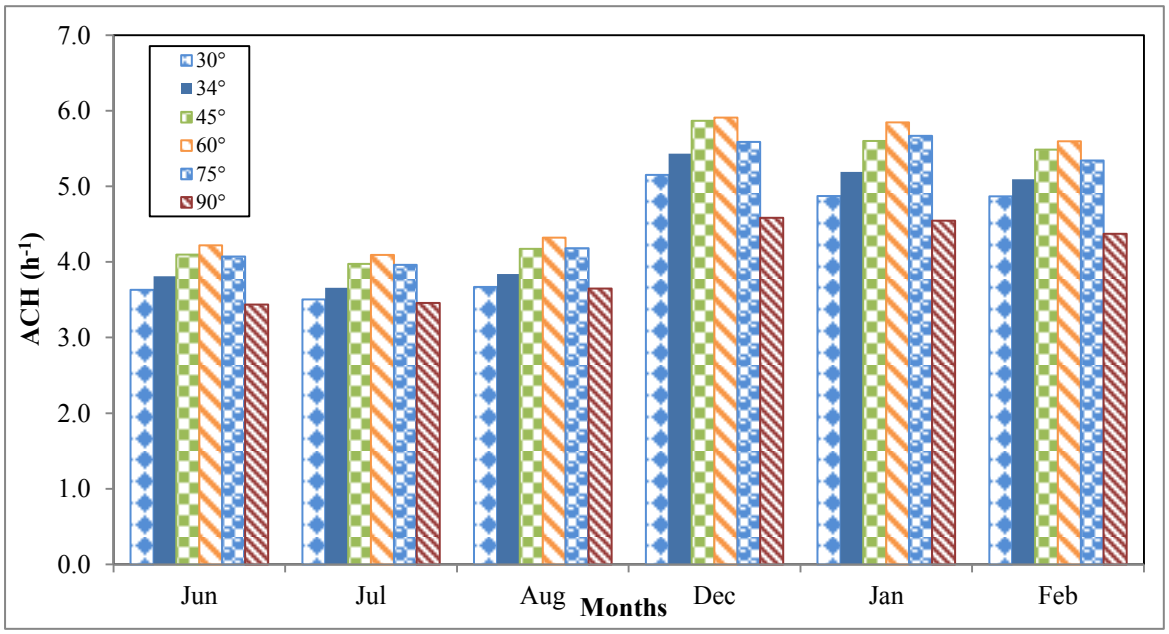

Figure 4.7: Effect of inclination angle on mean monthly hourly ACH in winter and summer for inclined and vertical solar chimneys; with d=0.25 m and L_{abs}=L_g=2 m.

The ACH results obtained in this study are fairly in agreement with the results obtained from previous studies. According to Mathur, Mathur and Anupma (2006), the optimum angle of inclination is 50° for a location at latitude of 35°. It has been further shown by Imran, Jalil and Ahmed (2015) that the optimum inclination angle for maximum ventilation rate is 60° for Baghdad, situated at latitude of 33.3°. Furthermore, a study carried out in Nanjing, at latitude of 32°, revealed that the optimum angle of inclination is 45° (Jianliu & Weihua, 2013). This also agrees with the results obtained in this research since it can be observed from Figure 4.7 that an inclination angle of 45° gives fairly similar results to that of 60°.

Additionally, the ACH values are higher in summer than in winter. This is due to the fact that in summer, the solar radiation level is higher and consequently, more heat can be transferred to the air stream, which in turn causes the fluid temperature to increase. This in turn causes a greater difference between the density of air at the inlet of the solar chimney and the density of air within the solar chimney channel. This higher density difference in summer causes a higher pressure difference between the inlet to the solar chimney and the chimney channel, thereby causing a higher rate of ventilation, thus leading to higher ACH values in summer, as compared to winter. This is also in accordance with the results obtained from previous studies (Bansal, Mathur & Bhandari, 1993; Chen *et al.*, 2003; Ong, 2003; Mathur *et al.*, 2006;

Bassiouny & Koura, 2008; Yan *et al*., 2011; Jianliu & Weihua, 2013; Al-Kayiem, Sreejaya & Gilani, 2014; Imran, Jalil & Ahmed, 2015; Suárez-López et al., 2015) which also showed that ventilation rate increases with an increase in the intensity of solar radiation.

According to SANS 10400-O: 2011 (SABS, 2011), the minimum ACH requirement is 2 for educational buildings (classrooms and libraries), meeting and waiting spaces in offices and for lobbies of hotels while the minimum ACH requirement for conference rooms, kitchens, assembly rooms or rooms associated with medical care ranges from 6 to 20. Consequently, it can be noted that all the solar chimneys, with tilt angles ranging from 30° to 90°, can only be integrated into educational buildings, meeting and waiting spaces in offices and in hotel lobbies since these solar chimneys produce ACH values which are above the minimum ventilation requirements for such spaces in buildings across South Africa.

4.4 Effect of air gap on ACH

The effect of air gap on ACH was investigated by varying the air gap from 0.15 m to 0.75 m. Figure 4.8 and Figure 4.9 illustrate the effect of air gap on ACH for the roof-mounted and wall-mounted solar chimneys respectively. In the context of this study, it was observed that an increase in the air gap causes the ACH to increase. For the roof-mounted solar chimney, the highest ventilation rate was achieved during the month of December, at an average ACH of 16.1 for an air gap of 0.75 m while for an air gap of 0.15 m, the ACH was 3.5 for the same month as can be observed from Figure 4.8. On the other hand, for the wall-mounted solar chimney, the highest ACH was found to be 13.4 for an air gap of 0.75 m in both December and January and for an air gap of 0.15 m, the ACH values were 2.9 and 2.8 in December and January respectively, as observed from Figure 4.9. An increase in air gap of 0.60 m can thus cause the ACH to increase by more than fourfold. The trend obtained in this study is in agreement with the results obtained from previous investigations (Hirunlabh *et al*., 1999; Chen *et al*., 2003; Mathur *et al*., 2006; Jing, Chen & Li, 2015; Imran, Jalil & Ahmed, 2015) which also showed an increase in ventilation rate as the air gap was increased.

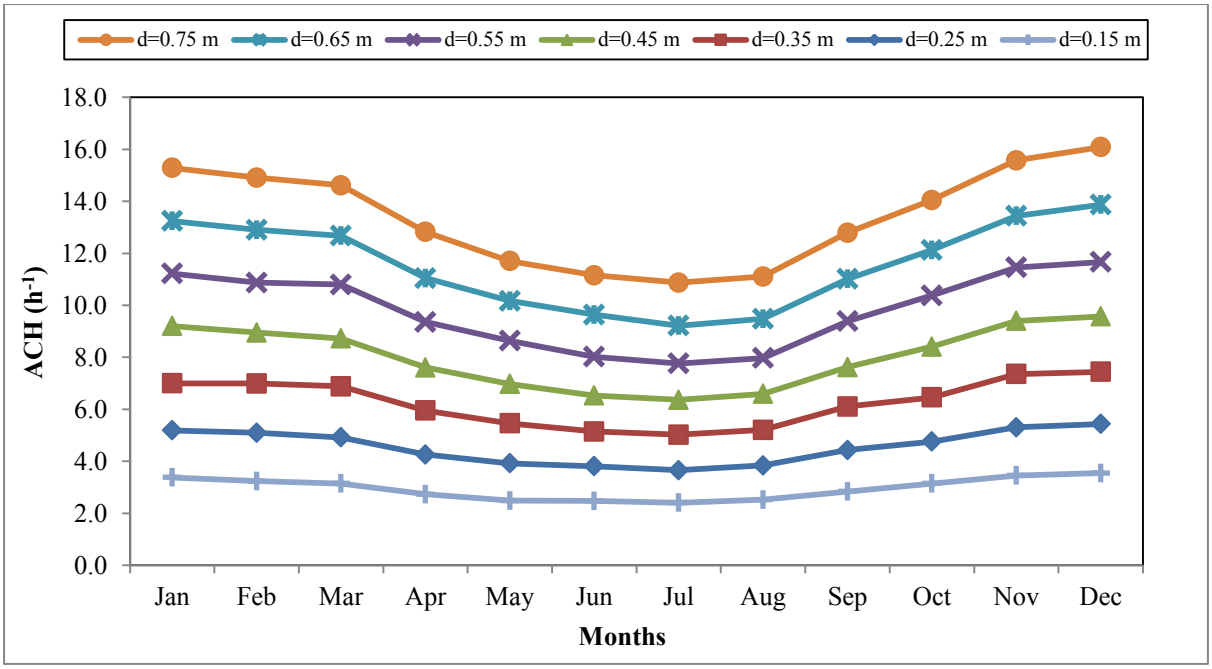

Figure 4.8: Effect of air gap on mean monthly hourly ACH for roof-mounted solar chimney with a tilt angle of 34°; with L_{abs}=L_g=2 m.

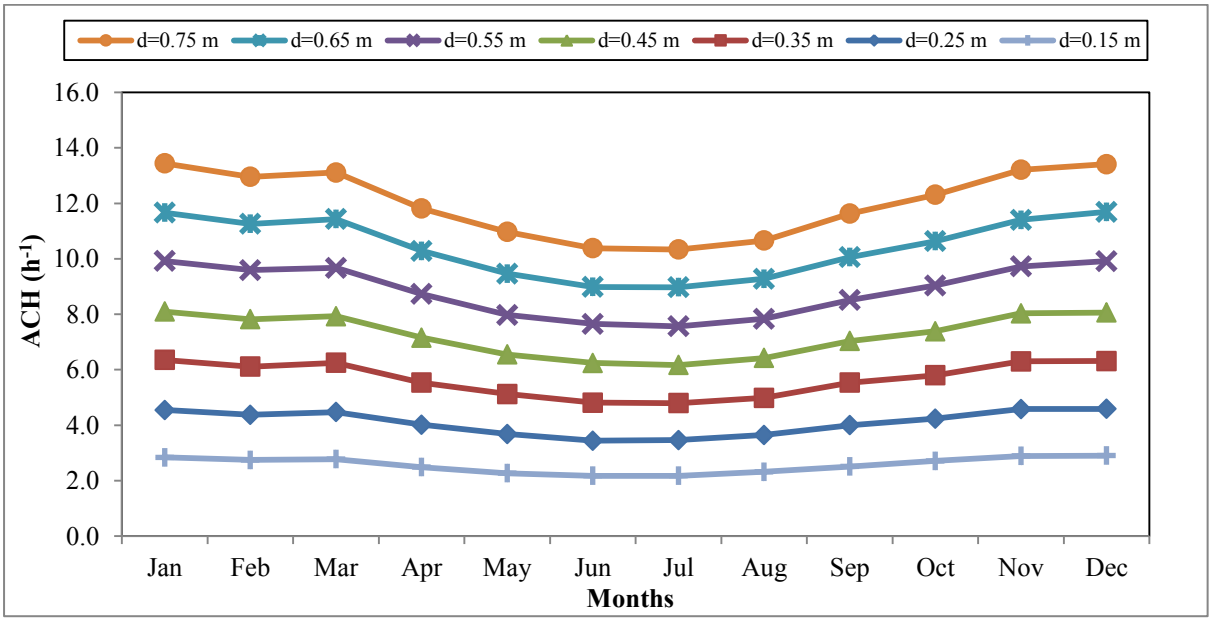

Figure 4.9: Effect of air gap on mean monthly hourly ACH for wall-mounted solar chimney; with L_{abs}=L_g=2 m.

Nonetheless, a few previous studies have revealed different results to that obtained in the context of this investigation. Lee and Strand (2009) found that the ventilation rate actually decreases with an increase in the air gap but they concluded that the air gap had almost no effect on the performance of the chimney since the decrease in ventilation rate with increase in air gap was almost negligible. Moreover, Gan and Riffat (1998) stated that the ventilation rate increases with increase in air gap up to the optimum air gap, but a further increase in air

gap causes the ventilation rate to decrease. They attributed this to the fact that reverse flow occurs within the channel of the solar chimney when the air gap is too large. Additionally, Miyazaki, Akisawa and Kashiwagi (2006) revealed that air flow rate increases with increase in air gap up to an optimum air gap but a further increase in the air gap has negligible effect on the flow rate of air.

4.4 Effect of chimney height on ACH

The length of the absorber wall (and the glass cover) was varied from 0.5 m to 3 m in order to investigate the effects of the chimney height on the ACH. As can be observed from Figure 4.10 and Figure 4.11, an increase in the chimney height causes the ACH to increase for both the roof-mounted and wall-mounted solar chimneys. This can be attributed to the fact that the surface area of the absorber wall increases as the chimney height increases and therefore, more solar radiation can be captured by the absorber wall and thus, more heat can be transferred to the air stream via convection, thereby leading to higher ventilation rates.

It was found that the ACH achieved for the month of December for the roof-mounted solar with a chimney height of 3 m was 6.8 while for a chimney height of 0.5 m, the ACH was 2.5 for the same month, as illustrated by Figure 4.10. On the other hand, the ACH values achieved in December by the wall-mounted solar chimney with chimney heights of 3 m and 0.5 m were 5.7 and 2.3 respectively, as can be observed from Figure 4.11. Consequently, it can be noted that an increase in the chimney height from 0.5 m to 3 m can cause the ventilation rate to increase by more than twofold.

The results obtained in this investigation agree with those obtained from previous studies which also indicated that higher ventilation rates could be achieved when the height of the chimney is increased (Hirunlabh *et al.,* 1999; Afonso & Oliveira, 2000; Ong, 2003; Lee & Strand, 2009; Maerefat & Haghighi, 2010; Al-Kayiem, Sreejaya & Gilani, 2014).

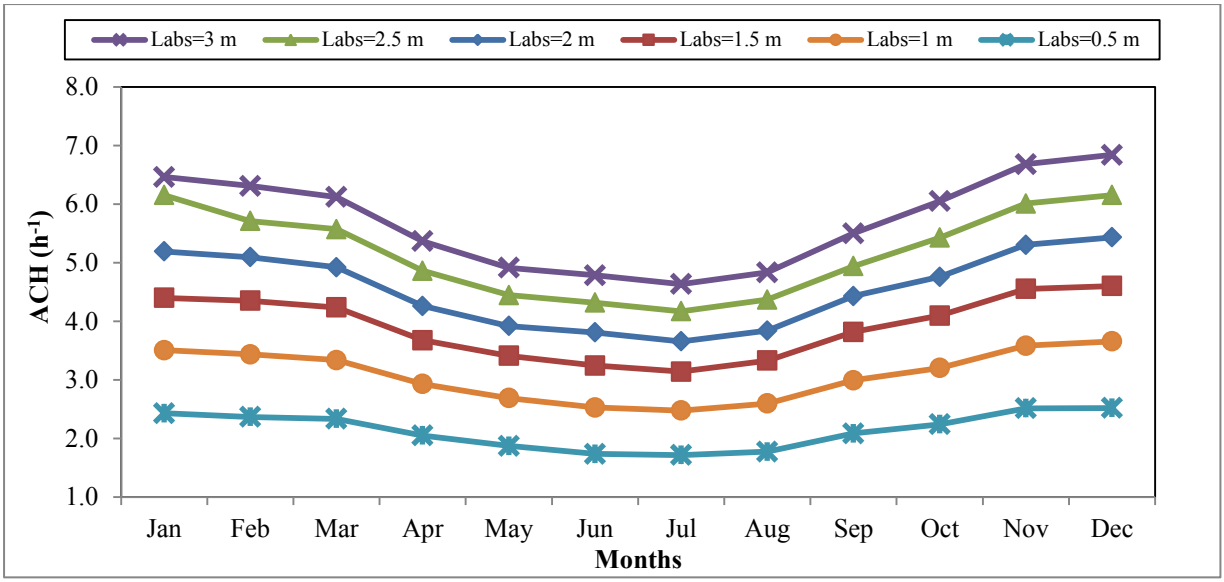

Figure 4.10: Effect of chimney height on mean monthly hourly ACH for roof-mounted solar chimney with tilt angle of 34°; with d= 0.25 m.

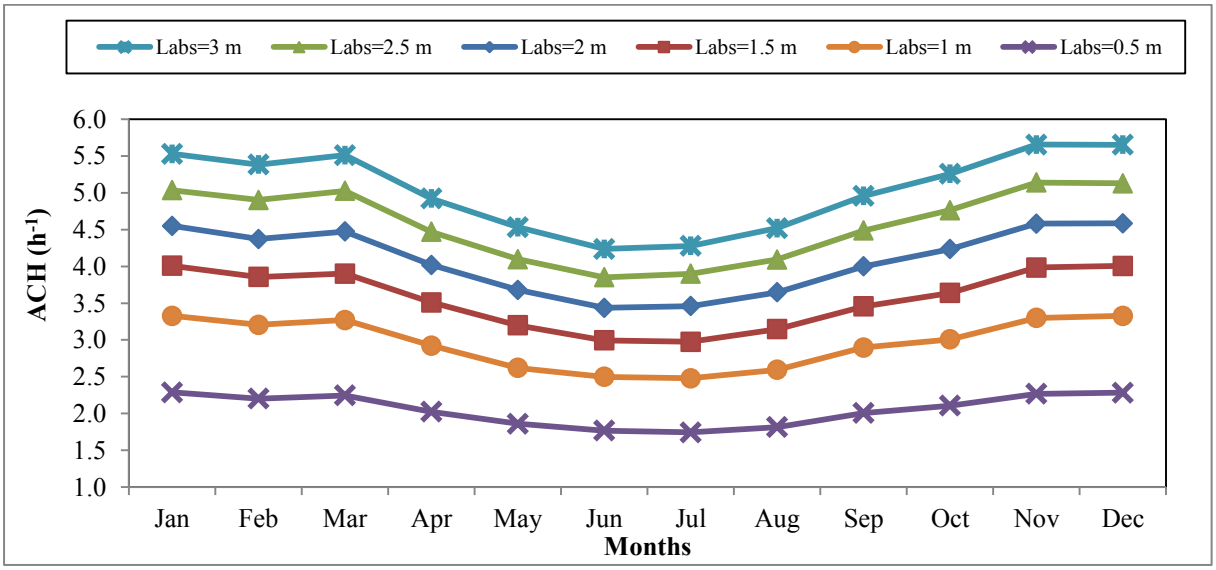

Figure 4.11: Effect of chimney height on mean monthly hourly ACH for wall-mounted solar chimney; with d= 0.25 m.

4.5 Effect of view factor

The view factor is an important parameter to consider when radiative heat is being transferred between two surfaces. The view factor depends on the geometries of the two surfaces exchanging radiative heat and consequently, it affects the rate of radiative heat transfer between the two surfaces. In the context of this research, the effect of view factor was investigated on the radiative heat transfer coefficient between the absorber wall and the glass cover, the temperature of the absorber wall and on ACH.

4.5.1 Effect of view factor on radiative heat transfer coefficient from the absorber wall to the glass cover

It was found that the radiative heat transfer coefficient from the absorber wall to the glass cover is lower when the view factor is taken into consideration as can be observed from Figure 4.12. This can be attributed to the fact that when the view factor is considered, a more realistic value for the amount of radiation leaving the absorber wall that reaches the glass cover is obtained; hence the radiative heat transfer coefficient from the wall to the glass is lower since no overestimation is done concerning the amount of radiation that reaches the glass cover from the absorber wall. A radiative heat transfer coefficient of 6.4 $W/m^2.K$ was obtained for the month of December for the inclined solar chimney when the view factor was ignored, while the coefficient was 4.8 $W/m^2.K$ when the view factor was accounted for. On the other hand, for the vertical solar chimney, during the month of December, it was found that the value for the radiative heat transfer coefficient is 5.3 $W/m^2.K$ without view factor and 3.9 $W/m^2.K$ with view factor. The heat transfer coefficient between the absorber wall and the glass cover was thus found to be more than 30 % lower when the view factor was accounted for.

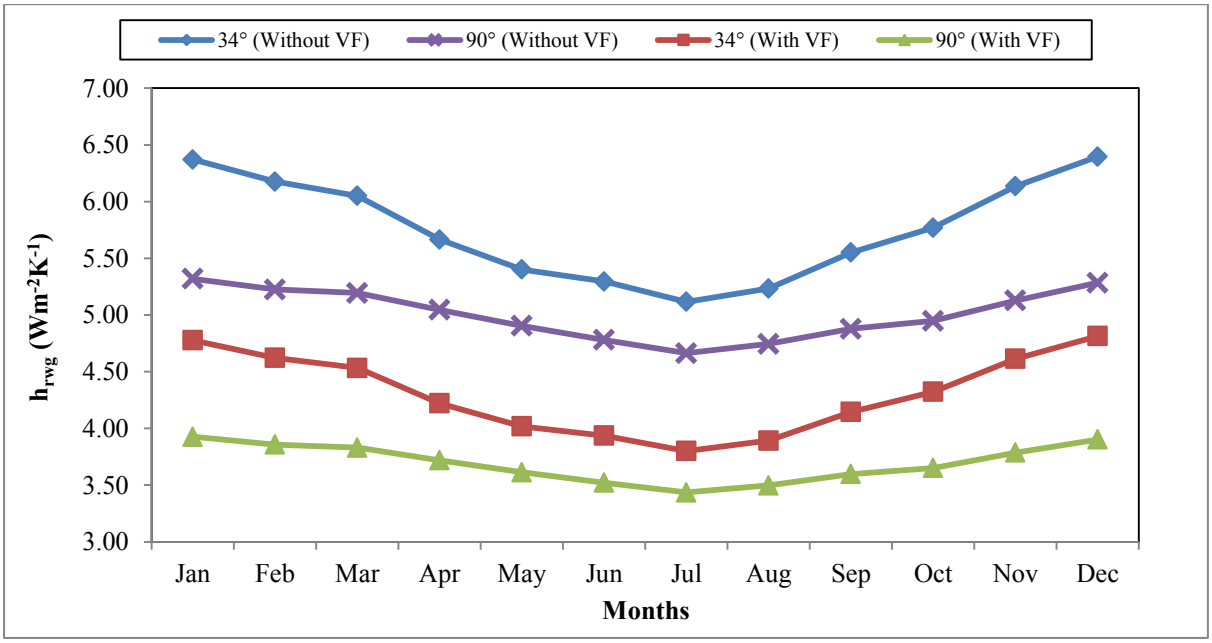

Figure 4.12: Effect of View Factor (VF) on mean monthly hourly radiative heat transfer coefficient from the absorber wall to the glass cover (h_{rwg}) for roof-mounted and wall-mounted solar chimneys; with d=0.25 m and $L_{abs}=L_g=2$ m.

4.5.2 Effect of view factor on absorber wall temperatures

Figure 4.13 shows the effect of view factor on the absorber wall temperatures for the solar chimney with a tilt angle of 34° and for the vertical solar chimney. It can be observed that the absorber wall temperatures are higher when the view factor is taken into consideration. This can be due to the fact that when the view factor is not accounted for, the amount of radiation that reaches the glass cover from the absorber wall is overestimated. Consequently, the amount of radiation that remains on the absorber wall tends to be underestimated, thereby leading to lower values of temperature.

Concerning the inclined solar chimney, for the month of December, it was found that the absorber wall temperature was 58.6 °C when the view factor was taken into consideration while it was only 54.3 °C without the view factor. On the other hand, for the vertical solar chimney, for the month of December, it was found that the temperature was 30.8 °C when the view factor was taken into consideration while it was only 29.8 °C when the view factor was not accounted for. Consequently, it can be observed that the absorber wall temperature was nearly 9 % higher for the inclined solar chimney and only around 3 % higher for the vertical solar chimney when the view factor was taken into account. Therefore, it is to be noted that the effect of view factor has a greater influence on the absorber wall temperature of the inclined solar chimney than the vertical solar chimney. This might be attributed to the fact that the amount of solar radiation captured by the absorber wall of the vertical chimney is much less than that of the inclined solar chimney and thus, a lower impact is observed on the absorber wall temperature of the vertical solar chimney.

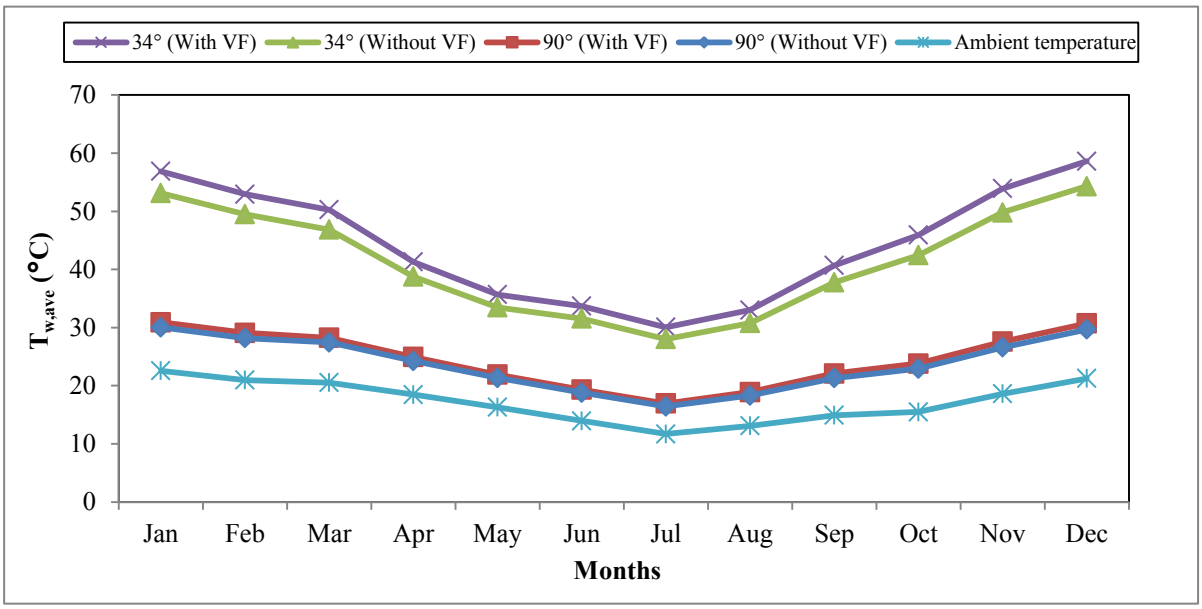

Figure 4.13: Effect of View Factor (VF) on mean monthly hourly absorber wall temperature for roof-mounted and wall-mounted solar chimneys; with d=0.25 m and Labs=Lg=2 m.

4.5.3 Effect of view factor on ACH

The ACH was found to be slightly higher for both the inclined and the vertical solar chimneys when the view factor was taken into consideration as can be depicted from Figure 4.14. It was found that the inclined solar chimney produced an ACH of 5.6 in December when the view factor was considered and an ACH of 5.4 without taking into consideration the view factor. For the vertical solar chimney, an ACH of 4.7 was obtained in December with view factor while a value of 4.5 was obtained for the ACH without the view factor. It can thus be deduced that the ACH is around 4 % higher when the view factor is considered for both the vertical and the inclined solar chimneys. This can be attributed to the fact that more heat can be transferred to the air stream when the view factor is considered and consequently, this causes a higher increase in the fluid temperature, which then causes a higher density difference which leads to a higher pressure difference and thus, more air can be expelled out of the solar chimney. Therefore, the ventilation rate is higher when the view factor is taken into account.

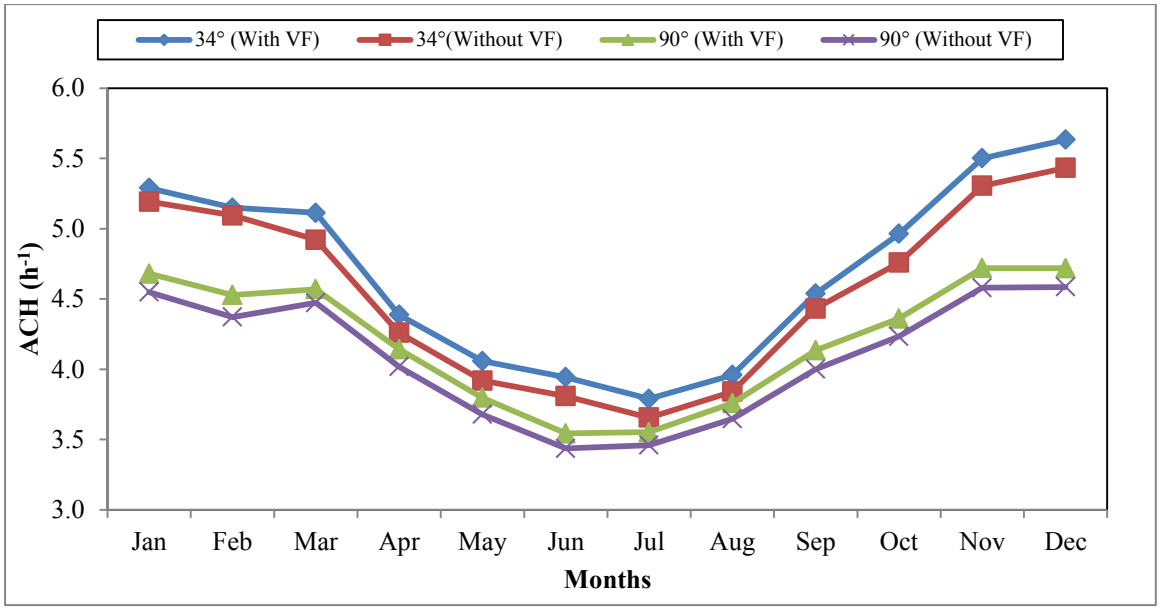

Figure 4.14: Effect of view factor on mean monthly hourly ACH for roof-mounted and wall-mounted solar chimneys; with d=0.25 m and L_{abs}=L_g=2 m.

4.5.5 Effect of view factor on ACH for different values of air gap

The effect of the view factor on ACH for different values of air gap was also investigated. Graphs of ACH for different values of air gap were plotted when the view factor was accounted for, as well as when the view factor was ignored so as to investigate the effect of view factor on ACH for different values of air gap.

Figure 4.15 and Figure 4.16 show the effect of view factor on ACH for different values of air gaps for the roof-mounted and wall-mounted solar chimney respectively. It was found that the effect of the view factor becomes more significant as the air gap increases as can be observed by the increasing distance between the curves as the air gap increases. For the roof-mounted solar chimney, the ACH value achieved in December with an air gap of 0.75 m with the view factor was 16.8 while the ACH achieved with the same air gap without the view factor was only 16.1. On the other hand, for the same month, the ACH achieved with an air gap of 0.15 m with view factor was 3.6, which was the same as that obtained with an air gap of 0.15 m without the view factor, as can be observed from Figure 4.15. Furthermore, for the wall-mounted solar chimney, an ACH of 14.7 was achieved in December with an air gap of 0.75 m with view factor while without the view factor, an ACH of only 13.4 was obtained. For the same month, an ACH of 2.9 was achieved by an air gap of 0.15 m when the view factor was considered, as well as when the view factor was ignored.

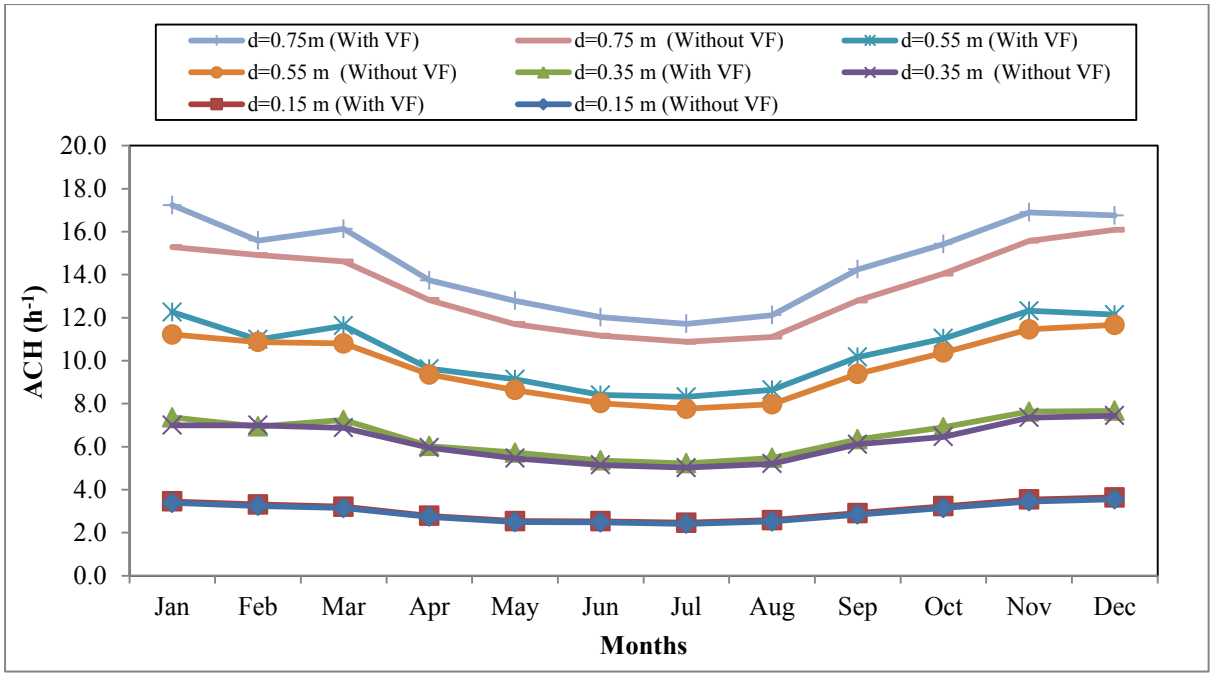

Figure 4.15: Effect of View Factor (VF) on mean monthly hourly ACH for varying air gaps for roof-mounted solar chimney with tilt angle of 34° and L_{abs}=L_g=2 m.

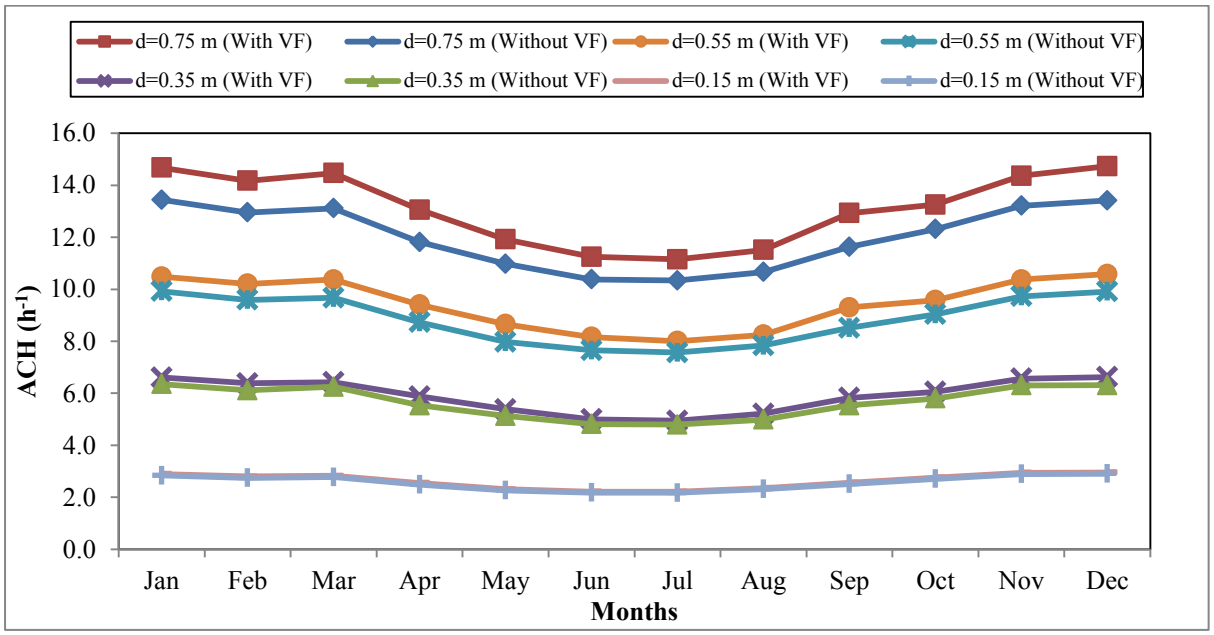

Figure 4.16: Effect of view factor on mean monthly hourly ACH for varying air gaps for wall-mounted solar chimney with L_{abs}=L_g=2 m.

4.5.6 Effect of view factor on ACH for different values of chimney height

Figure 4.17 and Figure 4.18 illustrate the effect of view factor on ACH for varying chimney heights. It can be observed that the ACH values are slightly higher when the view factor is taken into account for both the roof-mounted and wall-mounted solar chimneys. For the roof-mounted solar chimney with a chimney height of 3 m, an ACH of 7.1 was achieved in December when the view factor was accounted for, while an ACH of only 6.8 was achieved for the same month when the view factor was ignored as can be observed from Figure 4.17. On the other hand, for the vertical solar chimney with a chimney height of 3 m, an ACH of 5.8 was achieved in December when the view factor was considered while an ACH of 5.7 was obtained when the ACH was ignored as illustrated in Figure 4.18.

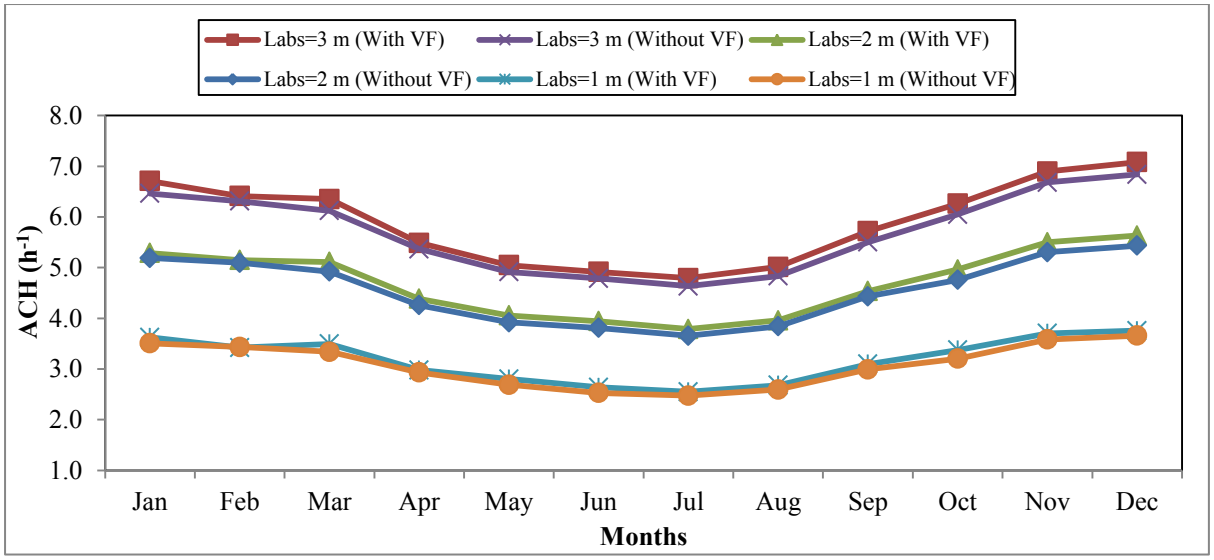

Figure 4.17: Effect of view factor on mean monthly hourly ACH for varying chimney heights for roof-mounted solar chimney with tilt angle of 34° and d=0.25 m.

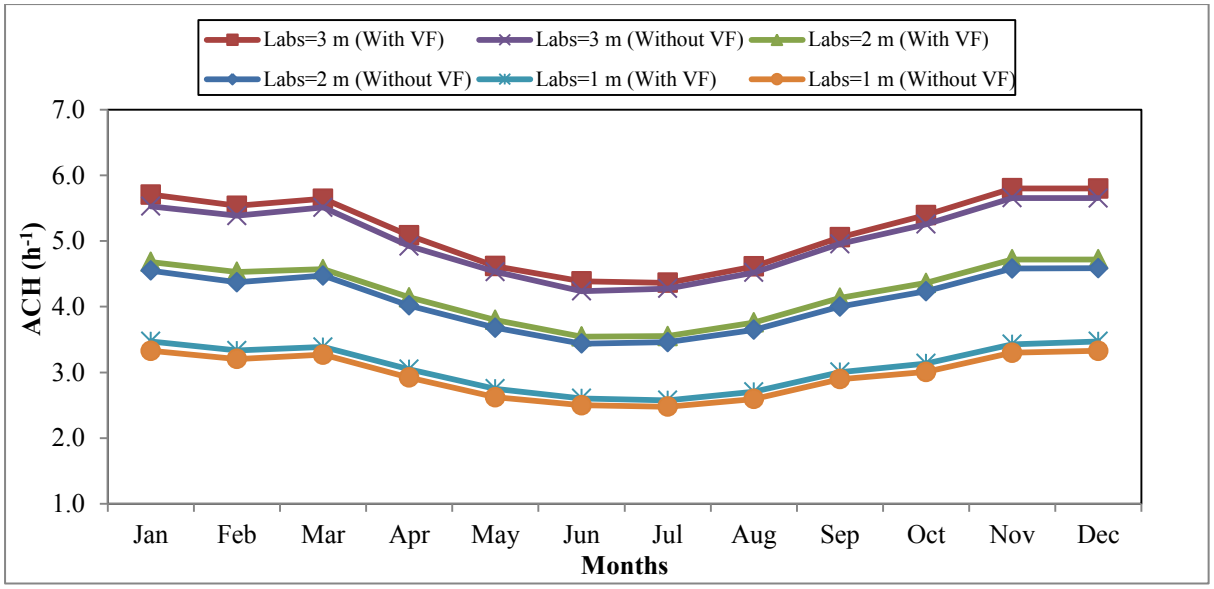

Figure 4.18: Effect of view factor on mean monthly hourly ACH for varying chimney heights for wall-mounted solar chimney with d=0.25 m.

It can also be observed that the view factor becomes more significant as the chimney height increases as represented by the increasing distance between the curves from Figure 4.17 and Figure 4.18. For a chimney height of 1 m, the ACH curve with view factor almost overlaps with the ACH curve without view factor. However, as the chimney height increases, the distance between the curves increases, showing that the effect of the view factor is more pronounced.

Chapter 5

CONCLUSIONS AND RECOMMENDATIONS

The importance of natural ventilation in buildings was discussed in Chapter 1. It was mentioned that a solar chimney can provide a successful means of minimising the electricity consumption associated with mechanical ventilation in buildings, thereby reducing the consumption of fossil fuels in an attempt to contribute towards the mitigation of climate change. The aim of this study was to assess the thermal performance of roof – mounted (inclined) solar chimneys and wall – mounted (vertical) solar chimneys. In order to achieve this aim, the following objectives were stipulated: (a) to design vertical and inclined solar chimneys; (b) to develop a mathematical model for the solar chimneys, based on previous studies done on solar chimneys; (c) to simulate the thermal performance of the solar chimneys and (d) to determine which configuration of the solar chimney is more efficient. The results from the MATLAB simulation were presented and discussed in Chapter 4. In this current chapter, the conclusions and recommendations are scrutinised.

5.1 Conclusions

In this investigation, the angle of inclination with the horizontal was varied from 30° to 90°, the air gap was varied from 0.15 m to 0.75 m and the chimney height was varied from 0.5 m to 3 m. Moreover, as mentioned in Chapter 4, the view factor is most often ignored in the design of solar chimneys and consequently, this study also sought to investigate the effect of the view factor on the thermal performance of the solar chimneys. Based on the results and discussion from Chapter 4, the following conclusions were drawn:

5.1.1 Validation of mathematical model

It was found that there is good agreement between the numerical results obtained from this investigation and experimental values obtained from literature. The errors for the inclined solar chimney models were found to be 13 % with the view factor and 20 % without the view factor. Consequently, it can be deduced that the mathematical model developed in this study is valid and that the inclusion of the view factor improves the accuracy of modelling of solar chimneys.

5.1.2 Optimum angle of inclination of solar chimney

It was found that the solar chimney with a tilt angle of 60° could achieve the highest number of air changes per hour (ACH) consistently throughout the whole year while the vertical solar chimney generated the lowest ACH across the whole year. It is thus concluded that the optimum thermal performance of a solar chimney at a location situated at latitude of 34° in the Southern Hemisphere can be achieved when the tilt angle is 60°.

5.1.3 Optimum air gap of solar chimney

In the context of this investigation, it was found that the highest ACH could be achieved with an air gap of 0.75 m; it was observed that the ACH increases with an increase in the air gap for both the roof-mounted and wall-mounted solar chimneys. It can thus be deduced that a solar chimney with a larger air gap gives a better performance as compared to solar chimneys with smaller air gaps.

5.1.4 Optimum chimney height of solar chimney

The highest ACH could be achieved with a chimney height of 3 m; the ACH was found to increase with an increase in the height of the chimney. Therefore, it can be concluded that a solar chimney with a chimney height of 3 m perform better than those with smaller heights.

5.1.5 Importance of view factor in designing solar chimneys

The results from the MATLAB simulation revealed that a higher absorber wall temperature can be achieved when the view factor is taken into consideration, both for the inclined solar chimney and the vertical solar chimney. It was also found that higher values of ACH could be achieved when the view factor is accounted for. Moreover, it was found that the effect of the view factor is more pronounced for larger air gaps and chimney heights. It can thus be deduced that the view factor is an important parameter to be considered in the design of both inclined and vertical solar chimneys as values for ACH tend to be underestimated when the view factor is not taken into consideration. Furthermore, it can also be deduced that the incorporation of the view factor improves the mathematical modelling of a solar chimney by nearly 7 %, based on the model validation.

5.2 Recommendations

In this investigation, it was found that a roof-mounted solar chimney gives a better thermal performance than a corresponding wall-mounted solar chimney. It was also found that a tilt angle of 60° is the optimum angle of inclination for a roof-mounted solar chimney in Stellenbosch. Moreover, it was found that solar chimneys with large values of air gaps and chimney heights lead to higher ventilation rates and also, the view factor is an important parameter to be considered in the design of solar chimneys as the inclusion of the view factor leads to more realistic values for ACH. However, there is a need for further research on this subject and some potential studies which could be done are mentioned below.

5.2.1 Build physical models for the roof-mounted and wall-mounted solar chimneys

Due to the time constraint of this investigation, it was not possible to build prototypes of the solar chimneys in order to assess their performance based on experimental observations. There is a need to build prototypes of the roof-mounted and wall-mounted solar chimneys in order to perform experiments on them and to compare the experimental values with those obtained from this numerical study.

5.2.2 Compare results with other sites

The mathematical model developed in this study could be applied to other sites across South Africa to investigate whether roof-mounted solar chimneys perform better than inclined solar chimneys at these locations. Furthermore, this model could also be used for simulating solar chimneys in any part of the world by changing the geographical parameters.

5.2.3 Use the model to investigate the effect of other parameters on the performance of solar chimneys

The mathematical model developed in this study could be used to investigate the effect of other parameters not considered in this research. For instance, the effect of type of glazing, type of insulation material and thickness of insulation material on the thermal performance of solar chimneys could be investigated.

5.2.4 Perform an economic feasibility study

An economic feasibility study could be carried out in order to investigate how much it would cost to integrate a solar chimney into a building. The mathematical model developed in this investigation could be applied to a real-case scenario. The reduction in the amount of electricity consumed due to the integration of a solar chimney into the building could be

calculated. Moreover, the effect of the type of glass used on the cost of the system could also be investigated.

REFERENCES

AboulNaga, M.M. & Abdrabboh, S.N. 2000. Improving night ventilation into low-rise buildings in hot-arid climates exploring a combined wall-roof solar chimney. *Renewable Energy*. 19(1-2): 47-54. DOI: 10.1016/S0960-1481(99)00014-2

Afonso, C. & Oliveira, A. 2000. Solar chimneys: simulation and experiment. *Energy and Buildings*. 32(1): 71-79. DOI: 10.1016/S0378-7788(99)00038-9

Al-Kayiem, H.H., Sreejaya, K.V. & Gilani, S.I.U. 2014. Mathematical analysis of the influence of the chimney height and collector area on the performance of a roof top solar chimney. *Energy and Buildings*. 68: 305-311. DOI: 10.1016/j.enbuild.2013.09.021

Al-Shemmeri, T. 2010. *Engineering Thermodynamics*. Available: http://bookboon.com/en/engineering-thermodynamics-ebook#download [2015, November 20].

American Society of Heating, Refrigerating and Air-conditioning Engineers. 1999. *Ventilation for Acceptable Indoor Air Quality. Standard 62-1999*. Available: https://gaia.lbl.gov/people/ryin/public/ASHRAE%20Standard%2062-1999%20-%20Ventilation%20for%20Acceptable%20Indoor%20Air%20Quality(1).pdf [2014, November 12].

American Society of Heating, Refrigerating and Air-conditioning Engineers. 2001a. *Ventilation for Acceptable Indoor Air Quality. Standard 62-2001*. Available: http://www.grntch.com/images/ASHRAE_Standard62-01_04_.pdf [2014, November 12].

American Society of Heating, Refrigerating and Air-conditioning Engineers. 2001b. *ASHRAE Handbook Fundamentals*. I-P Edition. Atlanta, United States.

Arce, J., Jiménez, M.J., Guzmán, J.D., Heras, M.R., Alvarez, G. & Xamán, J. 2009. Experimental study for natural ventilation on a solar chimney. *Renewable Energy*. 34(12): 2928-2934. DOI: 10.1016/j.renene.2009.04.026

Atkins, P. 2010. *The laws of thermodynamics: A very short introduction*. United States of America: Oxford University Press, Inc.

Bansal, N.K., Mathur, J., Mathur, S. & Jain, M. 2005. Modeling of window-sized solar chimneys for ventilation. *Building and Environment*. 40(10): 1302-1308. DOI: 10.1016/j.buildenv.2004.10.011

Bansal, N.K., Mathur, R. & Bhandari, M.S. 1993. Solar Chimney for Enhanced Stack Ventilation. *Building and Environment*. 28(3): 373-377. Available: http://www.eprint.iitd.ac.in/bitstream/2074/2258/1/bansalsol93.pdf [2014, October 14].

Bassiouny, R. & Korah, N.S.A. 2009. Effect of solar chimney inclination angle on space flow pattern and ventilation rate. *Energy and Buildings*. 41(2): 190-196. DOI: 10.1016/j.enbuild.2008.08.009

Bassiouny, R. & Koura, N.S.A. 2008. An analytical and numerical study of solar chimney use for natural ventilation. *Energy and Buildings*. 40(5): 865-873. DOI: 10.1016/j.enbuild.2007.06.005

Behar, O., Khellaf, A. & Mohammedi, K. 2015. Comparison of solar radiation models and their validation under Algerian climate – The case of direct irradiance. *Energy Conversion and Management*. 98: 236-251. DOI: 10.1016/j.enconman.2015.03.067

Belfuguais, B. & Larbi, S. 2011. Passive Ventilation System Analysis using Solar Chimney in South of Algeria. *International Journal of Mechanical, Aerospace, Industrial, Mechatronic and Manufacturing Engineering*. 5(10): 30-34. Available: http://waset.org/publications/8155/passive-ventilation-system-analysis-using-solar-chimney-in-south-of-algeria [2015, August 25].

Benghanem, M. 2011. Optimization of tilt angle for solar panel: Case study for Madinah, Saudi Arabia. *Applied Energy*. 88(4): 1427-1433. DOI: 10.1016/j.apenergy.2010.10.001

Bergman, T.L., Lavine, A.S., Incropera, F.P. & DeWitt, D.P. 2011. *Fundamentals of Heat and Mass Transfer*. Rev. 7th ed. United States of America: John Wiley & Sons, Inc.

Bourne, B. 2009. *PVSim and Solar Energy System Performance Modeling*. Available: http://us.sunpower.com/sites/sunpower/files/media-library/white-papers/wp-pvsim-solar-energy-system-performance-modeling.pdf [2015, June 02].

Burek, S.A.M. & Habeb, A. 2007. Air flow and thermal efficiency characteristics in solar chimneys and Trombe Walls. *Energy and Buildings*. 39(2): 128-135. DOI: 10.1016/j.enbuild.2006.04.015

Butt, R. 2009. *Introduction to Numerical Analysis Using Matlab*. United States of America: Jones & Bartlett Learning.

Çengel, Y.A. & Boles, M.A. 2006. *Thermodynamics: An engineering Approach*. Rev. 5th ed. McGraw-Hill.

Chai, T. & Draxler, R.R. 2015. Root mean square error (RMSE) or mean absolute error (MAE)? – Arguments against avoiding RMSE in the literature. *Geoscientific Model Development*. 7: 1247-1250. DOI: 10.5194/gmd-7-1247-2014

Chen, C.J. 2011. *Physics of Solar Energy*. United States of America: John Wiley & Sons, Inc. Available: http://www.vtsnis.edu.rs/Predmeti/obnovljivi_disperzivni_izvori_napajanja/fizika_solarne_energije.pdf [2015, June 02].

Chen, Z.D., Bandopadhayay, P., Halldorsson, J., Byrjalsen, C., Heiselberg, P. & Li, Y. 2003. An experimental investigation of a solar chimney model with uniform wall heat flux. *Building and Environment*. 38(7): 893–906 DOI: 10.1016/S0360-1323(03)00057-X

Cheney, E.W. & Kincaid, D.R. 2009. *Linear Algebra: Theory and Applications*. Massachusetts: Jones & Bartlett Learning.

City of Cape Town. 2014. *Planning and Building Development.* Available: https://www.capetown.gov.za/en/CityHealth/EnviroHealth/PlanningAndBuilding/Pages/PlanningBuildingDevelopment.aspx [2014, October 28].

Da Rosa, A.V. 2005. *Fundamentals of Renewable Energy Processes*. United States of America: Elsevier Academic Press.

DeBlois, J.C., Bilec, M.M. & Schaefer, L.A. 2013. Design and zonal building energy modeling of a roof integrated solar chimney. *Renewable Energy*. 52: 241-250. DOI: 10.1016/j.renene.2012.10.023

Demain, C., Journée, M. & Bertrand, C. 2013. Evaluation of different models to estimate the global solar radiation on inclined surfaces. *Renewable Energy*. 50: 710-721. DOI: 10.1016/j.renene.2012.07.031

Department of Energy. 2009. *Digest of South African Energy Statistics*. Available: http://www.energy.gov.za/files/media/explained/2009%20Digest%20PDF%20version.pdf [2014, November 10].

Department of Minerals and Energy. 2007. *Energy Security Master Plan – Liquid Fuels*. Available: http://www.sapia.co.za/pdf/legislation/Energy%20Security%20Master%20Plan%20-%20Liquid%20Fuels%20-%202007.pdf [2015, February 16].

Duffie, J.A. & Beckman, W.A. 2013. *Solar Energy Thermal Processes.* Rev. 4th ed. United States of America: John Wiley & Sons, Inc.

El-Sebaii, A.A. 2005. Thermal performance of a triple-basin solar still. *Desalination*. 174(1): 23-37. DOI: 10.1016/j.desal.2004.08.038

Encyclopaedia Britannica. 2015. *Cape Town - National legislative capital, South Africa*. Available: http://global.britannica.com/place/Cape-Town [2015, July 06].

European Commission. 2015. *Climate Action.* Available: http://ec.europa.eu/clima/change/consequences/index_en.htm [2015, February 06].

Evseev, E.G. & Kudish, A.I. 2009. The assessment of different models to predict the global solar radiation on a surface tilted to the south. *Solar Energy*. 83(3): 377-388. DOI: 10.1016/j.solener.2008.08.010

Gan, G. & Riffat, S.B. 1998. A numerical study of solar chimney for natural ventilation of buildings with heat recovery. *Applied Thermal Engineering*. 18(12): 1171-1187. DOI: 10.1016/S1359-4311(97)00117-8

Garg, H.P. & Prakash, J. 2000. *Solar Energy Fundamentals and Applications*. Delhi: Tata McGraw-Hill.

Gontikaki, M., Trcka, M., Hensen, J.L.M. & Hoes, P. 2010. Optimization of a solar chimney design to enhance natural ventilation in a multi-storey office building. *Proceedings of 10th International Conference for Enhanced Building Operations, Kuwait: ICEBO.* Available:

https://repository.tamu.edu/bitstream/handle/1969.1/94097/ESL-IC-10-10-50.pdf?sequence=1&isAllowed=y [2014, October 16].

Gonzalez, A., Navia, R. & Moreno, N. 2009. Fly ashes from coal and petroleum coke combustion: current and innovative potential applications. *Waste Management & Research*. 27(10): 976-987. DOI: 10.1177/0734242X09103190.

Gordon, J. 2001. *Solar Energy: The State of the Art*. United Kingdom. James & James (Science Publishers) Ltd.

Goswami, D.Y., Kreith, F. & Kreider, J.F. 2000. *Principles of Solar Engineering*. Rev. 2nd ed. Philadelphia: Taylor & Francis.

Handoyo, E.A., Ichsani, D. & Prabowo. 2013. The optimal tilt angle of a solar collector. *Energy Procedia*. 32: 166-175. DOI: 10.1016/j.egypro.2013.05.022

Harris, D.J. & Helwig, N. 2007. Solar Chimney and building ventilation. *Applied Energy*. 84(2): 135-146. DOI: 10.1016/j.apenergy.2006.07.001

Hewakandamby, B.N. 2012. *A First Course in Fluid Mechanics for Engineers*. Available: http://bookboon.com/en/a-first-course-in-fluid-mechanics-for-engineers-ebook [2015, February 10].

Hirunlabh, J., Kongduang, P., Namprakai, P. & Khedari, J. 1999. Study of natural ventilation of houses by a metallic solar wall under tropical climate. *Renewable Energy*. 18(1): 109-119. DOI: 10.1016/S0960-1481(98)00783-6

Hoffbeck, J.P., Sarwar, M. & Rix, E.J. 2001. Interfacing MATLAB with a parallel virtual processor for matrix algorithms. *Journal of Systems and Software*. 56(1): 77-80. DOI: 10.1016/S0164-1212(00)00087-X

Holman, J.P. 2010. *Heat Transfer*. Rev. 10th ed. Singapore: McGraw Hill.

Imran, A.A., Jalil, J.M. & Ahmed, S.T. 2015. Induced flow for ventilation and cooling by a solar chimney. *Renewable Energy*. 78: 236–244. DOI: 10.1016/j.renene.2015.01.019

Intergovernmental Panel on Climate Change. 2012. *Managing the risks of extreme events and disasters to advance climate change adaptation*. Available: https://www.ipcc.ch/pdf/special-reports/srex/SREX_Full_Report.pdf [2015, August 12].

Intergovernmental Panel on Climate Change. 2013. *Sea Level Change*. Available: http://www.ipcc.ch/pdf/assessment-report/ar5/wg1/WG1AR5_Chapter13_FINAL.pdf [2015, August 12].

International Energy Agency. 2013a. *Key World Energy Statistics*. Available: http://www.iea.org/publications/freepublications/publication/KeyWorld2013.pdf [2014, November 10].

International Energy Agency. 2013b. *Transition to Sustainable Buildings*. Available: http://www.iea.org/media/training/presentations/etw2014/publications/Sustainable_Buildings_2013.pdf [2015, August 08].

International Energy Agency. 2014. *Energy efficiency*. Available: http://www.iea.org/aboutus/faqs/energyefficiency/ [2014, November 10].

International Energy Agency. 2015a. *Building Energy Efficiency Policies*. Available: http://www.iea.org/beep/South%20Africa/ [2015, August 08].

International Energy Agency. 2015b. *Energy security*. Available: http://www.iea.org/topics/energysecurity/subtopics/whatisenergysecurity/ [2015, February 10].

Jaluria, Y. 2011. *Computer Methods for Engineering with MATLAB Applications*. Rev. 2nd ed. United States of America: Taylor & Francis.

Jianliu, X. & Weihua, L. 2013. Study on solar chimney used for room natural ventilation in Nanjing. *Energy and Buildings.* 66: 467-469. DOI: 10.1016/j.enbuild.2013.07.036

Jing, H., Chen, Z. & Li, A. 2015. Research for the Ventilation Properties of Solar Chimney with Vertical Collector. *Procedia Environmental Sciences*. 11: 1072-1077. DOI: 10.1016/j.proenv.2011.12.162

Jones, W.P. 1994. *Air Conditioning Engineering*. Rev. 4th ed. Great Britain: Arnold.

Kalogirou, S.A. 2014. *Solar Energy Engineering Processes and Systems*. Rev. 2nd ed. United States of America: Elsevier Inc.

Khalil, S.A. & Shaffie, A.M. 2013. A comparative study of total, direct and diffuse solar irradiance by using different models on horizontal and inclined surfaces for Cairo, Egypt.

Renewable and Sustainable Energy Reviews. 27: 853-863. DOI: 10.1016/j.rser.2013.06.038

Khan, N., Su, Y. & Riffat, S.B. 2008. A review on wind driven ventilation techniques. *Energy and Buildings.* 40(8): 1586-1604. DOI:10.1016/j.enbuild.2008.02.015

Khanal, R. & Lei, C. 2011. Solar chimney-A passive strategy for natural ventilation. *Energy and Buildings.* 43(8): 1811-1819. DOI: 10.1016/j.enbuild.2011.03.035.

Khanal, R. & Lei, C. 2014. A scaling investigation of the laminar convective flow in a solar chimney for natural ventilation. *International Journal of Heat and Fluid Flow*. 45: 98-108. DOI: 10.1016/j.ijheatfluidflow.2013.11.002

Khedari, J., Hirunlabh, J. & Bunnag, T. 1997. Experimental study of a roof solar collector towards the natural ventilation of new houses. *Energy and Buildings.* 26(2): 159-164. DOI: 10.1016/S0378-7788(96)01030-4

Larbi, S. Hella, A.E. 2013. Thermo-fluid aspect analysis of passive cooling system case using solar chimney in the south regions of Algeria. *Energy Procedia*. 36: 628-637. DOI: 10.1016/j.egypro.2013.07.072

Lee, D.S., Hung, T.C., Lin, J.R. & Zhao, J. 2015. Experimental investigations on solar chimney for optimal heat collection to be utilized in organic Rankine cycle. *Applied Energy*. 154: 651–662. DOI: 10.1016/j.apenergy.2015.05.079

Lee, K.H. & Strand, R.K. 2009. Enhancement of natural ventilation in buildings using a thermal chimney. *Energy and Buildings*. 41(6): 615-621. DOI: 10.1016/j.enbuild.2008.12.006

Li, Y. & Liu, S. 2014. Experimental study on thermal performance of a solar chimney combined with PCM. *Applied Energy*. 114: 172-178. DOI: 10.1016/j.apenergy.2013.09.022

Long, C. & Sayma, N. 2009. *Heat Transfer*. Available: http://bookboon.com/en/heat-transfer-ebook [2014, October 14].

Madhlopa, A. 2009. *Development of an advanced passive solar still with separate condenser.* Ph.D. Thesis. University of Strathclyde. Available: http://www.esru.strath.ac.uk/Documents/PhD/madhlopa.pdf [2015, June 29].

Madhlopa, A., Sparks, D., Keen, S., Moorlach, M., Krog, P. & Dlamini, T. 2015. Optimisation of a PV-wind hybrid system under limited water resources. *Renewable and Sustainable Energy Reviews*. 47: 324-331. DOI: 10.1016/j.rser.2015.03.051

Maerefat, M. & Haghighi, A.P. 2010. Passive cooling of buildings by using integrated earth to air heat exchanger and solar chimney. *Renewable Energy*. 35(10): 2316-2324.

Manz, O.E. 1997. Worldwide production of coal ash and utilization in concrete and other products. *Fuel*. 76(8): 691-696. DOI: 10.1016/S0016-2361(96)00215-3

Maor, T. & Appelbaum, J. 2012. View factors of photovoltaic collector systems. *Solar Energy*. 86(6): 1701-1708. DOI: 10.1016/j.solener.2012.03.017

Marti-Herrero, J. & Heras-Celemin, M.R. 2007. Dynamic physical model for a solar chimney. *Solar Energy*. 81(5): 614-622. DOI: 10.1016/j.solener.2006.09.003

Mathur, J., Bansal, N.K., Mathur, S., Jain, M. & Anupma. 2006. Experimental investigations on solar chimney for room ventilation. *Solar Energy*. 80(8): 927-935. DOI: 10.1016/j.solener.2005.08.008

Mathur, J., Mathur, S. & Anupma. 2006. Summer-performance of inclined roof solar chimney for natural ventilation. *Energy and Buildings*. 38(10): 1156-1163. DOI: 10.1016/j.enbuild.2006.01.006

McDowall, R. 2007. *Fundamentals of HVAC systems*. Great Britain: Academic Press.

Meawad, A.S., Bojinova, Y. & Pelovski. Y.G. 2010. An overview of metals recovery from thermal power plant solid wastes. *Waste Management.* 30(12): 2548-2559. DOI: 10.1016/j.wasman.2010.07.010

Miyazaki, T., Akisawa, A. & Kashiwagi, T. 2006. The effects of solar chimneys on thermal load mitigation of office buildings under the Japanese climate. *Renewable Energy*. 31(7): 987-1010. DOI: 10.1016/j.renene.2005.05.003

Mohammadi, K. & Khorasanizadeh, H. 2015. A review of solar radiation on vertically mounted solar surfaces and proper azimuth angles in six Iranian major cities. *Renewable and Sustainable Energy Reviews*. 47: 504-518. DOI: 10.1016/j.rser.2015.03.037

Moore, H. 2012. *MATLAB for Engineers*. Rev. 3rd ed. United States of America: Pearson Education, Inc.

Mora-Pérez, M., Guillén-Guillamón, I. & López-Jiménez, P.A. 2015. Computational analysis of wind interactions for comparing different buildings sites in terms of natural ventilation. *Advances in Engineering Software*. 88: 73-82. DOI: 10.1016/j.advengsoft.2015.06.003

Myers, D.R. 2013. *Solar Radiation. Practical Modeling for Renewable Energy Applications*. CRC Press. Available: https://www.crcpress.com/product/isbn/9781466502949 [2015, June 03].

Nag, P.K. 2008. *Engineering Thermodynamics*. Rev. 4th ed. New Delhi: Tata McGraw-Hill.

National Aeronautics and Space Administration. 2011. *How do photovoltaics work?* Available: http://science.nasa.gov/science-news/science-at-nasa/2002/solarcells/ [2015, February 10].

National Physical Laboratory. 2015. *Thermal conductivities.* Available: http://www.kayelaby.npl.co.uk/general_physics/2_3/2_3_7.html [2015, February 10].

Ng, M.O., Qu, M., Zheng, P., Li, Z. & Hang, Y. 2011. CO_2-based demand controlled ventilation under new ASHRAE Standard 62.1-2010: a case study for a gymnasium of an elementary school at West Lafayette, Indiana. *Energy and Buildings.* 43(11): 3216-3225. DOI: 10.1016/j.enbuild.2011.08.021

Nouanégué, H.F. & Bilgen, E. 2009. Heat transfer by convection, conduction and radiation in solar chimney systems for ventilation of dwellings. *International Journal of Heat and Fluid Flow*. 30(1): 150-157. DOI: 10.1016/j.ijheatfluidflow.2008.08.006

Ong, K.S. & Chow, C.C. 2003. Performance of a solar chimney. *Solar Energy*. 74(1): 1-17. DOI: 10.1016/S0038-092X(03)00114-2

Ong, K.S. 2003. A mathematical model of a solar chimney. *Renewable Energy*. 28(7): 1047–1060. DOI: 10.1016/S0960-1481(02)00057-5

Persily, A. 2015. Challenges in developing ventilation and indoor air quality standards: The story of ASHRAE Standard 62. *Building and Environment*. 91: 61-69. DOI: 10.1016/j.buildenv.2015.02.026

Popoola, O.M. & Burnier, C. 2014. Solar water heater contribution to energy savings in higher education institutions: Impact analysis. *Journal of Energy in Southern Africa*. 25(1): 51-58. Available: http://www.erc.uct.ac.za/jesa/volume25/25-1jesa-popoola-burnier.pdf [2015, February 10].

Razika, I., Nabila, I., Madani, B. & Zohra, H.F. 2014. The effects of volumetric flow rate and inclination angle on the performance of a solar thermal collector. *Energy Conservation and Management.* 78: 931-937. DOI: 10.1016/j.enconman.2013.09.051

Sailor, D.J., Resh, K. & Segura, D. 2006. Field measurement of albedo for limited extent test surfaces. *Solar Energy*. 80(5): 589-599. DOI: 10.1016/j.solener.2005.03.012

Sakonidou, E.P., Karapantsios, T.D., Balouktsis, A.I. & Chassapis, D. 2008. Modeling of the optimum tilt of a solar chimney for maximum air flow. *Solar Energy*. 82(1): 80-94. DOI: 10.1016/j.solener.2007.03.001

Santamouris, M. & Kolokotsa, D. 2013. Passive cooling dissipation techniques for buildings and other structures: The state of the art. *Energy and Buildings.* 57: 74-94. DOI: 10.1016/j.enbuild.2012.11.002

Sen, S.K. & Shaykhian, G.A. 2009. MatLab tutorial for scientific and engineering computations: International Federation of Nonlinear Analysts (IFNA); 2008 World Congress of Nonlinear Analysts (WCNA). *Nonlinear Analysis: Theory, Methods and Applications.* 71(12): 1005-1020. DOI: 10.1016/j.na.2009.01.069

South Africa Bureau of Standards. 2011. *The application of the National Building Regulations. Part O: Lighting and ventilation.* SANS 10400-O: 2011. Available: https://law.resource.org/pub/za/ibr/za.sans.10400.o.2011.html [2015, August 05].

South African Weather Service. 2015. *How are the dates of the four seasons worked out?* Available: http://www.weathersa.co.za/learning/weather-questions/82-how-are-the-dates-of-the-four-seasons-worked-out [2015, August 19].

Suárez-López, M.J., Blanco-Marigorta, A.M., Gutiérrez-Trashorras, A.J., Pistono-Favero, J. & Blanco-Marigorta, E. 2015. Numerical simulation and exergetic analysis of building ventilation solar chimneys. *Energy Conversion and Management*. 96: 1-11. DOI: 10.1016/j.enconman.2015.02.049

Tang, R. & Wu, T. 2004. Optimal tilt-angles for solar collectors used in China. *Applied Energy*. 79(3): 239-248. DOI: 10.1016/j.apenergy.2004.01.003

Tian, Y. & Zhao, C.Y. 2013. A review of solar collectors and thermal energy storage in solar thermal applications. *Applied Energy*. 104: 538–553. DOI: 10.1016/j.apenergy.2012.11.051

Tripathi, R. & Tiwari, G.N. 2004. Performance evaluation of a solar still by using the concept of solar fractionation. *Desalination*. 169(1): 69-80. DOI: 10.1016/j.desal.2004.08.008

Trollip, H., Butler, A., Burton, J. Caetano, T. & Godinho, C. 2014. *Energy Security in South Africa.* Available: http://www.mapsprogramme.org/wp-content/uploads/Energy-Security_in-South-Africa.pdf [2015, February 17].

United Nations Environment Programme. 2009. *Greenhouse Gas Emission Baselines and Reduction Potentials from Buildings in South Africa*. Available: http://www.unep.org/sbci/pdfs/SBCI-SAreport.pdf [2015, February 13].

US Department of Energy. 2003. *Improving Fan System Performance - a sourcebook for industry*. Available: https://www1.eere.energy.gov/manufacturing/tech_assistance/pdfs/fan_sourcebook.pdf [2015, February 19].

Wang, S.K. 2001. *Handbook of Air Conditioning and Refrigeration.* United States of America: McGraw-Hill. Available: http://www.gmpua.com/CleanRoom/HVAC/Cooling/Handbook%20of%20Air%20Conditioning%20and%20Refrigeration.pdf [2015, February 18].

Wang, S.K., Lavan, Z. & Norton, P. 2000. *Air Conditioning and Refrigeration Engineering.* United States of America: CRC Press.

Welty, J.R., Wicks, C.E., Wilson, R.E. & Rorrer, G.L. 2008. *Fundamentals of Momentum, Heat and Mass Transfer.* 5th ed. United States of America: John Wiley & Sons, Inc.

Winterbone, D.E. & Turan, A. 2015. *Advanced Thermodynamics for Engineers*. Rev. 2nd ed. United States of America: Butterworth-Heinemann.

Wlodarczyk, D. & Nowak, H. 2009. Statistical analysis of solar radiation models onto inclined planes for climatic conditions of Lower Silesia in Poland. *Archives of Civil and Mechanical Engineering*. 9(2): 127-144. DOI: 10.1016/S1644-9665(12)60064-8

World Health Organization. 2009. *Natural Ventilation for Infection Control in Health-Care Settings.* Available: http://www.ncbi.nlm.nih.gov/books/NBK143277/ [2015, November 20].

Yadav, A.K. & Chandel, S.S. 2013. Tilt angle optimization to maximize incident solar radiation: A review. *Renewable and Sustainable Energy Reviews*. 23: 503-513. DOI: 10.1016/j.rser.2013.02.027

Yan, Z., Guang-e, J., Xiao-hui, L. & Qing-ling, L. 2011. Research for Ventilation Properties of Solar Chimney with Vertical Collector. *Procedia.* 11(C): 1072-1077. DOI: 10.1016/j.proenv.2011.12.162

Zhai, X.Q., Song, Z.P. & Wang, R.Z. 2011. A review of the applications of solar chimneys in buildings. *Renewable and Sustainable Energy Reviews*. 15(8): 3757-3767. DOI: 10.1016/j.rser.2011.07.013

Zhou, L., Wang, B., Peng, X., Du, X. & Yang, Y. 2010. On the Specific Heat Capacity of CuO Nanofluid. *Advances in Mechanical Engineering*. 2: 1-4. DOI: 10.1155/2010/172085

Ziervogel, G., New, M., van Garderen, E.A., Midgley, G., Taylor, A., Hamann, R., Stuart-Hill, S., Myers, J. et al. 2014. Climate change impacts and adaptation in South Africa. *WIREs Climate Change*. 5: 605-620. DOI: 10.1002/wcc.295

APPENDICES

Appendix A: Correlations for calculating temperature-dependent properties

a) Air Density

The density of a substance is defined as the ratio of its mass to its volume, commonly expressed in its SI unit of kg/m^3. Values of air density were obtained from Welty et al. (2008: 679) for temperatures ranging from 250 K to 1000 K. A graph of air density against temperature was then plotted in Excel. A trend line was used to fit the data on a curve. Various trend lines of polynomial functions of orders 2, 3, 4 and 5 respectively were made to fit the data on a curve. It was found that a polynomial function of order 5 provided the best fit since the coefficient of determination, also known as the R-squared value, was 1 in this case. Figure A1 shows the relationship between the density of air and temperature.

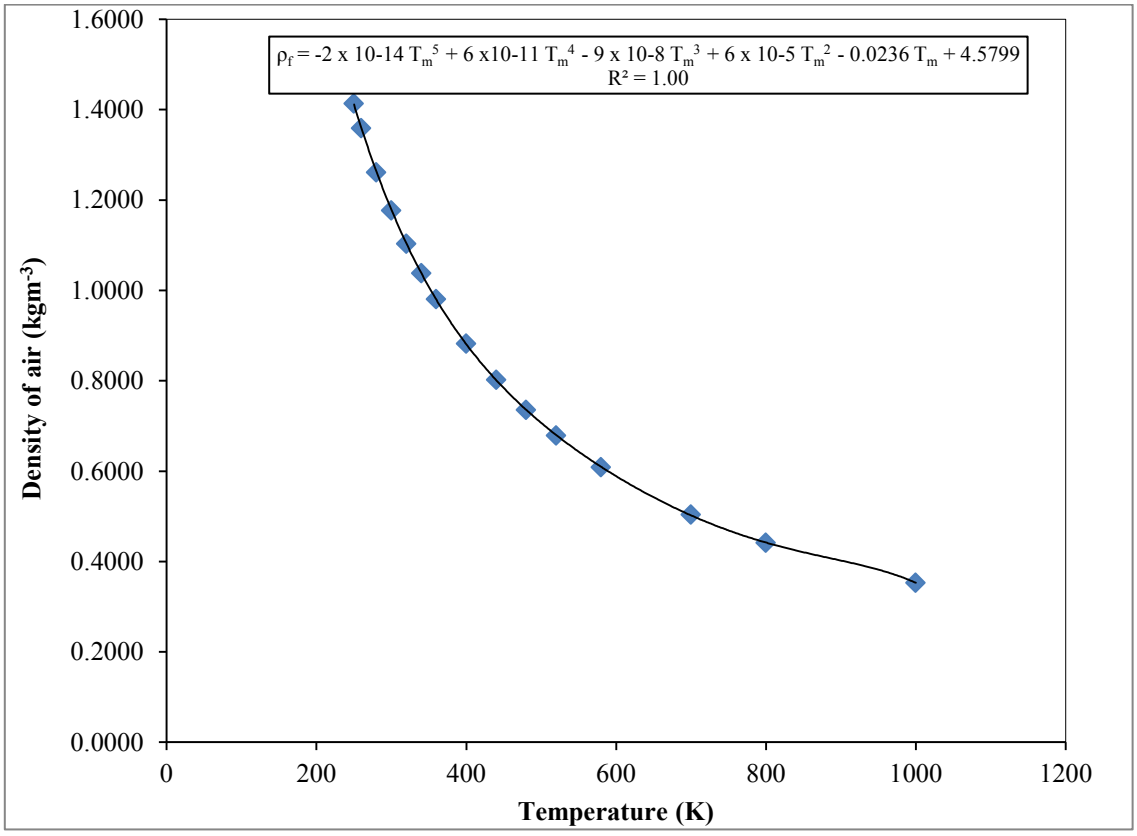

Figure A1: Variation of air density with temperature

The correlation equation relating air density with temperature (over a temperature range of 250 K to 1000 K) is thus given as follows:

For glass cover and air stream,

$$\rho_f = (-2 * 10^{-14})\, T_m^5 + (6 * 10^{-11})\, T_m^4 - (9 * 10^{-8})\, T_m^3 + (6 * 10^{-5})\, T_m^2 - 0.0236\, T_m + 4.5799 \tag{A.1}$$

Where, T_m is referred to as the mean temperature and is given as follows:

$$T_m = \frac{T_g + T_f}{2} \tag{A.2}$$

For absorber wall and air stream,

$$\rho_{f1} = (-2 * 10^{-14})\, T_{m1}^5 + (6 * 10^{-11})\, T_{m1}^4 - (9 * 10^{-8})\, T_{m1}^3 + (6 * 10^{-5})\, T_{m1}^2 - 0.0236\, T_{m1} + 4.5799 \tag{A.3}$$

$$T_{m1} = \frac{T_w + T_f}{2} \tag{A.4}$$

The same method as described above was used to obtain correlations for specific heat capacity, dynamic viscosity and thermal conductivity of air.

b) Specific heat capacity of air

The specific heat capacity of a substance is defined as the amount of energy required to change the temperature of 1 kilogram of the substance by 1 kelvin (Zhou *et al*., 2010: 2). The specific heat capacity is usually expressed in its SI unit of $Jkg^{-1}K^{-1}$. The relationship between the specific heat capacity of air and temperature (from 250 K to 1000 K) is shown in Figure A2.

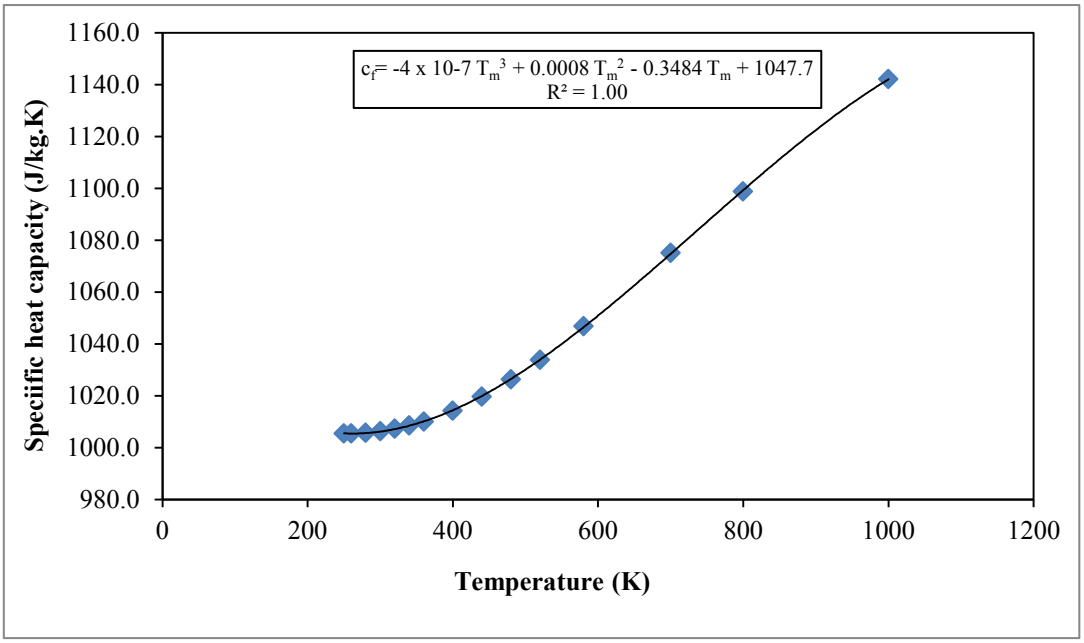

Figure A2: Variation of specific heat capacity of air with temperature

For this property, it was found that a polynomial function of order 3 gives an R-squared value of 1. Therefore, the relationship between the specific heat capacity of air and temperature over a range of 250 K to 1000 K can be expressed as follows:

For glass cover and air stream,

$$c_f = (-4 * 10^{-7})\, T_m^3 + 0.0008\, T_m^2 - 0.3484\, T_m + 1047.7 \qquad \text{(A.5)}$$

For absorber wall and air stream,

$$c_{f1} = (-4 * 10^{-7})\, T_{m1}^3 + 0.0008\, T_{m1}^2 - 0.3484\, T_{m1} + 1047.7 \qquad \text{(A.6)}$$

c) Dynamic viscosity of air

The viscosity of a fluid is a measure of its resistance to flow (Al-Shemmeri, 2012: 15). The dynamic viscosity is usually denoted by μ, and commonly expressed in units of Pa.s. Figure A3 shows the relationship between dynamic viscosity of air and temperature.

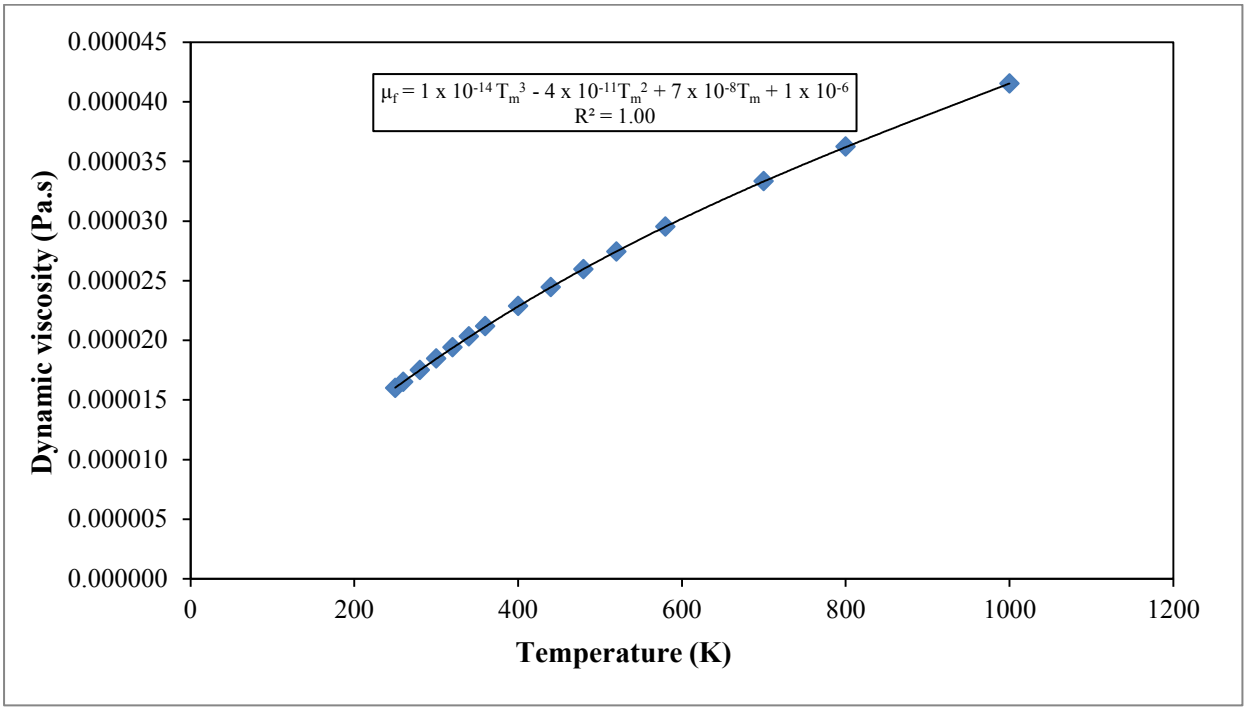

Figure A3: Variation of dynamic viscosity of air with temperature

A polynomial function of order 3 was found to be the best fit for the data and thus, the equation showing the relationship between dynamic viscosity of air and temperature is given as follows:

For glass cover and air stream,

$$\mu_f = (1 * 10^{-14})\, T_m^3 - (4 * 10^{-11})\, T_m^2 + (7 * 10^{-8})\, T_m + (1 * 10^{-6}) \qquad \text{(A.7)}$$

For absorber wall and air stream,

$$\mu_{f1} = (1 * 10^{-14})\, T_{m1}^3 - (4 * 10^{-11})\, T_{m1}^2 + (7 * 10^{-8})\, T_{m1} + (1 * 10^{-6}) \qquad \text{(A.8)}$$

d) Thermal conductivity of air

The thermal conductivity of a material is a property which gives an indication of the rate at which energy is transferred and is dependent on the physical matter that makes up the material (Bergman *et al*., 2011: 70). Thermal conductivity is typically expressed in W/mK. The relationship between thermal conductivity and temperature is depicted in Figure A4.

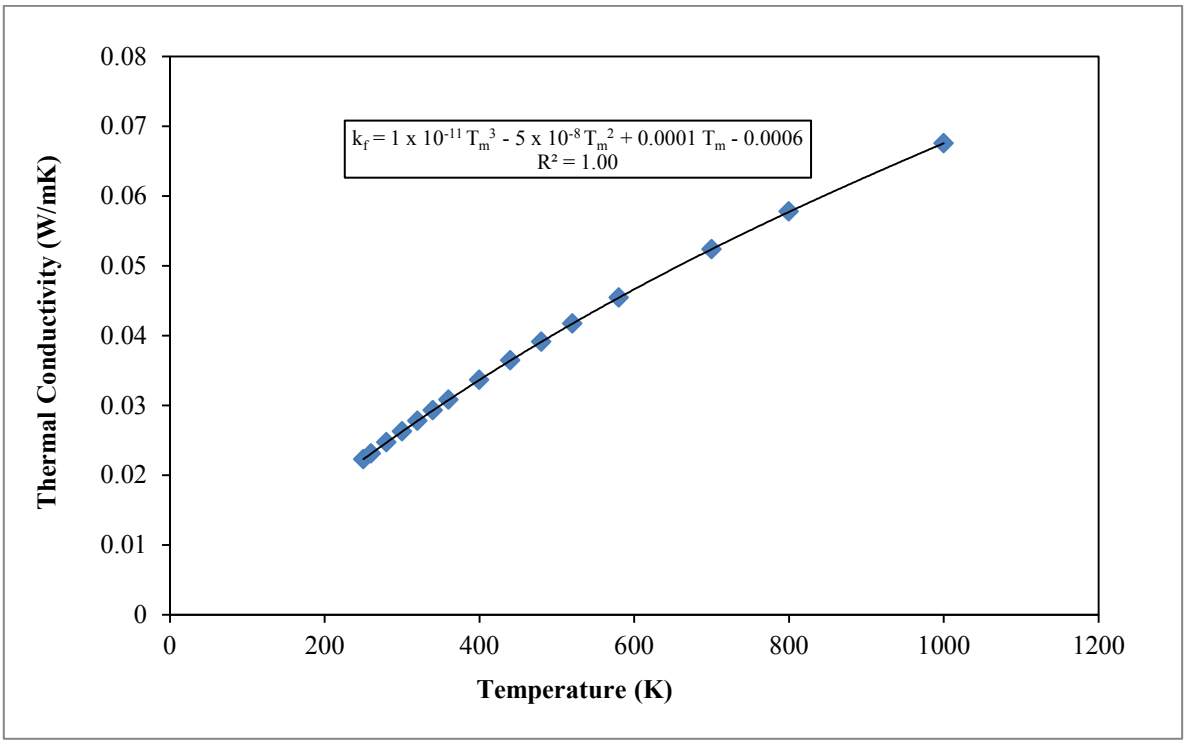

Figure A4: Variation of thermal conductivity of air with temperature

In this case as well, a polynomial function of order 3 was found to be the best fit for the data. The correlation relating the thermal conductivity of air with temperature can be expressed as follows:

For glass cover and air stream,

$$k_f = (1 * 10^{-11})\, T_m^3 - (5 * 10^{-8})\, T_m^2 + 0.0001\, T_m - 0.0006 \qquad \text{(A.9)}$$

For absorber wall and air stream,

$$k_{f1} = (1 * 10^{-11})\, T_{m1}^3 - (5 * 10^{-8})\, T_{m1}^2 + 0.0001\, T_{m1} - 0.0006 \quad \text{(A.10)}$$

e) Kinematic viscosity of air

Kinematic viscosity is the ratio of dynamic viscosity to the density of the fluid, commonly expressed in its SI unit of m^2s^{-1}, as given below (Hewakandamby, 2012: 16):

For glass cover and air stream,

$$\nu_f = \frac{\mu_f}{\rho_f} \quad \text{(A.11)}$$

For absorber wall and air stream,

$$\nu_{f1} = \frac{\mu_{f1}}{\rho_{f1}} \quad \text{(A.12)}$$

Appendix B: Algorithm for solving system of equations in MATLAB

The program which was written in MATLAB is given below. The name of the m-file was final_code.m while the name of the m-file in which the climatic data for Stellenbosch were transferred to was called Data_1.m. The latter comprised of numerous columns of data but the ones which were of relevance to this study were columns 3, 6, 8, 10 and 14, representing the day of the year, global radiation on a horizontal surface, diffuse radiation on a horizontal surface, ambient temperature and wind speed respectively. The green comments (preceded by the percentage sign) refer to non-executable commands which give the meaning of the symbol or equation. The percentage sign can also be seen in front of some equations in the program, which means for that particular run, that equation was not executed due to investigating the effect of other parameters in the study.

```
% The following program is used to simulate the thermal performance of roof-mounted and
% wall-mounted solar chimneys.

Gsc=1367;                % Solar constant
K_ecoeff=(4+32)/2;       % Extinction Coefficient
x=pi/180;                % conversion factor to radians
gamma=180;               % surface azimuth angle
long_s=30;               % standard meridian for local time zone
long=18.7817;            % longitude of Stellenbosch
phi=-33.93462;           % latitude
beta=90;                 % angle of inclination of roof solar chimney
rho_g=0.2;               % Ground Reflectance
g=9.81;                  % Acceleration due to gravity
alpha2=0.95;             % absorptivity of absorber wall
epsilon_g=0.90;          % emissivity of top of glass cover
epsilon_w=0.95;          % emissivity of absorber wall
Lg=2;                    % height of glass cover
Wg=1;                    % width of glass cover
Labs=Lg;                 % height of absorber wall
Wabs=1;                  % width of absorber wall
K_ins=0.027;             % thermal conductivity of wall insulation/polyurethane
w_ins=0.1;               % thickness of insulation
d=0.25;                  % air gap
z=0.1;                   % inlet height

if beta >= 90;
   Lstack=Labs+(z/2);          % stack height for wall solar chimney
else
   Lstack=Labs*sin(beta*x);    % stack height for inclined roof solar chimney
end

Lr=3;                    % length of room to be ventilated
Wr=3;                    % width of room
```

```
Hr=3;                    % height of room
Vr=Lr*Wr*Hr;             % volume of room
Cd=0.57;                 % coefficient of discharge
sigma=5.67*10^(-8);      % Stefan-Boltzmann constant (W/(m2.K4))
hc=5.91;                 % Conductive heat transfer for glass (W/m2.K)
gamma_mta=0.74;          % Mean temperature approximation
z_glass=4/1000;          % Thickness of glass
Ag=Lg*Wg;                % Area of glass cover
Aabs=Labs*Wabs;          % Area of absorber wall
Aoutlet=d*Wabs;          % Area of outlet of channel
Ainlet=Aoutlet;          % Area of inlet of channel
Ar=Aoutlet/Ainlet;

% view factor between wall and glass
X=Labs/d;
Y=Wabs/d;
F_w_g=2/(pi*X*Y)*(log(((1+X^2)*(1+Y^2)/(1+X^2+Y^2))^0.5)-X*atan(X)-
Y*atan(Y)+X*(1+Y^2)^0.5*atan(X/((1+Y^2)^0.5))+Y*(1+X^2)^0.5*atan(Y/((1+X^2)^0.5))
);

Wgr=0.5*(1-cos(x*beta));
Wsky=0.5*(1+cos(x*beta));

q0=0;       %initial useful energy
ACH0=0;     %initial ACH
S10=0;      %initial radiation absorbed by glass
hrwg0=0;    %initial radiative heat transfer between wall and glass
Itilted0=0; % initial amount of radiation on tilted plane
Eglass0=0; % initial energy captured by glass (J/m2)

% initial temperatures
Tg0=285.85;
Tf0=285.80;
Tw0=285.95;
tolerance=1;

h0=1;
h=744;

for i=h0:h
ncol=Data(:,3);ntrans=ncol';n=ntrans(:,i);      % day of the year
B=2*pi*(n-1)/365;
E_time=229.2*(0.000075+0.001868*cos(B)-0.032077*sin(B)-0.014615*cos(2*B)-
0.04089*sin(2*B))/60;
delta=0.006918-0.399912*cos(B)+0.07257*sin(B)-0.006758*cos(2*B)+0.000907*sin(2*B)-
0.002697*cos(3*B)+0.00148*sin(3*B);
timecol=Data(:,5);timetrans=timecol';
time=timetrans(:,i);                    % time of the day, midnight = 0
t_solar=time+E_time+(long_s-long)/15;   % solar time
omega_1=15*x*(t_solar-12);              % initial hour angle in radians
```

```
omega_2=omega_1+(x*15);                    % final hour angle in radians
omega=(omega_1+omega_2)/2;                 % midpoint of hour in radians
omega_ss=acos(-tan(x*phi)*tan(delta));
theta_z=acos(sin(delta)*sin(x*phi)+cos(delta)*cos(x*phi)*cos(omega));

% theta1: angle of incidence in radians
theta1=(acos((sin(delta)*sin(phi*x)*cos(beta*x))-
(sin(delta)*cos(phi*x)*sin(beta*x)*cos(gamma*x))+(cos(delta)*cos(phi*x)*cos(beta*x)*cos(
omega))+(cos(delta)*sin(phi*x)*sin(beta*x)*cos(gamma*x)*cos(omega))+(cos(delta)*sin(be
ta*x)*sin(gamma*x)*sin(omega))));
if abs(omega)< omega_ss-5*x
   R_b=cos(theta1)/cos(theta_z);
else R_b=0;
end
%
Igcol=Data(:,6); Igtrans=Igcol';      % global solar radiation on horizontal surface
Idcol=Data(:,8); Idtrans=Idcol';      % diffuse radiation on horizontal surface
if abs(omega)< omega_ss-5*x
Ig=Igtrans(:,i);
Id=Idtrans(:,i);
else Ig=0;Id=0;
end
%
Ib=(Ig-Id);             % beam radiation on horizontal surface
if Ig>0 ;
   f=sqrt(Ib/Ig);       % Modulating factor to account for cloudiness
else f=0;
end
if abs(omega)< omega_ss-5*x
Io=Gsc*(1+0.033*cos((2*pi)*n/365))*cos(theta_z);
else Io=0;
end
%
if Io>0
A_i=Ib/Io;                  % Anisotropic Index
else A_i=1;
end

if A_i>=0 && A_i<=1 && R_b>=0
Ibt=Ib*R_b;     % Beam radiation on inclined surface
Idt=Id*((1-A_i)*Wsky*(1+f*(sin(0.5*x*beta))^3)+A_i*R_b); % Diffuse radiation on
inclined surface
else Ibt=0; Idt=0;
end
%
Igr=Wgr*rho_g*Ig;      % Ground-reflected radiation on tilted surface
Itilted=(Ibt+Idt+Igr);    % Total radiation on inclined surface
Itilted_total=Itilted0+Itilted;
Itilted0=Itilted_total;
Eglass=Itilted*3600;    % Total radiation on inclined surface in J/m2
```

```
Eglass_total=Eglass0+Eglass;
Eglass0=Eglass_total;

% CALCULATING ABSORPTANCE, REFLECTANCE AND TRANSMITTANCE OF
GLASS
% Angle of incidence in radians
n1=1;n2=1.526;                          % Refractive indices of air and glass respectively
theta2=(asin((n1*sin(theta1))/n2));     % Angle of refraction in radians
K_extinctioncoeff=(4+32)/2;             % Extinction coefficient
tau_a=exp((-K_extinctioncoeff*z_glass)/cos(theta2));

r_perpendicular=(sin(theta2-theta1))^2/(sin(theta2+theta1))^2;
alpha_perpendicular=(1-tau_a)*((1-r_perpendicular)/(1-r_perpendicular*tau_a));%
absorptance associated with perpendicular component of radiation
tau_perpendicular=tau_a*(1-r_perpendicular)^2/((1-r_perpendicular*tau_a)^2);%
transmittance associated with perpendicular component of radiation
rho_perpendicular=1-(alpha_perpendicular+tau_perpendicular); % reflectance associated
with perpendicular component of radiation
%
r_parallel=(tan(theta2-theta1))^2/(tan(theta2+theta1))^2;
alpha_parallel=(1-tau_a)*((1-r_parallel)/(1-r_parallel*tau_a));% absorptance associated with
parallel component of radiation
tau_parallel=tau_a*(1-r_parallel)^2/((1-r_parallel*tau_a)^2); % transmittance associated with
parallel  component of radiation
rho_parallel=1-(alpha_parallel+tau_parallel);% reflectance associated with parallel
component of radiation

if alpha_perpendicular>0 && alpha_perpendicular<1 && alpha_parallel>0 &&
alpha_parallel<1
alpha_gc=0.5*(alpha_perpendicular+alpha_parallel);  % absorptance of glass cover
else alpha_gc=0;
end
%
if tau_perpendicular>0 && tau_perpendicular<1 && tau_parallel>0 && tau_parallel<1
tau_gc= 0.5*(tau_perpendicular+tau_parallel);   % transmittance of glass cover
else tau_gc=0;
end
%
if rho_perpendicular>0 && rho_parallel>0
rho_gc= 0.5*(rho_perpendicular+ rho_parallel); % reflectance of glass cover
else rho_gc=1;
end
%
S1=alpha_gc*Itilted;       % Solar radiation absorbed by glass cover
S1_total=S10+S1;
S10=S1_total;
S2=tau_gc*alpha2*Itilted;  % Solar radiation absorbed by absorber wall

% Ta=Tambient, Tr=Room temp,Ts=sky temp
Tacol=Data(:,10);
```

```
Tatrans=Tacol';
Ta=Tatrans(:,i)+273.15;
Tr=Ta;
Ts=0.0552*Ta^1.5;
solution=0;
%
while ~solution
% GLASS COVER AND AIR PROPERTIES
Tm=(Tg0+Tf0)/2;          % Mean temperature
Beta_volumetric=1/Tm;    % Coefficient of volumetric expansion
if Tg0>Tf0
Delta_T=Tg0-Tf0;         % Temperature difference
else Delta_T=0;
end
%
mu_f=((1*10^(-14))*(Tm^3))-((4*10^(-11))*(Tm^2))+((7*10^(-8))*Tm)+(1*10^(-6)); %
Dynamic viscosity of air
rho_f=((-2*10^(-14))*(Tm^5))+ ((6*10^(-11))*(Tm^4))- ((9*10^(-8))*(Tm^3))+ ((6*10^(-
5))*(Tm^2))-(0.0236*Tm) + 4.5799; % Density of air
K_f=((1*10^(-11))*(Tm^3))-((5*10^(-8))*(Tm^2))+(0.0001*Tm)-0.0006;  % Themal
conductivity of air
C_f=((-4*10^(-7))*(Tm^3))+ (0.0008*(Tm.^2))-(0.3484*Tm)+ 1047.7;    % Specific heat of
air
Pr=(mu_f*C_f)/K_f;                          % Prandtl number
nu_f=mu_f/rho_f;                            % Kinematic viscosity of air
Gr=(g*Beta_volumetric*Delta_T*(Lstack^3))/(nu_f^2); % Grashof Number
Ra=Gr*Pr;                                   % Rayleigh Number
%
if Ra<10^9
Nu=0.68+((0.67*(Ra^(1/4)))/(1+((0.492/Pr)^(9/16)))^(4/9)); %Nusselt's number
else
Nu=(0.825+(0.387*(Ra^(1/6)))/(1+((0.492/Pr)^(9/16)))^(8/27))^2;
end
%
% ABSORBER WALL AND AIR PROPERTIES
Tm1=(Tw0+Tf0)/2;
Beta_volumetric1=1/Tm1;
if Tw0>Tf0
Delta_T1=Tw0-Tf0;
else Delta_T1=0;
end
%
mu_f1=((1*10^(-14)))*(Tm1^3)-((4*10^(-11))*(Tm1^2))+((7*10^(-8))*Tm1)+(1*10^(-6));
% Dynamic viscosity of air
rho_f1=((-2*10^(-14))*(Tm1^5))+ ((6*10^(-11))*(Tm1^4))- ((9*10^(-8))*(Tm1^3))+
((6*10^(-5))*(Tm1^2))-(0.0236*Tm1) + 4.5799; % Density of air
K_f1=((1*10^(-11))*(Tm1^3))-((5*10^(-8))*(Tm1^2))+(0.0001*Tm1)-0.0006; % Themal
conductivity of air
C_f1=((-4*10^(-7))*(Tm1^3))+ (0.0008*(Tm1^2))-(0.3484*Tm1) + 1047.7;  % Specific heat
of air
```

```
Pr_1=(mu_f1*C_f1)/K_f1;  % Prandtl number
nu_f1=mu_f1/rho_f1;          % Kinematic viscosity of air
Gr_1=(g*Beta_volumetric1*Delta_T1*(Lstack^3))/(nu_f1^2);       % Grashof Number
Ra_1=Gr_1*Pr_1;                                    % Rayleigh Number
if Ra_1<10^9
Nu_1=0.68+(0.67*(Ra_1^(1/4)))/(1+((0.492/Pr_1)^(9/16)))^(4/9);  % Nusselt's number
else
Nu_1=[0.825+(0.387*(Ra_1^(1/6)))/(1+((0.492/Pr_1)^(9/16)))^(8/27)]^2;  % Nusselt's
number
end

%mass flow rate of air in kg/s
if Tf0-Tr>0
m=(Cd*rho_f1*Aoutlet/(sqrt(1+Ar^2)))*sqrt(((2*g*Lstack*(Tf0-Tr)))/Tr); % mass flow rate
of air
else m=0;
end

% HEAT TRANSFER COEFFICIENTS
hrs=((sigma*epsilon_g)*(Tg0^2+Ts^2)*(Tg0+Ts)); % radiative heat transfer between glass
cover and sky
% hrwg=(sigma*((Tg0^2+Tw0^2)*(Tg0+Tw0)))/((1/epsilon_g)+(1/epsilon_w)-1);       %
radiative heat transfer between wall and glass
% Taking into account VIEW FACTOR
hrwg= sigma*(Tg0^2+Tw0^2)*(Tg0+Tw0)/(((1-epsilon_w)/epsilon_w)+(((1-
epsilon_g)/(epsilon_g*Ag))*Aabs)+1/F_w_g); % radiative heat transfer with view factor
hrwg_total=hrwg0+hrwg;
hrwg0=hrwg_total;
%
Ub=K_ins/w_ins; % overall heat transfer coefficient between the insulation layer of the
absorber wall and the room that needs to be ventilated
%
Vcol=Data(:,14);Vtrans=Vcol';V=Vtrans(:,i); % Wind speed in m/s
if V<=5
hwind=2.8+3*V;            % heat transfer coefficient by convection due to wind
else hwind=6.15*V^0.8;
end
%
Ut=hwind+hrs;                % overall heat transfer coeff from top of glass to ambient
hg=(Nu*K_f)/Lg;              % convective heat transfer coefficient between glass and air
hw=(Nu_1*K_f1)/Labs;       % convective heat transfer coefficient between wall and air

% Computation of new temperatures
%
Tf=(hg*Ag*Tg0+hw*Aabs*Tw0+m*C_f1*Tr/gamma_mta)/(hg*Ag+hw*Aabs+m*C_f1/ga
mma_mta); % Fluid temperature
Tg=(S1*Ag+Ut*Ag*Ta+hg*Ag*Tf+hrwg*Aabs*Tw0)/(hg*Ag+hrwg*Aabs+Ut*Ag); %
Glass temperature
Tw=(S2*Aabs+Ub*Aabs*Tr+hrwg*Aabs*Tg+hw*Aabs*Tf)/(hw*Aabs+hrwg*Aabs+Ub*Aa
bs); % Absorber wall temperature
```

```
%
Tempold=[Tf0;Tg0;Tw0];
Tempnew=[Tf;Tg;Tw];
Tempdiff=abs(Tempnew-Tempold);
%
if all (Tempdiff)<=tolerance;
   solution=1;
end

temps=[Tf;Tg;Tw];
%
% updating temperatures
Tf0=Tf;
Tg0=Tg;
Tw0=Tw;
%
end
T(:,i)=temps;
%
v_rate=m/rho_f1;              % ventilation rate
ACH=(v_rate*3600)/Vr;         % no of air changes per hour
ACH_total=ACH0+ACH;
ACH0=ACH_total;
%
if Tf>Tr
q=3600*(m*C_f1*(Tf-Tr))/(Aabs*gamma_mta); % useful heat transferred to the air stream
else q=0;
end
%
q_total=q0+q;
q0=q_total;
end

Eff=(q_total/Eglass_total)*100; % Efficiency

% Temperature outputs
temp_matrix=T.';
Tf_col=temp_matrix(:,1);Tg_col=temp_matrix(:,2); Tw_col=temp_matrix(:,3);

%disp(q_total)
%disp(ACH_total)
%disp(S1_total)
% disp(hrwg_total)
%disp(Itilted_total)
%disp(Eff);

% Hours in a year
hourscol=Data(:,20);
hours=hourscol(h0:h,:);
```

```
% Final temperatures for plotting of graphs
%Tf_final=Tf_col(h0:h,:);
%disp(Tf_final);
%Tg_final=Tg_col(h0:h,:);
%disp(Tg_final);

%Tf_final=Tf_col(h0:h,:);
%Tf_average=mean(Tf_final);
%disp(Tf_average);

%Tg_final=Tg_col(h0:h,:);
%Tg_average=mean(Tg_final);
%disp(Tg_average);

%Tw_final=Tw_col(h0:h,:);
%Tw_average=mean(Tw_final);
%disp(Tw_average);

%Ta_final=Tacol(h0:h,:);
%Ta_average=mean(Ta_final);
%disp(Ta_average);
```